"We are dedicated to Innovative knowledge"

አዳማ ሳይንስና ቴክኖሎጂ ዩኒቨርሲቲ

Adama Science and Technology University

Modeling and Control of Dual Converters on a Grid Connected Wind Power Energy Conversion System with Doubly-Fed Induction Generator in the Case of Adama II Wind Farm

By:

Zebene Asitawos Reta

A Thesis Paper Submitted to School of Electrical Engineering and Computing Electrical Power and Control Engineering Program in Partial Fulfillment of the Requirement of the degree of Master of Science in Electrical Power and Control Engineering

(Specialization in Power Electronics)

Office of Graduate Studies

Adama Science and Technology University

Adama, Ethiopia

July, 2020

Modeling and Control of Dual Converters on a Grid Connected Wind Power Energy Conversion System with Doubly-Fed Induction Generator in the Case of Adama II Wind Farm

Zebene Asitawos Reta (Candidate)

Advisor: Milkias Berhanu Tuka (PhD)

A Thesis Paper Submitted to School of Electrical Engineering and Computing Electrical Power and Control Engineering Program in Partial Fulfillment of the Requirement of the degree of Master of Science in Electrical Power and Control Engineering

(Specialization in Power Electronics)

Office of Graduate Studies

Adama Science and Technology University

Adama, Ethiopia

July, 2020

Approval of Board of Examiners

We, the undersigned, members of the Board of Examiners of the final open defense by Zebene Asitawos Reta have read and evaluated his thesis entitled **"Modeling and Control of Dual Converters on a Grid Connected Wind Power Energy Conversion System with Doubly-Fed Induction Generator in the Case of Adama II Wind Farm"** and examined the candidate. This is, therefore, to certify that the thesis has been accepted in partial fulfillment of the requirement of the Degree of Master of Science Electrical Power and Control (Power Electronics).

Name	Signature	Date
______________	______________	______________
Name of Student		
______________	______________	______________
Advisor		
______________	______________	______________
External Examiner		
______________	______________	______________
Internal Examiner		
______________	______________	______________
Chair Person		
______________	______________	______________
Head of Department		
______________	______________	______________
School Dean		
______________	______________	______________
Post Graduate Dean		

DECLARATION

I hereby declare that this MSc. Thesis is my original work and has not been presented for a degree in any other university, and all sources of material used for this thesis have been duly acknowledged.

Name: __________________________

Signature____________

This MSc Thesis has been submitted for examination with my approval as thesis advisor.

Name: ______________________

Signature: ____________

Date of submission: _________________

ADVISOR'S APPROVAL SHEET

To: Electrical Power and Control Engineering department

Subject: Thesis Submission

This is to certify that the thesis entitled **"Modeling and Control of Dual Converters on a Grid Connected Wind Power Energy Conversion System with Doubly-Fed Induction Generator in the Case of Adama II Wind Farm"** submitted in partial fulfillment of the requirements for the degree of Masters of Master of Science Electrical Power and Control (Power Electronics), the Graduate program of the department of Electrical Power and Control and has been carried out by Zebene Asitawos Reta Id. No PGR/18354/11, under our supervision. Therefore, we recommend that the student has fulfilled the requirements and hence hereby he can submit the thesis to the department.

Advisor	Signature	Date

ACKNOWLEDGEMENTS

First, I would like to thanks more for my God and his mother saint Mary. Then I would like to express my gratitude to my supervisor Dr. Milkias Berhanu Tuka for guiding me through with his expertise, and also many thanks to my Lecturer for their contribution and assistance and fruitful ideas. I further wish to thank all of them who had guided me through all the technical difficulties throughout the research work. This research would not have been successful without the valuable guidance and constructive criticisms throughout the research. I also would like to express my sincere thanks to my best friends Mr.Assefa Sefu and Mr.Tesifaye Birara who have helped me throughout the research.

ABSTRACT

The demand of energy is drastically increasing now days mainly in developing countries like Ethiopia. It is global and increasing demand in developed countries. The penetration of wind energy generation in to existing power system network is increasing rapidly during recent years. But Ethiopia electric power corporation is using wind power to solve electric power shortage in the existing grid. Currently 153MW from Adama II wind farm, 120MW from Ashegoda wind farm and 51MW from Adama I wind farm of the country's power is generated from wind power. The number of Doubly- Fed Induction Generator has grown over the last few years in several countries. In Ethiopia, among the most commonly used generators Adama II wind farm use Doubly-Fed Induction Generator nowadays. Its stator is directly connected to the grid, whereas the rotor is tied via dual (back-to-back) converters. Doubly fed induction generator connected to a grid through back-to-back converter have problems, such as converter control, and power quality. Therefore, improving the reliability of the wind turbine system in power generation sector with optimal performances is one of the important tasks. A detail study of the performance of wind turbine systems in various case scenarios namely, using different pulse width modulation types namely, sinusoidal pulse width modulation (SPWM), third harmonics injection pulse width modulation (THIPWM), space vector pulse width modulation (SVPWM) and using different converter topologies are investigated. This thesis is mainly focused on back-to back converter modeling and pulse width modulation techniques comparison in order to reduce voltage and current harmonic distortion and control real and reactive power. From the comparative study the DFIG based wind turbine system studied in this thesis, using either two-level converter or three-level NPC converter using SVM achieve the IEEE 519 criteria of THD which is less than 5%. Analysis and modeling have been developed using MATLAB/SIMULINK software based on data obtain from Ethiopian Electric Power (EEP) and Adama II wind farm site.

Key Word*: Back-to-Back Converter, PWM, DFIG, MATLAB/SIMULINK, SPWM, THIPWM SVPWM.*

Contents

LIST OF FIGURES

LIST OF TABLES

LIST OF ACRONYMS

AC	Alternating Current
DC	Direct Current
CHB	Cascaded H-Bridge
DFIG	Doubly Fed Induction Generator
DM	Delta Modulation
EEP	Ethiopian Electric Power
GB	Gear Box
GSC	Grid Side Converter
GVOVC	Grid Voltage Oriented Vector Control
IGBT	Insulated Gate Bipolar Transistor
IGCT	Insulated Gate commutated Transistor
MLI	Multilevel Inverter
MOSFET	Metal Oxide Semiconductor Field Effect Transistor
MPWM	Modified Pulse Width Modulation
MSC	Machine Side Converter
NPC	Neutral Point Converter
PCC	Point of Common Coupling
PI	Proportional Integral controller
PLL	Phase Locked Loop
PMSG	Permanent Magnet Synchronous Generator
PWM	Pulse Width Modulation
RPWM	Random Pulse Width Modulation
SCIG	Squirrel-Cage Induction Generator
SHE	Selective Harmonics Elimination
SVM	Space Vector Modulation
TCPWM	Triangular Comparison Pulse Width Modulation
THIPWM	Third Harmonics Injection Pulse Width Modulation
WECS	Wind Energy Conversion System
WT	Wind Turbine

LIST OF SYMBOLS

C	Filter Capacitance
C_{dc}	DC Link Capacitor
f_r	Rotor Frequency
f_s	Rated Stator Frequency
f_{sw}	Switching Frequency
G_B	Gearbox Ratio
i_{As}, i_{Bs}, i_{Cs}	Three-Phase Stator Currents
i_{Ar}, i_{Br}, i_{Cr}	Three-Phase Rotor Volt
i_{ca}, i_{cb}, i_{Cc}	Filter Capacitor Current
i_{g-dc}	DC Current Flowing from the DC Fink to the Grid
i_{r-dc}	DC Current Flowing from the Rotor to the Dc Link
I_{res}	Current Through the Resistance
i_{a1}, i_{b1}, i_{c1}	Inverter-Side Current
i_{a2}, i_{b2}, i_{c2}	Grid-Side Current
L_m	Mutual Inductance
L_r	Rotor Inductance
L_s	Stator Inductance
M_a	Modulation Index
p	Number of pole pairs
p_{mech}	Mechanical power
P_r	Rotor-side converter active power
P_s	Stator active power
R_s, R_r	Stator and Rotor Resistances of the Phase Windings
s	Generator Slip

S_{a-g}, S_{b-g}, S_{c-g}	Switching Function of the Converter
T_m	Mechanical Torque of the Shaft
ω_m	Machine Angular Frequency
ω_s	Synchronous Angular Frequency
ω_r	Angular Frequency
Ψ	Flux
Ω_m	Mechanical Angular Speed

CHAPTER ONE

1. INTRODUCTION

1.1. Background of Study

Renewable energy resources have gained significant attention of the industry and the academic researcher, because it is environmentally friendly [1]. Nowadays, wind power plants are becoming dominant in serving as source of renewable energy next to hydro power in Ethiopia. This is because of the advancement and better understanding of the technology, energy security, generation mix, and aim to decrease the greenhouse gases or global warming. The Doubly-Fed Induction Generators (DFIG) are currently the most popular wind generators in the market among variable-speed wind turbines used because of their high energy efficiency and controllability [2]. The main advantages of using variable-speed operation of wind turbines are: the possibility to reduce stresses on the mechanical structure, acoustic noise reduction, and the possibility to control active and reactive power [3].

The general shape of the DFIG is that, its stator side is connected to the grid directly while, the rotor windings are connected to the grid via AC/DC/AC insulated bipolar power converter [4]. A typical block diagram of the DFIG in a wind energy system is shown in Figure 1-1.

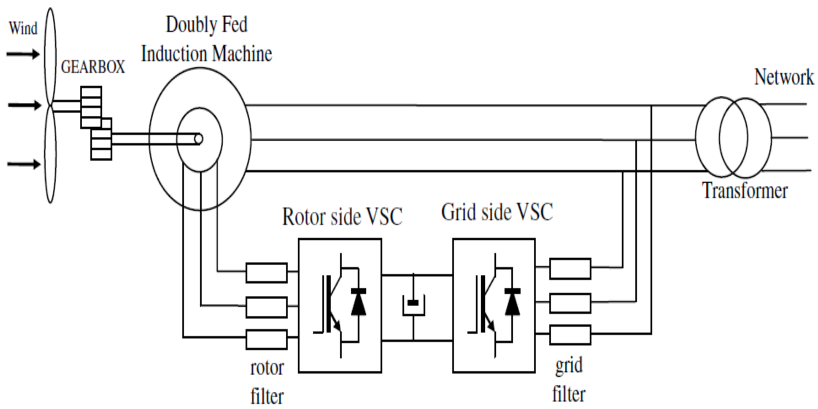

Figure 1-1: Block diagram of DFIG wind energy conversion system

The interest focused on wind energy is due to the importance of this source of power in terms of quality of energy and its environmental impact. From this power, Adama II wind farm is one of the sources of power in Ethiopia, which is located in the middle of Ethiopia, about 7 km west of Nazret, and 3.5 km west of Adama I wind power project, with altitude elevation of 1741-2200m. The central geographical position of the wind power project is $39^{0}13^{'}6.46^{''}$ E, $8^{0}34^{'}48.12^{''}$ N, stretching from Northeast to Southwest. The total installed capacity of Adama II wind power project is of 102 turbines with a 1.5 MW each which gives 153 MW. Since Ethiopia has high wind resource potential, Ethiopian Electric Power (EEP) has a plan to increase the power generated from wind more than 600 MW. Thus, the growing level of wind power penetration in to the power system requires detailed analysis of grid connected converters.

In recent years, different back-to-back PWM power converters techniques have been developed to integrate wind turbines with the electrical grid. The use of power electronics converters allows for variable speed operation of wind turbines as well as enhanced power extraction. The converter system combined with the rotor of DFIG guarantees superior grid connection capabilities but the converter-inverter system used in wind farms generate harmonic emissions; hence it may result a power quality problem within the wind farm and the grid connected to it. This thesis focuses on developing various pulse width modulation and control methods for grid connected back-to-back converters so as to improve their performance in wind energy generation.

In order to efficiently obtain the available power in wind and allow stable power flow at machine terminals, the control of DFIG is very important. As the voltage variation is directly related to real and reactive power variations, where the voltage is not stiffly constant, the DFIG may be ordered to produce or absorb an amount of reactive power to or from the grid as per the grid code requirements with the purpose of voltage control. Hence, adapting the well-known control methods employed with back-to-back converters in DFIG play a greater role. The rotor side voltage source converter is used to control stator active and reactive power; whereas the grid side voltage source converter controls the DC link voltage to be used as a stable voltage source. Grid voltage orientation technique is used in this paper for grid side voltage source converter control. Several types of research are still underway in investigating the best control strategies to improve the performance of DFIG [5], which shows a key emphasis of the machine. Even though design, simulation, as well as practical results from the previous studies, have offered useful hints for DFIG, there is a lack of detail analysis especially on regarding converter control issues. For this and adding an additional contribution, the study of DFIG through modeling and simulation in the well-known MATLAB/Simulink software would help to justify ideas that will be investigated in further works and control techniques.

1.2. Statement of Problem

The EEP has a plan to use wind power plants to solve the shortage of electric power supply. Modern wind turbines are equipped with power converters and generators, mainly Doubly

Fed Induction Generator (DFIG) and Permanent Magnet Synchronous Generator (PMSG). These thesis focus on DFIG, being a rotating electrical machine and switching in the power electronics converter, introduces harmonics that could result in voltage distortions at point of common coupling (PCC) to the grid. This effect increases as the number of DFIG wind energy conversion system (WECS) connected to the grid increases. The voltage distortions resulting from the rotor side voltage source converter of the power electronics converter cause increase in eddy current losses in the generator and the voltage distortion in grid side converter grid side voltage source converter resulting power quality problem at the grid. The power converters will affect the power quality, which can affect the operation and the reliability of the electrical grid. In this thesis, harmonics issue will be considered. The complete modeling of a back-to-back converter developed using a MATLAB-Simulink software.

1.3. Objective of Study

1.3.1. General Objective

The main goal of this thesis is to develop enhanced back-to-back converter control strategies for DFIG based wind turbines and to investigate their performance in terms of harmonics distortion level and switching losses.

1.3.2. Specific Objective

- ❖ To model back-to-back PWM converter connected to the electric grid.
- ❖ Analyze the performance of grid connected wind energy conversion system (WECS) employing DFIG machine with two level back to back Converters by implementing PI controller based SPWM, THIPWM, and SVPWM techniques.
- ❖ Analyze the performance of grid connected DFIG based WECS with three level neutral point clamped (NPC) Converters by employing SVPWM techniques.
- ❖ To simulate the system using MATLAB software.

1.4. Significance of Study

The benefits that can be achieving from this research are:

- ➢ To reduce the cost and size of filter connected with grid by reducing the harmonics of converters output voltage and currents. It also increases the efficiency of the grid.
- ➢ Since multilevel voltage source inverter is recently applied in many applications such as ac power supplies, flexible AC transmission systems, renewable energy sources, and active power filters and drive system, so having knowledge in such area can contribute to transfer technology of the above listed applications in Ethiopia.

1.5. Scope of Study

All studies for each of the above stated objectives will be modeled and simulated in MATLAB/SIMULINK simulation software. Renewable generation technologies currently existing in the fields are of many types, including solar, hydro power, wind power and biomass. Thus, this thesis focuses only on wind energy for case study on technologies mainly available in Ethiopia, particularly in the Adama II wind farm where wind power is found in abundance. All elements data type exist in MATLAB and all equipment specification are from data obtained at Adama II wind farm.

1.6. Limitation of Study

This study is limited to investigating the modeling and Control of dual converters for a grid connected wind power system of Adama II wind farm. There was a limitation of harmonics voltage and current data collector device. Furthermore, due to the provision of Internet accesses and other side effects on the research work during pandemic and un expected cases like Covid-19, there was a problem to collect farther data from the site.

1.7. Thesis organization

The thesis is organized into five chapters which are briefly summarized below:

Chapter one, presents the back ground, statement of problem, Objective of study and significance of study. It also highlights scope of study, limitation of study and thesis outline. The second chapter introduces the literature review, basic configurations and characteristics of different wind generator systems. This chapter further discusses the power converter topologies and pulse width modulation techniques to mitigate harmonic distortion. The third chapter briefly looks the detailed doubly-fed induction generator models expressed in the ABC reference frame and DQO reference frames, the PWM converter models and different control schemes for a wind turbine system, which include the grid-side converter control, machine-side converter control. The main focus is introducing a space vector PWM technology and compared with the traditional sinusoidal PWM and third harmonics injected PWM for a two-level inverter. Besides, a three-level neutral-point-clamped converter is studied, and the corresponding space vector modulation is developed. The fourth chapter present simulation result and discussion of a space vector PWM, third harmonics injected PWM and traditional sinusoidal PWM for a two-level converter, three-level converters and two-level converters modulated by space vector PWM. Finally, chapter five summarizes the main results and conclusions within the scope of the research work performed and reported in this thesis. Possible further research topics are also highlighted.

CHAPTER TWO

2. LITRATURE REVIEW

2.1. Introduction

Factor that influences the performance and efficiency of wind energy system is proper selection of Pulse Width Modulation (PWM) technique that controls gating sequence of converters. The main objective of PWM technique is to generate a sinusoidal output voltage with minimum harmonic distortion in the grid side converter. PWM techniques are broadly classified into two types-Space Vector Pulse Width Modulation (SVPWM) and Triangle Comparison Pulse Width Modulation (TCPWM). Comparison of modulating signals with a high frequency triangular carrier signal is performed in TCPWM which results in generation of PWM signals. Thus, turn on and turn off instants of power semiconductor switches of the inverter will be decided. TCPWM technique is suitable to be employed for both single phase and three phase inverter circuits. In SVPWM, a rotating voltage vector is considered as the reference. For every sector rotation, the switching sequence of the inverter will change and output voltage is generated accordingly. The SIMULINK models of Space Vector Pulse Width Modulation and Sinusoidal Pulse Width Modulation techniques for three phase Voltage Source Inverter are developed using MATLAB and results are compared. Peak value of phase voltage obtained at the output of the grid inverter is much higher when SVPWM technique is employed [6]. It is observed that Space Vector Modulation technique utilizes DC bus voltage more efficiently and generates less harmonic distortion when compared with Sinusoidal PWM (SPWM) technique. Thus, prominence of SVPWM in three phase Voltage Source Inverters has increased and its application is extended for controlling Induction motors, Brushless DC, Switched Reluctance and Permanent Magnet Synchronous motors.

With advances in solid-state power electronic devices, various converter control techniques employing pulse-width-modulation (PWM) techniques are becoming increasingly popular in induction motor drive applications. These PWM-based drives are used to control both the frequency and the magnitude of the voltages applied to machines [7]. Various pulse width modulation (PWM) strategies, control schemes, and realization techniques have been developed in the past two decades [8]. Modulation strategy plays an important role in the minimization of harmonics and switching losses in converters, especially in three-phase applications. The first modulation techniques were developed in the mid-1960s by Kirnnich, Heinrick, and Bowes as reported in [9]. The research in PWM schemes has intensified in the last few decades. The main aim of any modulation technique is to obtain a variable output with a maximum fundamental component and minimum harmonics [10]. The carrier-based PWM methods were developed first and were widely used in most applications. One of the earliest modulation signals for carrier-based PWM is sinusoidal PWM (SPWM). The SPWM technique was introduced by Schonung and Stemmler in 1964 as reported in [11]. It The utilization rate of the DC voltage for traditional sinusoidal PWM is only 78.5% of the DC bus voltage, which is far less than that of the six-step wave (100%). Improving the utilization rate of the DC bus voltage has been a research focus in power electronics [8]. This problem of the under-utilization of the DC bus voltage led to the development of the third-harmonic-injection pulse-width modulation (THIPWM). In 1975, Buja developed this improved sinusoidal PWM technique, which added a third-order harmonic content into the sinusoidal reference signal leading to a 15.5% increase in the utilization rate of the DC bus voltage [12]. Another method of increasing the output voltage is the space-vector PWM (SVPWM) technique.

SVPWM was first introduced in the mid-1980s and was greatly advanced by Van Der Broeck in 1988 [13]. Compared to THIPWM, the two techniques have similar results but their methods of implementation are completely different. With the development of microprocessors, SVPWM has become one of the most important PWM methods for three-phase inverters [14]. Many SVPWM schemes have been developed and extensively investigated in the literature. The goal in each modulation strategy is to lower the switching losses, maximize bus utilization, reduce harmonic content, and still achieve precise control [15].

The SVPWM technique utilizes the DC bus voltage more efficiently and generates less harmonic distortion when compared with the SPWM technique [12]. The maximum peak fundamental magnitude of the SVPWM technique is about 90.6% of the inverter capacity. This represents a 15% increase in the maximum voltage compared with conventional sinusoidal modulation. In 1991, Holtz proposed a classical over-modulation technique based on SVPWM, which divided the over-modulation range into two modes of operation and increased the utilization rate of the DC voltage to that of a six-step wave [12,16,17]. Holtz proposed this technique using switching time calculations in the over-modulation region of SVPWM. In 1998, Lee analyzed Holtz's over-modulation technique graphically, gave some approximate linear expressions between the modulation index and its own auxiliary parameter, and discussed the harmonic problem [18]. He showed that this technique generated less harmonic distortion in the output voltages (or) the currents applied to the phases of an AC motor and provided more efficient use of the DC input voltage. Because of its superior performance characteristics, it has found widespread application in recent years. Accordingly, many other researchers have explored various aspects of this technique in the literature [12, 19].

2.2. Basics of wind energy conversion system

In this section, a detailed literature review describing various wind turbine generator, back-to back converter and PWM modulation techniques are presented. More specifically, the related previous studies and researches on the modeling, control strategies, and the state-of-the-art converter topologies applied in doubly-fed induction generator (DFIG) based wind turbine-generator systems can be presented.

2.3. Wind energy conversion system topologies

Wind Energy Conversion Systems (WECS) have several different topologies depending on the type of machine used as well as the application. WECS can also be classified according to their speed of operation, that is, fixed-speed or variable-speed operation of the systems. The simple design and low maintenance of fixed-speed WECS made them popular in the past. This type of system consists of an induction machine connected directly to the grid. The term fixed speed is due to the fact that there is no speed control in this system and the operating speed is constant and not dependent on the changing wind speed. This means they can only achieve optimal aerodynamic efficiency at a single wind speed [20]. Variable speed WECS are more preferred owing to the ability for independent speed control. This is due to the technological advances in power converters. Furthermore, the ability to change the speed of operation of the generator allows the system to operate at higher aerodynamic efficiencies over a wider range of wind speeds [20]. In this section, some common topologies are discussed and then the one that is used for this thesis is outlined.

2.3.1. Squirrel Cage Induction Machine

Squirrel Cage Induction machines are used for variable speed operation. The back to back converter is connected to the stator windings and has to be rated for the full machine power. Figure 2-1 below shows the layout of the Squirrel Cage Induction Generator (SCIG) wind energy conversion system (WECS) topology with full bridge back to back converters. According to [22], squirrel cage induction machines are not to be overlooked among the WECS technologies. They are low cost and have a low maintenance requirement which further reduces the cost. They are also robust and have the full speed range operation and complete control of active and reactive power [23]. However, the full power rating of the converter can be costly. The back- to back converter is used to transfer the generated power from the SCIG induction machine to the three-phase grid.

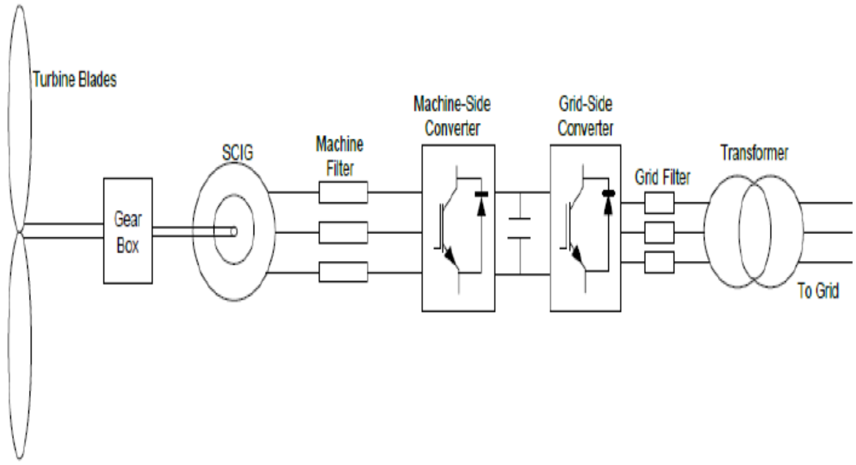

Figure 2-1: Layout out of SCIG WECS topology [21]

2.3.2. Permanent magnet synchronous machine

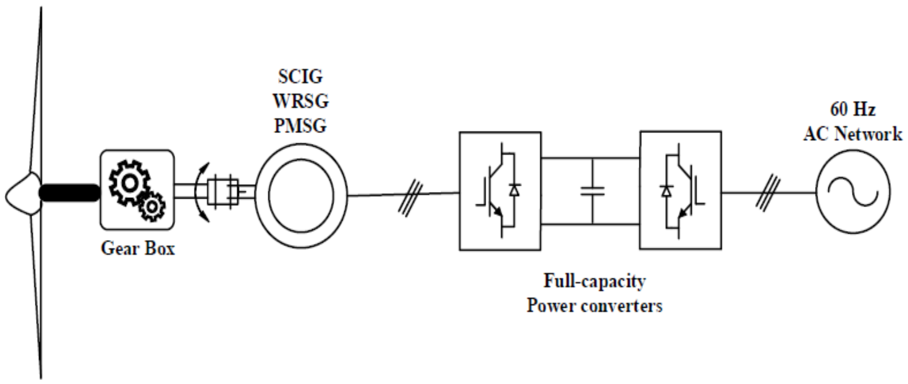

Figure 2-2: Layout of PMSG WECS topology [21]

Figure 2-2 above shows the layout of Permanent Magnet Synchronous Generator (PMSG) WECS topology with back to back converter. This topology is used for variable speed operation made possible by the power converter. PMSGs do not require reactive power hence they can be connected with various converter topologies. PMSGs have the advantage of the full operating speed as well as independent control of active and reactive power exchanged with the grid. They do not require much maintenance because they have no brushes on the generator. However, PMSGs consist of permanent magnets which are rare earth metals, hence they become very expensive to make as the MW capacity increases.

2.3.3. Doubly fed Induction machine

A typical block diagram of the doubly fed induction generator (DFIG) wind energy system is shown in figure 2-3, the power factor of the system can be adjusted by the power converters. A DFIG WECS topology is the basis of this thesis. In this topology the back to back converter is connected to the rotor windings resulting in a much lower rating for the converter, about 30 % of the stator power, which reduces the cost of the converter [21]. The stator is connected directly to the grid. There is independent control of the active and reactive power as well as a wide range of operating speed which is controlled by the machine side converter.

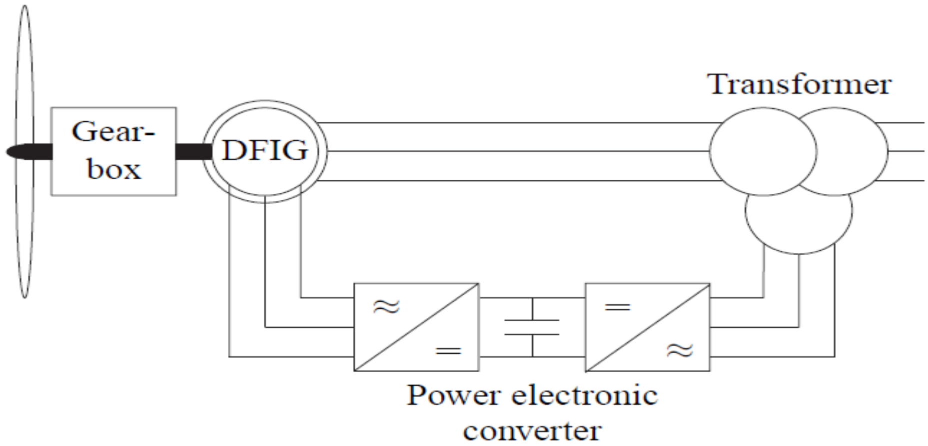

Figure 2-3: Layout of DFIG WECS Topology with Full bridge back to back converters [21]

The use of the converters also allows bidirectional power flow in the rotor circuit and increases the speed range of the generator. This system features improved overall power conversion efficiency, extended generator speed range (±30%), and enhanced dynamic performance as compared to the fixed-speed WECS. These features have made the DFIG wind energy system widely accepted in today's market.

2.4. Two-level converter

Two-level voltage source converter has been the most widely used power converter for three phase motor drive applications. Probably, due to the maturity obtained in the drives industry during more than a decade, the two-level voltage source converter was widely adopted by the wind turbine industry for use in large scale wind turbines in the late nineties [24]. In two-level inverter output voltage waveform is produced by using SPWM with two voltage levels, this causes the converter output phase to neutral, line to line voltage and current to be distorted and the total harmonics distortion (THD) of the voltage is poor. In high power and high voltage applications this two level inverter however, have some limitations in operating at high frequency mainly due to switching losses and constraints of device rating.

2.5. Diode clamped or neutral point clamped (NPC) multilevel converter

One of the traditionally accepted and widely used topology for various industrial and power sector applications is diode clamped or neutral point clamped converter which was proposed by Nabae, Takahashi and Akagi in 1981[25]. The diode-clamped inverter is also known as neutral-point clamped (NPC) inverter. This inverter is consisting of two pairs of series switches (upper and lower). Each phase has complementary switch pairs such that turning on, one of the switches of the pair require that the other complementary switch be turned off. Here common dc voltage source is share by both upper and lower switches which is then subdivided by two series connected capacitor. In between two capacitor the midpoint is there which divides the main DC voltage into smaller voltages. As the two-level inverter has the drawback of achieving higher power levels so three level inverter configurations was developed to meet the requirement of high voltage level. Since all semiconductors are operated at a commutation voltage of half the dc-link voltage, the topology offered a simple solution to extend voltage and power ranges of the existing two-level technology, which were previously limited by the blocking voltages of power semiconductors with active turn-on and turn-off capabilities. Hence, the converter was of particular interest for medium voltage applications. However, as the number of levels has increased the number of clamping diodes, switching devices and dc capacitors also increases, thus the circuit configuration becomes more complicated [26]. In general, for an m-level diode clamped inverter, for each leg $2(n-1)$ switching devices, $(n-1) * (n-2)$ clamping diodes and $(n-1)$ dc link capacitors are required. Generally, the voltage across each capacitor for an m-level diode clamped inverter at steady state is ${V_{dc}}/{(n-1)}$. The operation of NPC topology is simple and straightforward but as the number of inverter levels increases, number of devices increases and also increased the capacitor voltage balancing which becomes a major problem. Hence, design and implementation become more complicated for higher number of levels.

There are different modulation schemes to generate the desired converter voltage. Commonly applied modulation methods in industry for diode clamped inverter are the carrier-based sine-triangle modulation [27], based on multiple-carrier arrangements in vertical shifts. In addition, the space-vector modulation has been extended for the multilevel case. From all these modulation technique any one can be preferred depend on in which application this inverter is used, but the most preferable is carrier-based sine-triangle modulation in which the sine wave is compared with triangular wave and provide PWM signal for the switches used in the inverter and also its implementation is easy.

Following are the advantages of diode clamped or neutral point clamed MLI

1. All the phases share a common dc bus, due to which the capacitor requirements for the converter minimizes.
2. As a group, capacitors can be pre-charged.
3. Converter efficiency is high.

While the disadvantages are the number of switches, capacitors, and diodes required in the circuit increases with the increase in the number of output voltage levels. Currently, the three-level neutral point clamped inverter is the most widely spread topology in medium voltage drives.

2.6. Flying capacitor (FC) MLI

This inverter topology is similar to that of the NPC topology except the usage of clamping diodes. This inverter topology uses capacitors instead of clamping diodes. Flying capacitor MLI has capacitors on dc side and connected like ladder structure, where the voltage across each capacitor differs from that of the next capacitor. The voltage increment between two adjacent capacitor legs gives the size of the voltage steps in the output waveform. Similar to neutral point clamped inverter, the capacitor clamped inverter requires a large number of bulk capacitors of voltage clamping. The voltage rating of each capacitor used will be the same as that of the main power switch, therefore, an m-level converter will require a total of $\frac{(n-1)(n-2)}{2}$ clamping capacitors per phase leg in addition to $(\mathrm{n}-1)$ main DC-bus capacitors. Thus, as the number of levels has increased, more number of storage capacitors are required which results in a bulky and expensive structure when compared to diode clamped inverter topology [28].

The main advantages of this topologies are as follows,

1. Phase redundancy due to which balancing the voltage levels of the capacitors is possible.
2. The large number of capacitors enables the inverter to ride through short duration outages and deep voltage sags.
3. Real and reactive power flows can be controlled

The disadvantages are the requirement of more numbers of capacitors results in bulky and expensive structure than diode-clamped multilevel inverter and complex control is required to maintain the capacitors voltage balance so the inverter control is complicated for higher number of levels.

2.7. Cascaded H-Bridge (CHB) multilevel converter

The basic idea of connecting single-phase H-Bridge inverters in cascade with multiple isolated dc supplies to realize multilevel waveforms was first introduced in 1990 for plasma stabilization. This topology structure has been subsequently extended for three-phase applications, such as reactive power compensation by Peng F.Z., et.al [29]. The CHB is designed by the series connection of H-bridge power cells. Each cell includes a single-phase H-bridge inverter, a capacitive dc-link, a rectifier, and an isolated voltage source. The number of output phase voltage level is given by m=2s+1, where s is number of separate dc sources and by cascading H bridges the inverter voltage get added.

The three modulation techniques mentioned for the diode clamped inverter can also be implemented for the CHB but they present some drawbacks that makes them not the preferred for this inverter. So selective harmonic elimination (SHE) is slightly modified and referred as staircase modulation for CHB. For low-switching frequency applications, the staircase modulation is used. The main advantage of this method is that the converter switches very few times per cycle, reducing the switching losses to a minimum and low-order harmonic are eliminated. However, this method needs important offline calculations to compute the angles for a variety of modulation indexes and is therefore not very suited for highly dynamic systems. Advantage of cascaded H bridge MLI are the number of possible output voltage levels is more than twice the DC sources $(n = 2s + 1)$, simple voltage balancing and no extra clamping diodes or voltage balancing capacitors are necessary. The separate DC sources are required for each of the H bridges is major disadvantage of the topology which increases cost of the inverter [30].

2.8. Switching devices

There is a large variety of power semiconductors that function as switching devices in a converter such as metal oxide semiconductor field effect transistors (MOSFETs), insulated gate bipolar transistors (IGBTs), gate turn-off thyristors (GTOs), and integrated gate commutated thyristors (IGCTs). IGBTs were introduced on the market in 1988. Nowadays, they have become especially important for the “mass markets” of mains powered systems and equipment with a medium or high switching performance. With recent advances in semiconductor technology, IGBTs of a rating up till 6.5 kV with DC current ratings up to 3.6 kA are commercially available today. The selection of semiconductor devices is always a compromise between controllability and dynamic requirements of the generator system on the one hand, and moderate losses on the other hand. In the DFIG based wind turbine, the IGBTs are clearly the dominating semiconductor devices used in various converter topologies. They offer switch-on and switch-off capability and thus provide full controllability at a wide range of switching frequencies.

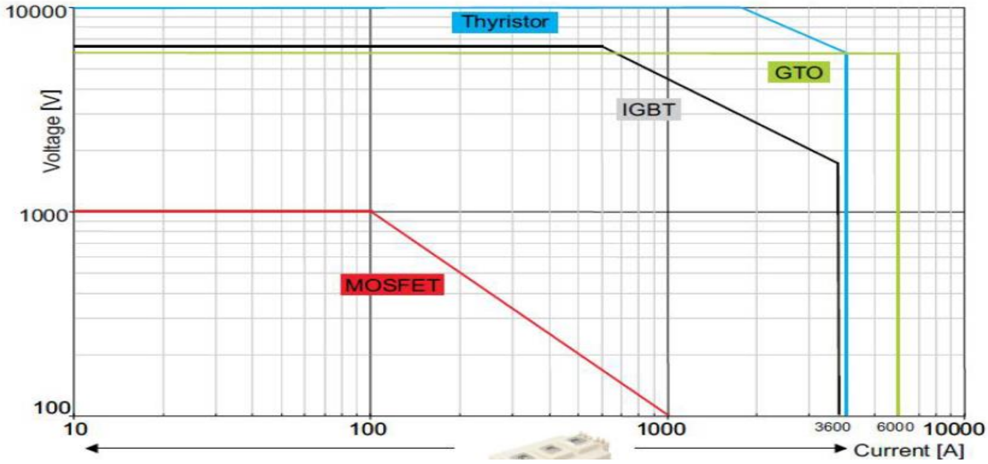

Figure 2-4: Switching devices [31]

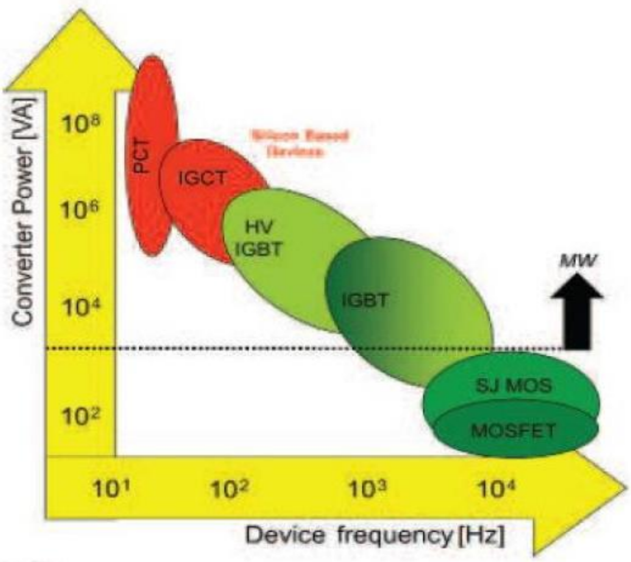

Figure 2-5: switching frequency ranges for various power semiconductors [32]

As shown in Figure 2-5, the upper limit of the frequency range is determined by the semiconductor switching losses and is approximately at 5 kHz for power applications. The lower limit is due to the increased harmonic generation at low switching frequencies and the corresponding increased filter size. Other switching devices like GTOs or IGCTs also offer switch-off capability, but work at lower switching frequencies. Therefore, in this study, the IGBTs are selected as the switching devices.

2.9. Pulse width modulation techniques

In power electronic converters, the electrical energy from one level of voltage/current/ frequency is converted into another using semiconductor-based electronic switch. The essential characteristic of these types of circuits is that the switches are operated only in one of two states – either ON or OFF.

As the power electronics industry developed, various families of power electronic converters have evolved, often linked by power level, switching devices, and topological origins. Application areas of power converters improved vastly in semiconductor technology, which offer higher voltage and current ratings as well as better switching characteristics. Meanwhile, the main advantages of modern power electronic converters are high efficiency, low weight, small dimensions, fast operation, and high-power densities.

The process of switching the electronic devices in a power electronic converter from one state to another is called 'modulation'. Each family of power converters has preferred modulation strategies associated with it that aim to optimize the circuit operation for the target criteria most appropriate for that family. Parameters such as switching frequency, distortion, losses, harmonic generation, and speed of response are typical of the issues that must be considered when developing modulation strategies for a particular family of converters. The output voltage of power inverter should be a pure sinusoidal waveform with minimum distortion. However, for practical inverters, the output voltage is a series of rectangular waveforms. The major issues for the control of the power inverters are to get suitable modulation methods to control the output rectangular waveforms to synthesize the desired waveforms. Therefore, a modulation control method is required to get a desired fundamental frequency voltage and to eliminate higher-order harmonics as much as possible.

Modulation techniques are used for switching and operating inverters and controlled converters in order to produce output voltages and currents with higher qualities for different types of loads. By using these modulation techniques, the switching electronic device get the desired amplitude and frequency with the desired quality. Broadly, these modulation techniques can be subdivided into two classes [32]: Carrier based modulation and Carrier less modulation. There are many types of carrier-based modulation such as;

1- Sinusoidal pulse width modulation (SPWM)

2- Modified pulse width modulation (MPWM)

3-Random pulse width modulation (RPWM)

4-Third harmonic injection (THIPWM)

5- Space vector modulation (SVM)

Carrier less modulation, such as;

1- Delta modulation (DM)

2- Specific harmonic elimination (SHE)

3- Wavelet modulation (WM).

The main aim of all of these techniques is to enhance the output of the converters in terms of the following reasons. In other words, these various techniques are designed to control the inverter switches in order to shape the output ac voltage and currents to be as close to sine wave as possible. The quality of these techniques can be measured by six factors:

1- The amplitude of the fundamental output voltage,

2- The harmonic content in the converter output,

3- The switching losses,

2.9.1. Sinusoidal pulse width modulation (SPWM)

This modulation is the simplest technique that can be implemented in both two level and multilevel inverters [33]. Basically, in SPWM, two signals - a sinusoidal reference signal and a high frequency carrier signal (triangular signal) are compared to give two states (high or low). The amplitude of the fundamental component of the output voltage of the inverter can be controlled by varying Modulation Index (MI). Modulation Index is defined as the ratio of the magnitude of the reference signal V_r to that of the magnitude of the carrier signal V_{cr}.Thus, by keeping V_{cr} constant and varying V_r, the modulation index can be varied. This conventional pulse-width modulation is the most widely used technique all over the world because of its advantages. Some of the advantages of PWM based switching power converter over the other techniques can be in its easy to implement and control and in its compatibility with almost all the modern digital applications. However it has also some disadvantages that might reduce its volubility in some applications, such as its attenuation of the fundamental frequency amplitude, its THD is reduced by increasing the switching frequency but that will lead to the increase of switching losses; which means greater stresses on the associated switching devices and creation of high-frequency components with high amplitudes.

2.9.2. Modified Pulse width modulation (MPWM)

The main principle of the MPWM is based on the comparisons between two low-frequency modulating signals with a triangular high frequency carrier. The first modulating signal is similar to the fundamental signal of the desired output voltage. The other modulating signal is also similar to the first signal but with a phase shift of 180 electrical degrees. The advantage of the MPWM over the conventional SPWM is in the location of the first harmonic. Where the SPWM is pushing back the harmonics towards the high frequencies by which the first significant sideband of the output voltage spectrum is located in the switching frequency sideband, However the MPWM is able to shift back the first significant harmonic to a frequency equal to twice of the switching frequency. This means that the THD of the MPWM is less than that of the SPWM with the same switching frequency, but the fundamental component is not too high. This method is easy to implement and control, but it has some disadvantages in high switching stresses on the semiconductor devices and also its effect of the harmonic content on the input side is high as well [34].

2.9.3. Random pulse width modulation (RPWM)

Random pulse width modulation technique is basically based on randomizing the frequency of the carrier signal in order to distribute the concentrated energy of the harmonic frequency of the inverter output voltage in a narrow high frequency band. The main purpose and advantage of this technique is to reduce the energy of the harmonics, which in turn will reduce the THD of the inverter output voltage. However, this action will also affect the energy of the fundamental frequency component, i.e. the amplitude of the fundamental frequency component will be reduced as well, which is the main disadvantage of this technique. Also, it has a significant drawback, which is the rapid deterioration of quality of operation at low values of modulation index. Moreover, randomizing the carrier frequency adds an extra switching losses and extra stresses to the semiconductor devices which in turn lead to add more harmonics to the current signal in the input side [34].

2.9.4. Third harmonic injection PWM (THPWM)

By injecting the third harmonic to the three-phase sinusoidal modulating signals, the inverter fundamental frequency voltage can also be increased without causing over modulation. In which, the modulating signal is composed of the fundamental component and the third harmonic component, making the signal somewhat flattened on the top. As a result, the peak fundamental component can be higher than the peak triangular carrier wave which boosts the fundamental voltage.

The injected third harmonic component will not increase the harmonic distortion in the output voltage. Although it appears in each of the inverter terminal voltages, the third-order harmonic voltage does not exist in the line to line voltage. This is because the line to line voltage is given by the difference of the phase voltage relation, where the third-order harmonics in the phase voltage are zero sequence with the same magnitude and phase displacement and thus cancel each other. The main disadvantage of this technique is that there is no defined procedure for determining the proper amount of the added third harmonic component [35].

In this work from different Pulse width modulation techniques space vector pule width modulation can present more detailed. The Space Vector Pulse Width Modulation is a fast, advanced and efficient Pulse width modulation technique among all others for voltage source inverter fed loads with superiority of good DC utilization voltage and less harmonic problems as compared to other techniques. It is a more advanced technique for generating sine wave that provides a higher voltage to the load side with lower total harmonic distortion.

2.9.5. Space vector pulse width modulation (SVM)

The use of SVM based voltage source inverter is suitable for many high-power industrial applications such as wind energy conversion system as SVM shows good utilization of dc link voltage, easier implementation of the system, less switching loss, & also less total harmonic distortion. Consequently, inverter performance improves to a great level as the overall THD becomes reduced. In this thesis a topology of a two-level inverter and three level NPC based on space vector pulse width modulation technique is described.

Sinusoidal pulse width modulation technique is often used for many applications for controlling the inverter. In this thesis space vector pulse width modulation technique is implemented and it is compared with sinusoidal pulse width modulation technique in view of voltage utilization and total harmonic distortion. SVM technique is more popular in these days compared to conventional techniques because of its excellent features such as more efficient use of DC supply voltage, more output voltage than conventional modulation, lower total harmonic distortion and prevent un-necessary switching hence less commutation losses. The objective of SVM technique is to approximate the reference voltage vector using the eight switching patterns. In the implementation of SVM, determination of reference voltage, switching time duration, and switching time of each switch, are vital steps and switching sequence should be such that it gives less switching losses.

CHAPTER THREE

3. METHODOLOGY

3.1. Introduction

In this chapter, a necessary collected data required for this study has been described in the appendix. The study is based on Adama II wind farm which is found in the middle of Ethiopia, about 7 km west of Nazret, and 3.5 km west of Adama I wind power project and its generator and converter data has been collected. To analysis the performance of DFIG WECS, all procedures and mathematical modelling of doubly fed induction generator and grid connected converter with filter using various modulation technique and finally model the system using MATLAB software.

3.2. Steady State Model of the Doubly Fed Induction Machine

In order to set a good basis for understanding of the machine behavior, a brief look at the steady state model is presented below. The steady state model of the induction machine is very useful in testing the performance of the machine in steady sate. The dynamic behavior of the machine will then be developed with this understanding.

The following assumptions are made about the machine so as to allow for it to be modelled in steady state [36];

1. The stator is supplied by balanced and constant three-phase ac signals from the grid, i.e. frequency and voltage amplitude.
2. The rotor is also supplied by balanced and constant three-phase ac signals through the back to back power converters independently from the stator.

The above assumptions are incorporated into the development of the electric models and derivations of the electric equations. The doubly fed induction machine is made of a stator and a rotor each carrying three phase windings which are spatially shifted by 120^0. The rotor is mounted on bearings and separated from the stator by a gap known as the airgap. The two sets of windings are independently supplied and below are the equations of the balanced three-phase currents flowing through the windings [36].

$$i_a = i_m \cos(120^0)$$
$$i_b = i_m \cos(\omega_t - 120^0)$$
$$i_c = i_m \cos(\omega_t + 120^0) \tag{3.1}$$

In the stator, when the windings are supplied by a balanced three-phase voltage at the grid frequency f_s, a stator flux is induced in the air gap and rotates at synchronous speed which is given by [37] and p is the number of pole pairs;

$$n_s = \frac{120 f_s}{p} \tag{3.2}$$

This flux then induces an emf in the rotor windings. The angular frequency of the induced rotor voltages and currents is given by [36];

$$\omega_r = \omega_s - \omega_m \tag{3.3}$$

ω_r is the angular frequency of the voltage that is supplied to the rotor winding externally, ω_m is the machine's electrical angular frequency and is related to the mechanical angular speed Ω_m in [37] as; $\omega_m = p\Omega_m$

The relationship between the stator and rotor angular frequency can now be looked at below;

$$s = \frac{\omega_s - \omega_m}{\omega_s} \tag{3.4}$$

s is the slip of the rotor;

Rotor frequency can also be expressed as;

$$f_r = s f_s \tag{3.5}$$

The machine can be operated in the following three modes and the sign of the slip is determined by the mode in which the machine is operating.

3.2.1. Sub-synchronous speed mode

Figure 3.1 illustrates the case where the rotor magnetic field rotates at a slower speed than the stator magnetic field.

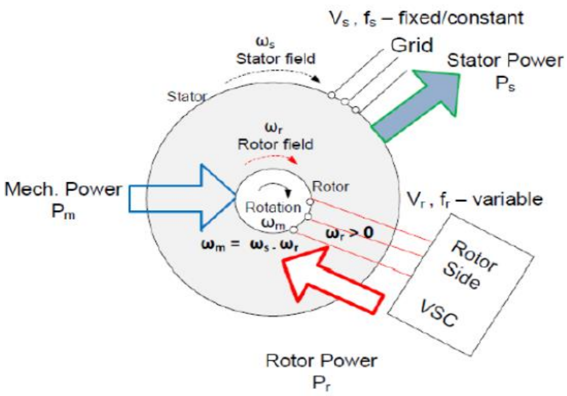

Figure 3-1: Sub-synchronous operating mode of DFIG [38]

The machine is operated in the sub-synchronous mode, i.e., $\omega_m < \omega_s$,

- If and only if its speed is exactly $\omega_m = \omega_s - \omega_r > 0$, $s > 0$ and
- Both the phase sequences of the rotor and stator magnetomotive force are the same and in the positive direction, as referred to as positive phase sequence $(\omega_r > 0)$. This condition takes place during slow wind speeds. In order to extract power from the wind turbine, the following conditions should be satisfied:
- The rotor side VSC shall provide low frequency AC current for the rotor winding.
- The rotor power shall be supplied by the DC bus capacitor via the rotor side voltage source converter (VSC), which tends to decrease the DC bus voltage. The grid side VSC increases/controls this DC voltage and tends to keep it constant. Power is absorbed from the grid via the grid side VSC and delivered to the rotor via the rotor side VSC. During this operating mode, the grid side VSC operates as a rectifier and rotor side VSC operates as an inverter. Hence power is delivered to the grid by the stator.

3.2.2. Super-synchronous speed mode

The super-synchronous speed mode is achieved by having the rotor magnetic field rotate counterclockwise. Figure 3.2 represents this scenario. However, in order to represent the counterclockwise rotation of the rotor, which is analytically equivalent to inverting the direction of the rotor magnetic field.

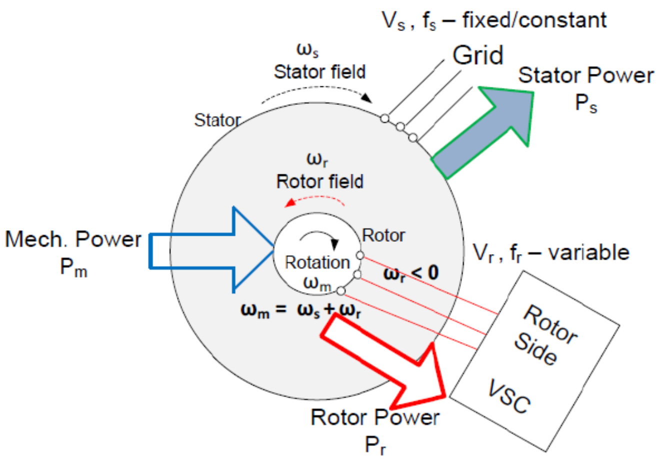

Figure 3-2: Super-synchronous operating mode of DFIG [38]

The machine is operated in the super-synchronous mode, i.e., $\omega_m > \omega_s$,

- if and only if its speed is exactly $\omega_m = \omega_s - (-\omega_r) > 0$, $s < 0$ and
- The phase sequence in the rotor rotates in opposite direction to that of the stator, i.e., negative phase sequence $(\omega_r < 0)$. This condition takes place during the condition

of high wind speeds. The following conditions need to be satisfied in order to extract maximum power from the wind turbine and to reduce mechanical stress:

- The rotor winding delivers AC power to the power grid through the VSCs.
- The rotor power is transmitted to DC bus capacitor, which tends to raise the DC voltage. The grid side VSC reduces/controls this DC-link voltage and tends to keep it constant. Power is extracted from the rotor side VSC and delivered to the grid. During this operating mode, the rotor side VSC operates as a rectifier and the grid side VSC operates as an inverter. Hence power is delivered to the grid directly by the stator and via the VSCs by the rotor.

3.2.3. Synchronous speed mode

The synchronous speed mode is represented by figure 3.3.

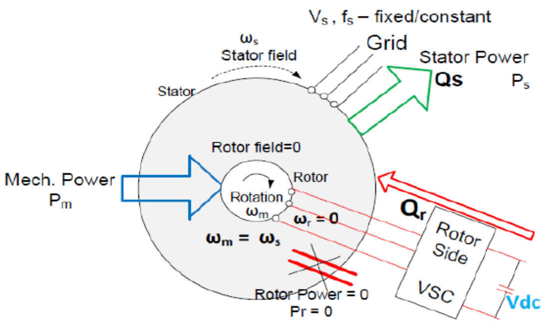

Figure 3-3: Synchronous operating mode of DFIG [38]

The machine is operated in the synchronous speed mode, i.e., $\omega_m = \omega_s$,

- If and only if its speed is exactly $\omega_m = \omega_s - 0 > 0$, $s = 0$ and
- The phase sequence in the rotor is the same as that of the stator, but no rotor magnetomotive force is produced ($\omega_r = 0$). The following conditions are necessary in order to extract power from the wind turbine under this condition:
- The rotor side converter shall provide DC excitation for the rotor, so that the generator operates as a synchronous machine. The rotor side VSC will not provide any kind of AC current/power for the rotor winding. Hence the rotor power is zero ($P_r = 0$).
- A substantial amount of reactive power can still be provided to the grid by the stator. As per the operating modes described above, at any wind speeds a wide range of variable speed operation can be performed to achieve maximum wind power extraction.

3.2.4. Steady-State Equivalent Circuit of DFIG with Rotor-Side Converter

In order to investigate the steady-state performance of the DFIG wind energy system, the rotor-side converter can be modeled by equivalent impedance. Figure 4.1 shows a steady-state equivalent circuit of DFIG WECS. This equivalent circuit is developed by adding the converter equivalent impedance to the SCIG steady-state model. The equivalent impedance of the converter is defined by [39];

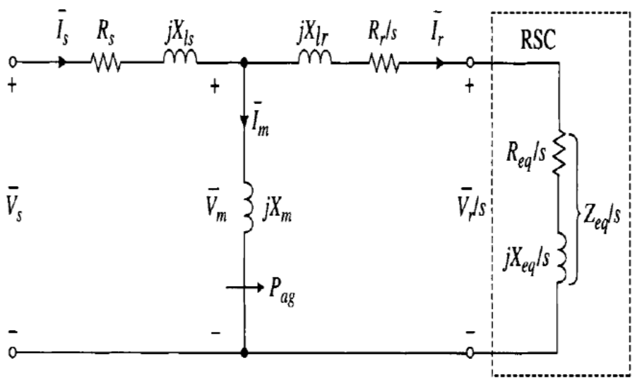

Figure 3-4: Steady-state equivalent circuit of DFIG with the rotor-side converter [39]

$$Z_{eq} = R_{eq} + jX_{eq} = R_{eq} + j\omega_{sl}L_{eq}$$

(3.6)

Where ω_{sl} is the angular slip frequency and L_{eq} is the equivalent inductance of the rotor side converter. The frequency of the rotor current in the actual rotor winding flowing into the converter is the angular slip frequency not the stator frequency ω_s. In order to integrate the converter equivalent impedance into the steady-state model with the stator frequency ω_s. The impedance Z_{eq} should be divided by slip (s). The equivalent impedance referred to the stator side is then given by [39];

$$\frac{Z_{eq}}{s} = \frac{R_{eq}}{s} + \frac{j\omega_{sl}L_{eq}}{s} = \frac{R_{eq}}{s} + j\omega_{sl}L_{eq} \tag{3.7}$$

Where, $\omega_{sl} = s\omega_s$

Assuming that the stator operates at a unity power factor, the air-gap power of the generator can be calculated by

$$P_{ag} = 3(V_S - I_S R_S)I_S \tag{3.8}$$

From the induction machine theory, the air-gap power can also be calculated by

$$P_{ag} = \frac{\omega_S T_m}{P} \tag{3.9}$$

Where T_m is the mechanical torque and P is the number of pole pairs of the generator.

Substituting equation (3.9) into (3.8) yields

$$\frac{\omega_s T_m}{P} = 3(V_s - I_s R_s) I_s \tag{3.10}$$

Solving equation (3.10), we have

$$Is = \frac{V_s \pm \sqrt{V_s^2 - \frac{4R_s T_m \omega_s}{3P}}}{2R_s} \tag{3.11}$$

With the magnitude of the stator current calculated, we can use the equivalent circuit of Figure 3-4 to find the rotor voltage V_r and rotor current I_r. The voltage across the magnetizing branch is given [39] as;

$$\bar{V}_m = \bar{V}_s - \bar{I}s(R_s + j\omega_s L_{ls}) \tag{3.12}$$

Where the stator voltage and current are given by

$$\begin{aligned} \bar{V}_s &= V_s < 0^0 \\ I_s &= I_s < 180^0 \end{aligned} \tag{3.13}$$

The stator voltage and current are 180° out of phase, indicating that the DFIG is in the generating mode and the stator power factor (PF) is unity. The magnetizing current can be determined by [39];

$$\bar{I}m = \frac{\bar{V}_m}{j\omega_s Lm} \tag{3.14}$$

The rotor current is

$$\bar{I}_r = \bar{I}_s - \bar{I}_m \tag{3.15}$$

The rotor voltage can be calculated by [39];

$$\frac{\bar{V}_r}{s} = \bar{V}_m - \bar{I}_r\left(\frac{R_r}{s} + j\omega L_{lr}\right) \qquad (3.16$$

From which

$$\bar{V}_r = s\bar{V}_m - \bar{I}_r(R_r + js\omega_s L_{lr}) \tag{3.17}$$

The rotor voltage and current relate to the equivalent resistance R_{eq} and reactance X_{eq} by

$$\frac{\bar{V}_r/s}{\bar{I}_r} = \frac{R_{eq}}{s} + jX_{eq}/s \tag{3.18}$$

Case 1: Equivalent Impedance of Rotor-Side Converter

A 1.5 MW, 690 V, 50 Hz, 1500 rpm DFIG wind energy system. The parameters of the generator are given in Appendix D. The stator power factor is unity. This case study investigates the relationship between the rotor voltage, rotor current, and the equivalent impedance of the rotor-side converter when the DFIG operates at super synchronous, synchronous, and sub synchronous speeds.

In the manufacturer manual named "ABB wind turbine converters: System description and start-up guide: ACS800-67 wind turbine converters", it is mentioned as X_{ls} and X_{lr} are typically about 5% of the X_m. R_s and R_r are typically about 0.5% of the X_m.

Converter Equivalent Impedance at 1800 RPM (Super synchronous Mode):

From Equation (3.11), the rated mechanical torque is calculated [39];

$$T_m = \frac{3P[V_s^2 - (2R_sI_s - V_s)^2]}{4R_s\omega_s} \tag{3.19}$$

In the manufacturer's manual, the rated stator current, I_s is given as 1110A. It has negative sign during generating mode. Thus, Rated Mechanical Torque, T_m can be calculated us:

$$T_m = \frac{3P[V_s^2 - (2R_sI_s - V_s)^2]}{4R_s\omega_s} = \frac{6[\frac{690^2}{3} - \{2*0.006243*1110 - (\frac{690}{\sqrt{3}})\}^2}{4*0.006243*2*50*\pi} = 8.2984kNm \cong 8.3kNm$$

Where, P is number of pole pairs

Using the equivalent circuit of Figure 3-4, the voltage across the magnetizing branch is

$$\bar{V}_m = \bar{V}_s - \bar{I}s(R_s + j\omega_s L_{ls}) \tag{3.20}$$

$$\bar{V}m = \frac{690}{\sqrt{3}} - 1110\angle180^0[0.006243 + (j100*pi*0.0001988)]$$

$$= 411.19\angle9.71^0$$

The magnetizing current is calculated by

$$\bar{I}m = \frac{\bar{V}_m}{j\omega_s Lm} \tag{3.21}$$

$$\bar{I}m = \frac{411.19\angle9.71^0}{(100*pi*0.003976)\angle90^0}$$

$$= 329.10\angle-80.29^0 A$$

From equation (3.15) the rotor current is

$$-1110-[55.522-j324.5A]$$
$$=1290.852\angle -15.56^{0}$$

The rotor voltage from equation (3.17) is calculated us:

$$-0.2[405.30+j69.333[-[9-1165.522+j324.5)*\{0.011014-j0.2*100pi*0.0001988\}]$$
$$=78.99\angle 23.92$$

Where

$$s=\frac{\omega s-\omega r}{\omega s}=-0.2$$

The equivalent impedance for the rotor-side converter is given by

$$\overline{Z}eq=\frac{\overline{V}r}{\overline{I}r} \tag{3.22}$$

$$\overline{Z_{eq}}=\frac{78.99<23.92^{0}}{1209.852<-15.56^{0}}=0.065<39.48^{0}=0.05+j0.04133\Omega$$

From which

$$\mathrm{Re}\,q=0.05\Omega$$
$$Xeq=0.04133\Omega$$

Following the same procedure, the calculated rotor voltage, rotor current, and the equivalent impedance of the rotor-side converter in the subsynchronous mode (1250rpm) and synchronous (1500rpm) are summarized in Table 3-1. For the convenience of comparison, the calculated results for the DFIG operating in supersynchronous (1800).

Table 3-1: Equivalent impedance of RSC in 1.5 MW/690 V DFIG WECS (PF = 1)

Rotor speed (rpm)	1250	1500	1800
T_m (kNm)	-4.091	-5.8909	-8.3
Slip	0.1667	0	-0.2
V_r (V)	$76.89<5.84^0$	$9.59<-21.89^0$	$79.02<23.91^0$
I_r (A)	$664.72<25.73^0$	$865.78<-21.89^0$	$1209.852<-15.56^0$
R_{eq} (Ω)	-0.0986	-0.0111	0.05
X_{eq} (Ω)	-0.0606	0	0.042

From the above table 3.1 analysis, it can be remarked that at synchronous speed, the rotor equivalent reactance is zero implying due to DC excitation, DC current flowing into the rotor circuit by the rotor side converter.

Case 2: Steady-State Analysis of DFIG in WECS with stator power factor (PF = 1)

To facilitate the steady-state analysis of the DFIG wind energy system, the equivalent circuit of Figure3-4 can be rearranged as shown in Figure 3-5, where the mechanical power P_m, the rotor power P_r , and stator and rotor winding losses, $P_{cu,s}$ and $P_{cu,r}$ can be easily calculated by a general equation of $P = 3I^2R$. The rotor power P_r is the power transferred from or to the rotor-side converter.

Neglecting the rotational losses P_{rot} of the turbine, the power transferred or dissipated in the generator can be calculated by [39];

$$\begin{aligned} P_m &= 3I_r^2(R_r + \mathrm{R}_{eq})(1-s)/s \\ \mathrm{P_r} &= 3I_r^2\,\mathrm{R}_{eq} \\ P_{cu,r} &= 3I_r^2\,\mathrm{R}_r \\ P_{cu,s} &= 3I_r^2\,\mathrm{R}_s \\ \mathrm{P}_s &= 3V_s I_s \cos\phi_s \end{aligned} \tag{3.23}$$

Where P_s is the stator power and ϕ_s is the stator power factor angle. The power delivered to the grid, P_g, is the sum of the stator and rotor power, given by

$$P_g = \begin{cases} P_r + P_s \\ P_s - P_r \end{cases} \tag{3.24}$$

During a super synchronous operating mode, equivalent resistance Req of the rotor-side converter has a positive value and the rotor power P_r is positive. This implies that the resistance Req consumes power similar to the winding resistances Rr and Rs. In reality, the rotor power P_r is not dissipated in Req, but transferred from the rotor to the grid through the converters. In the sub synchronous mode, Req has a negative value and the rotor power P_r is also negative. This indicates that the rotor circuit receives power from the grid through the converters.

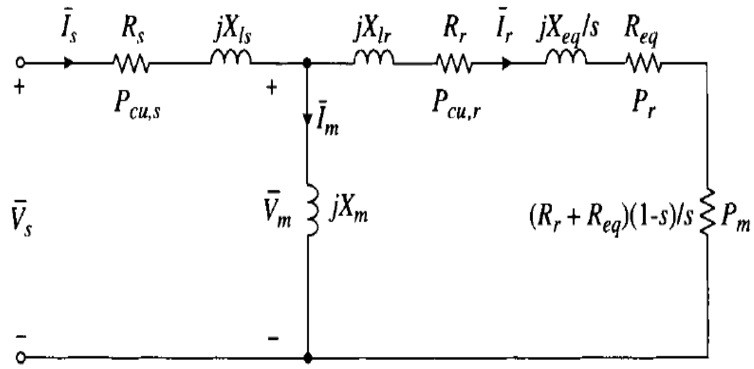

Figure 3-5: Steady-state equivalent circuit of DFIG WECS [39]

This case is a continuation of previous case 1, where the equivalent impedance for the rotor-side converter of a 1.5 MW/690 V DFIG wind energy system was developed. The steady-state operation of the system at the super synchronous, synchronous, and sub synchronous speeds is analyzed below.

DFIG Operation at Rotor Speed of 1800 Rpm (Super synchronous Mode):

At the rated rotor speed of 1800 rpm, the rotor current calculated in Case 1 is 1209.86A, from which the mechanical power of the generator is calculated:

$$P_m = T_m.\omega_m \tag{3.25}$$

$$8294.4*1800*2*pi/60$$
$$=1.56MW$$

The rotor power is

$$P_r = 3I_r{}^2R_{eq} \tag{3.26}$$

$$3*1209.86^2*0.05$$
$$= 219.56KW$$

The rotor and stator winding losses are

$$P_{cu,r} = 3I_r{}^2R_r \tag{3.27}$$

$$3*1209.86^2*0.011074$$
$$= 48.63KW$$

$$P_{cu,s} = 3I_s{}^2R_s \tag{3.28}$$

$$3*1110^2*0.006243$$
$$= 23.1KW$$

The stator active power is

$$P_s = 3V_sI_s\cos\phi_s \tag{3.29}$$

$$3*690/\sqrt{3}*11108\cos(180^0)$$
$$= -1326.58KW$$

Where the stator power factor angle ϕ_s is 180° since the DFIG operates in the generating mode with a unity power factor. The total power delivered to the grid at Super synchronous Mode is

$$|P_g| = |P_s| + |P_r| \tag{3.30}$$

$$1326.58 + 219.56$$
$$= 1546.14KW$$

The difference between P_m and P_g is the losses on the stator and rotor windings, that is,

$$|P_{loss}| = P_{cu,r} + P_{cu,s} = |P_m| - |P_g| \tag{3.31}$$

$$48.63 + 23.1$$
$$= 71.73KW$$
$$Pm - Pg$$
$$1609.16 - 1546.14$$
$$= 63.02KW$$

There is small deviation between two cases

$$71.73 - 63..02 = 8.71KW$$

The efficiency of the DFIG is

$$\eta = \frac{P_g}{P_m} \tag{3.32}$$

$$\frac{1546.14}{1609.16} = 96.1\%$$

DFIG Operation at the Synchronous and Sub synchronous Speeds following the same procedure presented above. Table 3.2 summarizes the calculation results. It is noted that in the sub synchronous mode the rotor circuit receives power from the grid through the converters.

Table 3-2: Three operating modes of 1.5 MW/690V DFIG WECS (PF = 1)

Operating mode	Subsynchronous operation (1250rpm)	Synchronous operation (1500rpm)	Supersynchronous operation (1800rpm)
Slip	0.1667	0	-0.2(rated)
T_m(kNm)	4.091	5.8909	8.3

$R_{eq}(\Omega)$	-0.0986	-0.0111	0.05
$X_{eq}(\Omega)$	-0.0606	0	0.042
$I_s(A)$	533.2434	765.1	1110
$P_m(kW)$	535.512	925.34	1609.16
$P_r(kW)$	130.7	24.961	219.56
$P_s(kW)$	637.29	914.383	1326.58
$P_g(kW)$	506.59	889.422	1546.14
$\eta(\%)$	94.6	96.12	96.1

3.3. Dynamic modelling of the doubly fed Induction machine

Nowadays doubly fed induction machine has been widely used in wind power generation system. These types of machines can be used resolutely as a generator or a motor. Though demands as motor is less because of its mechanical wear at the slip rings but they have gained their prominence for generator application in wind and hydro power plant because of its obvious adoptability capacity and nature of controllability of power. Before proceeding to the control and analysis of the machine for its performance, a model of the machine in space vector form using Clarke and park transformations is very important to facilitate the simulation and implementation of control schemes in wind power systems. The Induction Generator space-vector model is generally composed of three sets of equations: voltage equations, flux linkage equations, and motion equation [40].

3.3.1. State space model in the a-b-c natural frame

The Doubly-fed induction machine (DFIM) is provided with laminated stator and rotor cores with uniform slots in which three-phase winding are placed as shown in Figure 3-4. Usually, the rotor winding is connected to copper slip-rings. Brushes on the stator collect the rotor currents from the rotor-side static power converter. For the time being, the resistances of slip-ring-brush system are lumped into rotor phase resistances, and the converter is replaced by controllable voltage source. The three-phase model of a DFIG can be described as:

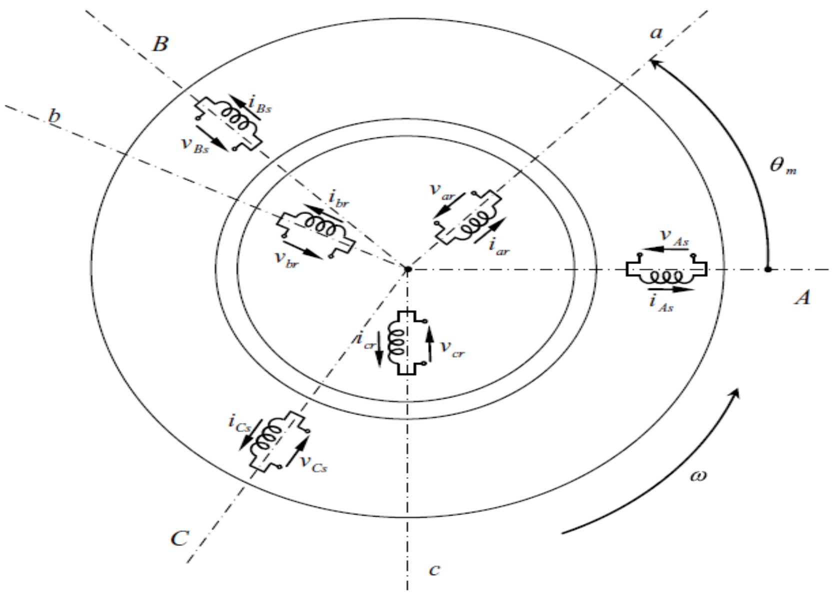

Figure 3-6: Three-phase stator and rotor windings of the DFIG [40]

From the ideal model above, the following equations showing the relationship of the instantaneous stator voltages to the currents and fluxes of the machine are obtained [41].

$$\begin{cases} V_{As}(t) = R_s i_{As}(t) + \dfrac{d\psi_{As}(t)}{dt} \\ V_{Bs}(t) = R_s i_{Bs}(t) + \dfrac{d\psi_{Bs}(t)}{dt} \\ V_{Cs}(t) = R_s i_{Cs}(t) + \dfrac{d\psi_{Cs}(t)}{dt} \end{cases} \tag{3.33}$$

The rotor electric relationships can be described by the equations below [40]

$$\begin{cases} V_{ar}(t) = R_r i_{ar}(t) + \dfrac{d\psi_{ar}(t)}{dt} \\ V_{br}(t) = R_s i_{br}(t) + \dfrac{d\psi_{br}(t)}{dt} \\ V_{cr}(t) = R_s i_{cr}(t) + \dfrac{d\psi_{cr}(t)}{dt} \end{cases} \tag{3.34}$$

From the above equations, a complete representation of the DFIG is shown below in figure 3-5 [40];

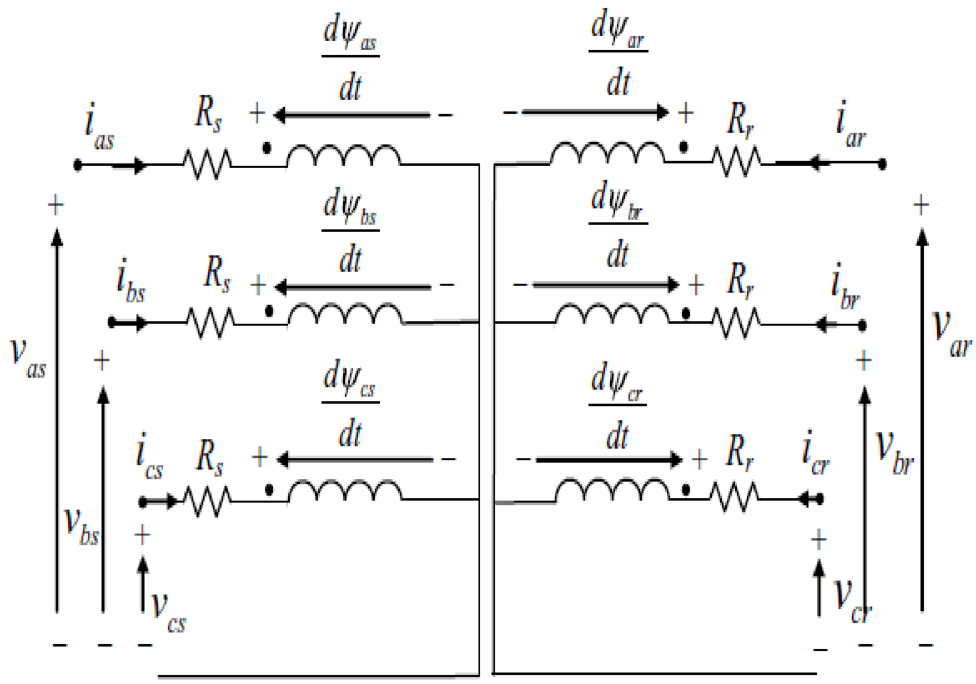

Figure 3-7: Equivalent circuit of the DFIG [40]

Where $i_{As}(t)$, $i_{Bs}(t)$, $i_{Cs}(t)$ are the three-phase stator currents; $i_{Ar}(t), i_{Br}(t), i_{Cr}(t)$ are the three-phase rotor currents; $V_{As}(t)$, $V_{Bs}(t)$, $V_{Cs}(t)$ are the three-phase stator voltages; $V_{ar}(t), V_{br}(t), V_{cr}(t)$ are the three-phase rotor voltages; $\Psi_{As}(t)$, $\Psi_{Bs}(t)$, $\Psi_{Cs}(t)$ are the three-phase stator flux linkages; Ψ_{ar}, Ψ_{br}, Ψ_{cr} are the three-phase rotor flux linkages; R_s and R_r are stator and rotor resistances. The stator equations are represented in the stator natural frame, and the rotor equations are described in the rotor natural frame.

3.3.2. Clarke transformation

Considering a symmetrical three phase induction machine with stationary a-phase, b-phase and c-phase axes are placed at 120◦ angle to each other, as shown in Figure 3-8. The main aim of a Clarke transformation is to transform the three-phase stationary frame variables into a two-phase stationary frame variables α - β, and vice versa. Any three-phase voltage or current χ in a-b-c components can be converted into α - β components via Clarke transformation and can be represented in the matrix as;

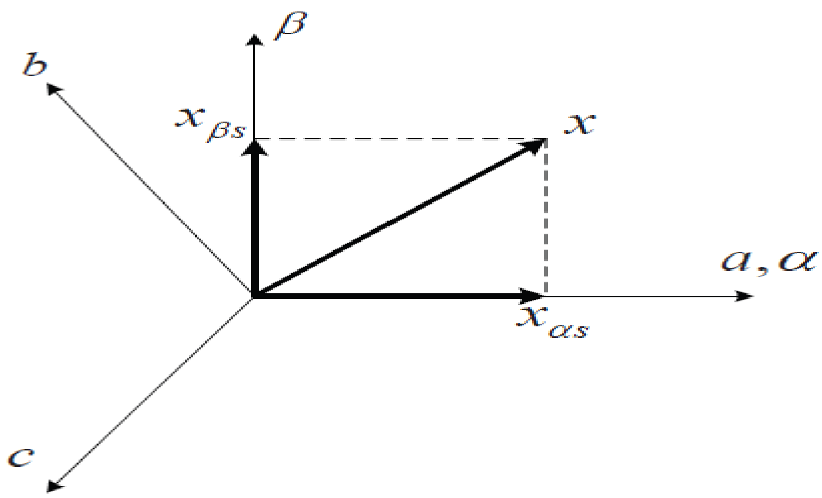

Figure 3-8: a-b-c to α - β axes transformation of stationary frame

$$\begin{bmatrix} \chi_\alpha \\ \chi_\beta \\ \chi_o \end{bmatrix} = Tc \begin{bmatrix} X_a \\ X_b \\ X_c \end{bmatrix} \tag{3.35}$$

Where T_c is the transformation matrix of Clarke transformation.

$$T_c = \frac{2}{3}\begin{bmatrix} 0 & -\frac{1}{2} & -\frac{1}{2} \\ 0 & \frac{\sqrt{3}}{2} & -\frac{\sqrt{3}}{2} \\ \frac{1}{2} & \frac{1}{2} & \frac{1}{2} \end{bmatrix} \tag{3.36}$$

χ_0 is the zero-sequence component, which equals to zero for symmetrical three phase variable. The reference transformation of stator and rotor currents are described as follows, and the reference frames can be seen in Figure 3-8.

$$\begin{bmatrix} i_{\alpha s} \\ i_{\beta s} \\ i_{os} \end{bmatrix} = Tc \begin{bmatrix} i_{as} \\ i_{bs} \\ ics \end{bmatrix} \tag{3.37}$$

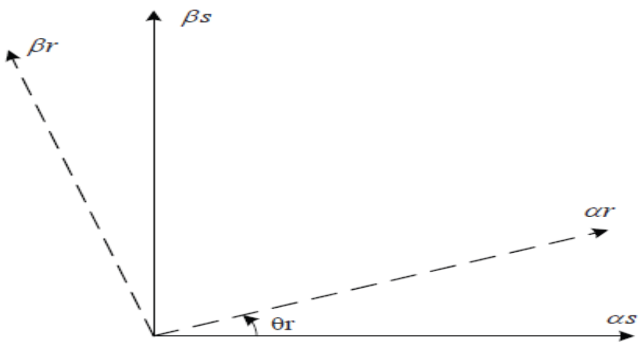

Figure 3-9: Transformation between stationary reference frames for stator and rotor

$$\begin{bmatrix} i_{\alpha r} \\ i_{\beta r} \\ i_{or} \end{bmatrix} = Tc \begin{bmatrix} i_{ar} \\ i_{br} \\ i_{cr} \end{bmatrix} \tag{3.38}$$

Where i_{0s} and i_{0r} are the zero sequence components of stator and rotor current, respectively. The rotor variables represented in the rotor stationary reference frame can be referred to the stator stationary reference frame by a transformation matrix T_r, as shown in Figure 3-9.

$$\begin{bmatrix} i^{s}{}_{\alpha r} \\ i^{s}{}_{\beta r} \end{bmatrix} = T_r \begin{bmatrix} i_{\alpha r} \\ i_{\beta r} \end{bmatrix} \tag{3.39}$$

Where

$$T_r = \begin{bmatrix} \cos\theta r & -\sin\theta r \\ \sin\theta r & \cos\theta r \end{bmatrix} \tag{3.40}$$

3.3.3. Park transformation

A Park transformation transfer variable from a two-phase stator stationary reference frame to a two-phase rotating reference frame through the rotation transformation matrix $T_p(\theta)$, as shown in Figure 3-10.

$$\begin{bmatrix} i_{ds} \\ i_{qs} \end{bmatrix} = T_{p(\theta)}) \begin{bmatrix} i_{\alpha s} \\ i_{\beta s} \end{bmatrix} \tag{3.41}$$

Where $T_p(\theta)$ is the transformation matrix,

$$T_p(\theta) = \begin{bmatrix} \cos\theta & -\sin\theta \\ \sin\theta & \cos\theta \end{bmatrix} \tag{3.42}$$

where θ is the angle between d-axis and α-axis.

The same transformation in general orthogonal coordinates, rotating at genetic electric speed $\omega = \frac{d\theta}{dt}$, is valid for all currents and flux linkages.

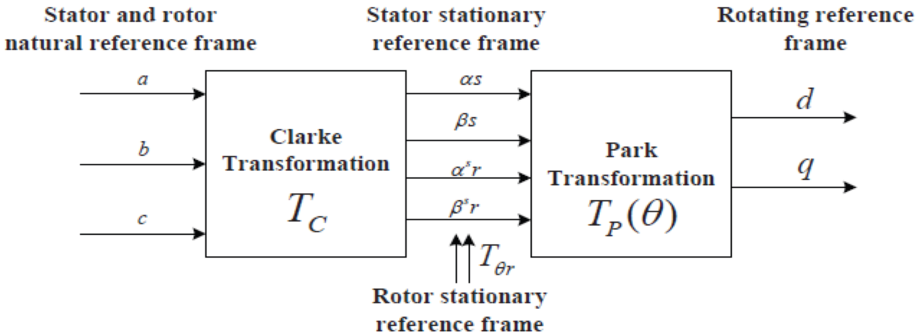

Figure 3-10: Transformation of reference frames

The transformation from three-phase (a-b-c) to two-phase stationary reference frame (α-β) and to a two-phase rotating reference frame (d-q) is summarized in Figure 3-10.

For the design of controllers, the stator and rotor equations should be referred to the same reference frame. The stator equations in the stator stationary reference frame α_s, β_s can be derived from (a-b-c) three-phase model by using Clarke transformation T_c:

$$U_{\alpha S} = R_s i_{\alpha s} + \frac{d\Psi_{\alpha s}}{dt} \quad (3.43)$$

$$U_{\beta s} = R_s i_{\beta s} + \frac{d\Psi_{\beta s}}{dt} \quad (3.44)$$

where $i_{\alpha s}$ and $i_{\beta s}$ are α-axis and β-axis stator currents, respectively; $\Psi_{\alpha s}$ and $\Psi_{\beta s}$ are α-axis and β-axis stator-flux linkages, respectively.

The state variables in equation below are aligned with the rotating d-q frame by substituting the Park transformation matrix $T_p(\theta)$ into equation (3.43) and equation (3.44), after the computations of each variables from stationary to rotating reference frame, the equations can be written as:

$$U_{ds} = R_s i_{ds} + \frac{d\psi_{ds}}{dt} - \omega\psi_{qs} \quad (3.45)$$

$$U_{qs} = R_s i_{qs} + \frac{d\psi_{qs}}{dt} - \omega\psi_{ds} \quad (3.46)$$

where all the variables are in rotating reference frame, ω is the rotation speed. The last terms in equation (3.45) and (3.46) can be defined as speed emf due to rotation of the axes, that is, when ω = 0, the equations revert to stationary form.

Since the rotor actually moves at speed ω_r against to the stator, the d-q axes fixed on the rotor move at a speed $\omega - \omega_r$. Therefore, in d-q frame, the rotor equations represented in the d-q frame as:

$$U_{dr} = R_r i_{dr} + \frac{d\psi_{dr}}{dt} - \left(\omega - \omega_r\right)\psi_{qr} \quad (3.47)$$

$$U_{qr} = R_r i_{qr} + \frac{d\psi_{qr}}{dt} + (\omega - \omega_r)\psi_{dr} \quad (3.48)$$

Figure 3.9 shows the equivalent circuits for d-q dynamic model that satisfy equations (3.45)-(3.48), in which$U_s = U_{ds} + jU_{qs}$, i_s, i_r, Ψ_s, Ψ_r can be presented in the same form, $L_s = L_{ls} + L_m$ is the stator self-inductance;

$L_r = L_{lr} + L_m$ is the rotor self-inductance; L_{ls} is the stator leakage inductance; L_{lr} is the rotor leakage inductance; L_m is the mutual inductance. The flux linkage expressions in terms of the currents can be obtained as follows:

$$\begin{cases} \psi_{ds} = L_s i_{ds} + L_m i_{dr} \\ \psi_{qs} = L_s i_{qs} + L_m i_{qr} \end{cases} \tag{3.49}$$

$$\begin{cases} \psi_{dr} = L_r i_{dr} + L_m i_{ds} \\ \psi_{qr} = L_r i_{qr} + L_m i_{qs} \end{cases} \tag{3.50}$$

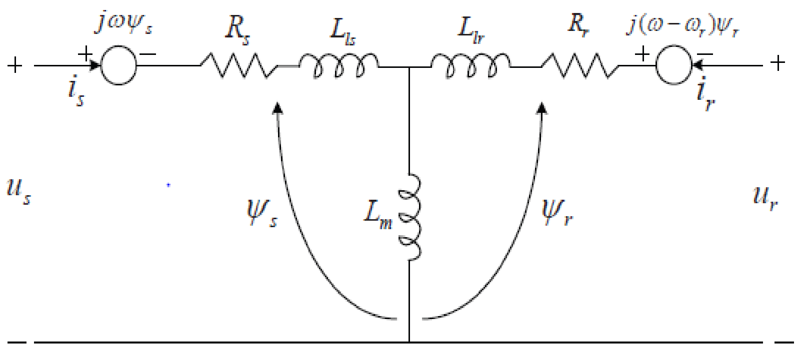

Figure 3-11: Dynamic d-q equivalent circuits of machine

The electromagnetic torque equation is represented as:

$$T_e = \psi_{ds} i_{qs} - \psi_{qs} i_{ds} = L_m (i_{qs} i_{dr}) = \psi_{dr} i_{qr} - \psi_{qr} i_{dr} \tag{3.51}$$

The active and reactive stator power equations are presented as:

$$P_s = \frac{3}{2}(U_{ds} i_{ds} + U_{qs} i_{qs}) \tag{3.52}$$

$$Q_s = \frac{3}{2}(U_{qs} i_{qs} - U_{ds} i_{qs}) \tag{3.53}$$

With the mathematical equations for computing the active and reactive powers of rotor side

$$P_r = \frac{3}{2}(U_{dr} i_{dr} + u_{qr} i_{qr}) \tag{3.54}$$

$$Q_r = \frac{3}{2}(U_{qr} i_{qr} + u_{dr} i_{qr}) \tag{3.55}$$

3.4. Back-to-Back voltage source converter (VSC) models

The AC/DC/AC converter model based on two-level voltage source converter topology is widely used in renewable energy systems. The converter provides good abilities to transmit the generated power from wind turbine to grid effectively, respond quickly and accurately. Nowadays, some kinds of power electronics semiconductors are popular [42], including Power MOS Field Effect Transistors (Power MOSFETs), Gate Turn Off Thyristors (GTOs), and Insulated Gate Bipolar Transistors (IGBTs). The AC/DC/AC converter usually utilizes IGBT devices in the power industry. The IGBT combines the advantages of the MOSFETs and the advantages of the bipolar transistors by using an isolated gate FET as the control unit, and utilizing a bipolar power transistor as the switch to transmit high currents. The IGBT is used in medium to high power applications. The control unit in an IGBT is much simpler than a GTO, and the switch frequency can be up to 40 kHz. High power IGBT modules may consist of many devices in parallel and can have very high current handling capabilities.

Figure 3-12 shows a typical a back-to-back converter consists of two converters, i.e., the left-hand side is an AC/DC converter (machine-side converter) and the right-hand side is a DC/AC converter (also called grid side converter) with a DC-link capacitor which is placed between the two converters. The main objective for the grid-side converter is to keep the variation of the DC-link voltage small. With the control of the generator-side converter, it is possible to control the torque, the speed of a DFIG as well as its active and reactive power at the stator terminals.

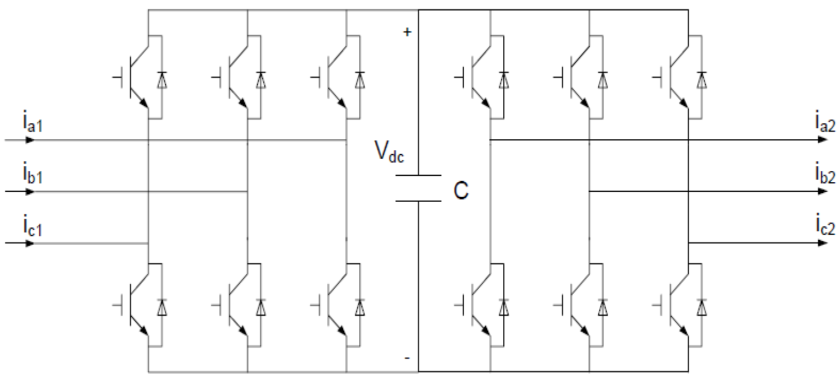

Figure 3-12: A typical AC/DC/AC converter

Actually, these two types of converters are very similar to each other, the fundamental control theories of these two types of converter are almost the same.

3.4.1. Three-phase voltage source converter model

The main power circuit of a three-phase PWM voltage source converter is shown in Figure 3-13. It consists of six IGBTs with six antiparallel freewheeling diodes, three-phase AC input inductances and resistances, and a DC output capacitor.

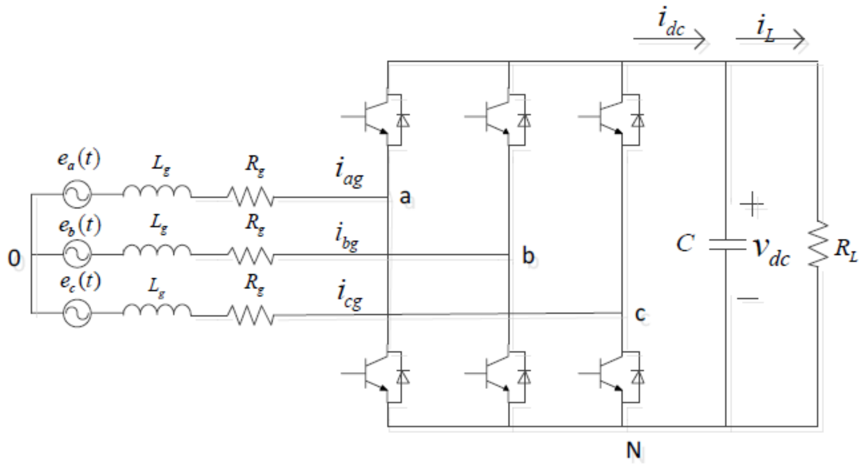

Figure 3-13: Configuration of a PWM voltage source rectifier [43]

Here, $e_a(t)$, $e_b(t)$ and $e_c(t)$ are the three-phase voltage sources as a feed node in the power system, R_g, is the AC side resistances, and L_g, is the AC side inductances. Here, C, is the DC-link capacitor, R_L, is the load resistance, while, i_{ag}, i_{bg} and i_{cg}, are the input currents of a three-phase PWM rectifier. Here also, i_{dc}, is the DC-link current, i_L, is the load current, and V_{dc}, is the DC-link voltage.

First, let us define $S_k(\ k = a, b, c\ )$ as the switch function of phase, k. Based on the principle that any two switches in the same leg cannot be on at the same time, one can write the following definition [44]:

$$S_K = \begin{cases} 1 \text{ The upper IGBT is ON} \\ 0 \text{ The upper IGBT is OFF} \end{cases} \tag{3.56}$$

Applying Kirchhoff's laws to the circuit of Figure 3-13, the instantaneous values of the currents can be obtained, and written as following:

$$\begin{cases} L_g \dfrac{di_{ag}}{dt} = e_a - R_a i_{ag} \\ L_g \dfrac{di_{bg}}{dt} = e_b - R_b i_{bg} \\ L_g \dfrac{di_{cg}}{dt} = e_c - R_c i_{cg} \end{cases} \tag{3.57}$$

Here, $V_{(a,o)}$, $V_{(b,o)}$, and $V_{(c,o)}$, are the voltages from the AC side of the PWM rectifier to the power neutral point 0, and can be obtained by using the following equations:

$$\begin{cases} V_{(a,o)} = V_{(a,N)} + V_{(N,o)} \\ V_{(b,o)} = V_{(b,N)} + V_{(N,o)} \\ V_{(c,o)} = V_{(c,N)} + V_{(N,o)} \end{cases} \tag{3.58}$$

Where, $V_{(N,O)}$, is the voltage from point N to point 0. Here, $V_{(a,N)}$, $V_{(b,N)}$ and $V_{(c,N)}$, are the voltages from the AC side of the PWM rectifier to point N.

For a balanced three-phase system, one can write:

$$V(a,o) + V(b,o) + V(c,o) = 0 \tag{3.59}$$

Substituting from equation (3.58) into (3.59), the following equation can be deduced:

$$V(N,o) = -\frac{V(a,N) + V(b,N) + V(c,N)}{3} \tag{3.60}$$

Considering phaseA, when the upper IGBT is on and lower IGBT is off, one can derive; $S_a = 1$ and $V_{(a,N)} = V_{dc}$. Similarity, when the upper IGBT is off and lower IGBT is on, one can also write; $S_a = 0$ and $V_{(a,N)} = 0$. Therefore, based on the above characteristic, $V_{(a,N)}$, $V_{(b,N)}$, $V_{(c,N)}$ and $V_{(N,O)}$, can be rewritten as follows:

$$\begin{cases} V_{(a,N)} = S_a V_{dc} \\ V_{(b,N)} = S_b V_{dc} \\ V_{(c,N)} = S_c V_{dc} \end{cases} \tag{3.61}$$

Substituting from equations (3.58) and (3.61) into equation (3.57), the following set of equations can be derived:

$$\begin{cases} L_g \dfrac{di_{ag}}{dt} = e_a - R_a i_{ag} - V_{dc}(S_a - \dfrac{1}{3}\sum\limits_{k=abc} S_k) \\ L_g \dfrac{di_{bg}}{dt} = e_b - R_b i_{bg} - V_{dc}(S_b - \dfrac{1}{3}\sum\limits_{k=abc} S_k) \\ L_g \dfrac{di_{cg}}{dt} = e_c - R_c i_{cg} - V_{dc}(S_c - \dfrac{1}{3}\sum\limits_{k=abc} S_k) \end{cases} \tag{3.62}$$

Under the assumption that the power switch resistances of a balanced three-phase system could be neglected, the power relationship between the AC side and DC side is given as follows:

$$\sum_{k=a,b,c} i_{kg}(t)V_{kN}(t) = i_{dc}(t)V_{dc} \tag{3.63}$$

By combining equation (3.62) with (3.63), one can write:

$$i_{dc}(t) = i_{ag}(t)S_a + i_{bg}(t)S_b + i_{cg}(t)S_c \tag{3.64}$$

By applying Kirchhoff's laws to the positive node of the DC-link capacitor, one can easily reach the following equations:

$$i_c = i_{dc} - i_L \tag{3.65}$$

$$C\frac{dV_{dc}}{dt} = S_a i_{ag} + S_b i_{bg} + S_c i_{cg} - \frac{V_{dc}}{R_L} \tag{3.67}$$

3.4.2. Two level grid-side converter model

The grid side system is composed by the grid side converter feed by the DC link, the grid side filter, and the grid voltage. Since, the wind turbine and machine side converter are not the main issue for this thesis, the modified layout of the modeling system can be seen in below.

Figure 3-14 shows a typical DC/AC inverter, there are six IGBTs in this inverter, which inverts a DC power input into a controlled three phase AC power output based on the control signals applied on the gate circuits of IGBTs.

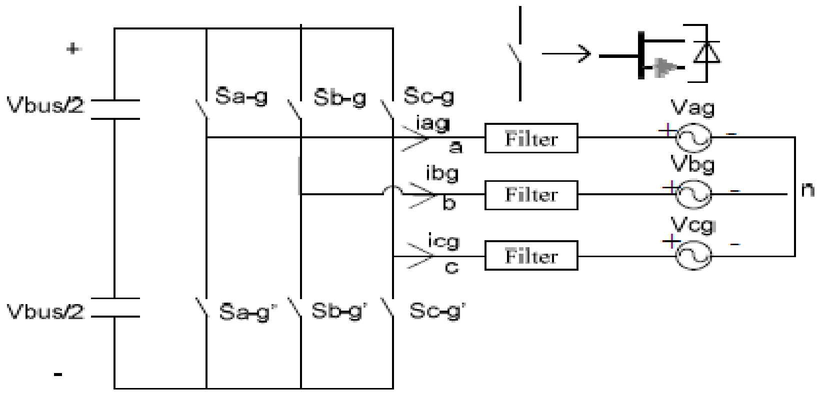

Figure 3-14: Simplified converter, filter, and grid model [45]

The control signals used for the gate circuits of IGBT are usually generated through a PWM signal generator. To model the grid side inverters, the following elements are considered.

- The grid side converter is modeled with ideal bidirectional switches. It converts voltage and currents from DC to AC, while the exchange of power can be in both directions from AC to DC (rectifier mode) and from DC to AC (inverter mode).

The ideal switch normally is created by a controlled semiconductor with a diode in antiparallel to allow the flow of current in both directions.

- The grid side filter is normally composed of inductances and capacitor, which are the link between each output phase of the converter and the grid voltage. When a high filter requirement is needed, each inductance can be by one capacitor and one more inductance (LCL).
- The grid voltage is normally supplied through a transformer. This AC voltage is supposed to be balanced and sinusoidal under normal operation conditions. The effect of the transformer or grid impedances is neglected.

There are eight different combinations of output voltages, according to the eight permitted switching states of S_{a-g}, S_{b-g}, and S_{c-g} given in Table 3.3 below. The circuit satisfies the Kirchhoff's Voltage Law and the Kirchhoff's current Law, both of the switches in the same leg cannot be turned ON at the same time, as it would short the input voltage violating the Kirchhoff's Voltage Law. Thus, the nature of the two switches in the same leg is complementary.

$$\begin{cases} S_{a\text{-}g} + S'_{a\text{-}g} = 1 \\ S_{b\text{-}g} + S'_{b\text{-}g} = 1 \\ S_{c\text{-}g} + S'_{c\text{-}g} = 1 \end{cases} \tag{3.66}$$

Different output voltages can be distinguished in a converter, for instance, the voltages referenced to the zero point of the DC bus:

$$V_{jo} = V_{bus} S_{j\text{-}g} \tag{3.67}$$

Where $S_{j-g} \in \{0,1\}$ and j = a, b, c

Thus, by different combinations of S_{a-g}, S_{b-g}, and S_{c-g} it is possible to create AC output voltages with a fundamental component of different amplitude and frequency. The converter provides two possible voltage levels at each phase.

The converter output voltages referred to the neutral point of the grid three-phase system (n). As Figure 3-15 illustrates, the following voltage relationships are true:

$$\begin{cases} V_{an} = V_{ao} - V_{no} \\ V_{bn} = V_{bo} - V_{no} \\ V_{cn} = V_{co} - V_{no} \end{cases} \tag{3.68}$$

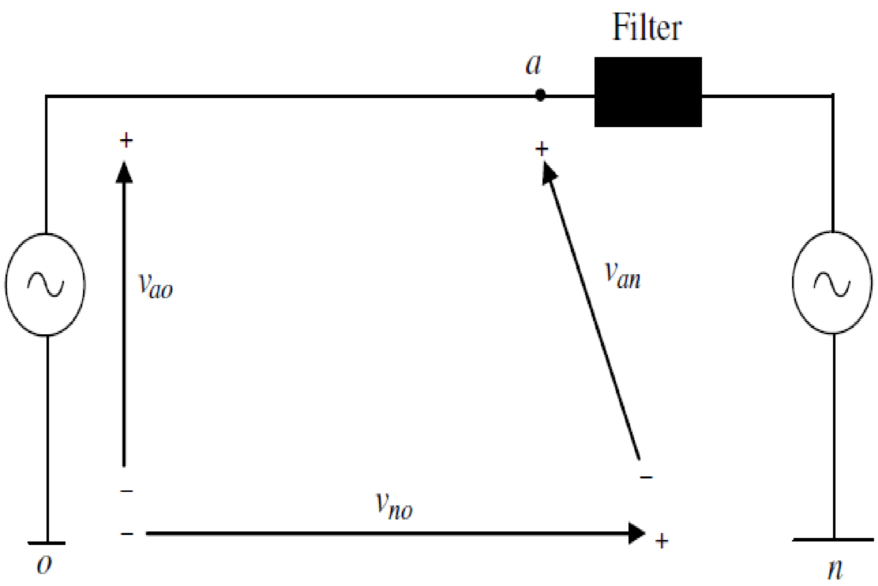

Figure 3-15: Simplified equivalent single-phase grid circuit (a phase).

The voltage between the neutral point (n) and the negative point of the DC bus (o) is needed, so assuming holds, the grid AC voltage is supposed to be balanced and sinusoidal under normal operation conditions.

$$V_{an} + V_{bn} + V_{cn} = 0 \tag{3.69}$$

Substituting expression (3.66) into (3.67) yields

$$V_{no} = \frac{1}{3}(V_{ao} + V_{bo} + V_{co}) \tag{3.70}$$

Substituting expression (3.68) into equation (3.66)

$$V_{an} = \frac{2}{3}V_{ao} - \frac{1}{3}(V_{b0} + V_{co}) \tag{3.71}$$

$$V_{bn} = \frac{2}{3}V_{bo} - \frac{1}{3}(V_{a0} + V_{co}) \tag{3.72}$$

$$V_{cn} = \frac{2}{3}V_{co} - \frac{1}{3}(V_{b0} + V_{ao}) \tag{3.73}$$

Or more simply, directly from the order commands,

$$\begin{cases} V_{an} = \frac{V_{bus}}{3}(2S_{a\text{-}g} - S_{b\text{-}g} - S_{c\text{-}g}) \\ V_{bn} = \frac{V_{bus}}{3}(2S_{b\text{-}g} - S_{a\text{-}g} - S_{c\text{-}g}) \\ V_{cn} = \frac{V_{bus}}{3}(2S_{c\text{-}g} - S_{a\text{-}g} - S_{b\text{-}g}) \end{cases} \tag{3.74}$$

Table 3-3: Different Output Voltage Combinations of grid side converter

S_{a-g}	S_{b-g}	S_{c-g}	V_{ao}	V_{bo}	V_{co}	V_{an}	V_{bn}	V_{cn}
0	0	0	0	0	0	0	0	0
0	0	1	0	0	V_{bus}	$-\frac{V_{bus}}{3}$	$-\frac{V_{bus}}{3}$	$2\frac{V_{bus}}{3}$
0	1	0	0	V_{bus}	0	$-\frac{V_{bus}}{3}$	$2\frac{V_{bus}}{3}$	$-\frac{V_{bus}}{3}$
0	1	1	0	V_{bus}	V_{bus}	$-2\frac{V_{bus}}{3}$	$\frac{V_{bus}}{3}$	$\frac{V_{bus}}{3}$
1	0	0	V_{bus}	0	0	$2\frac{V_{bus}}{3}$	$-\frac{V_{bus}}{3}$	$-\frac{V_{bus}}{3}$
1	0	1	V_{bus}	0	V_{bus}	$\frac{V_{bus}}{3}$	$-2\frac{V_{bus}}{3}$	$\frac{V_{bus}}{3}$
1	1	0	V_{bus}	V_{bus}	0	$\frac{V_{bus}}{3}$	$\frac{V_{bus}}{3}$	$-2\frac{V_{bus}}{3}$
1	1	1	V_{bus}	V_{bus}	V_{bus}	0	0	0

Current on the DC side can be calculated as a function of phase currents and switches configuration:

$$i_{dc} = S_{a\text{-}g} i_{ag} + S_{b\text{-}g} i_{bg} + S_{c\text{-}g} i_{cg} \tag{3.75}$$

3.4.3. Grid side two-level converter model with LCL-filter

The PWM output voltage of the grid-connected inverters contains abundant of switching harmonic components, which results in the harmonic current injecting into the grid. Therefore, a filter is required to interface between the inverter bridge and the power grid. Figure 3-16 show the topology of a three-phase grid-connected inverter with LCL filter, where switches Q1–Q6 compose the three-phase legs, and three sets of inductors L1, L2, and capacitor C compose the three-phase LCL filter.

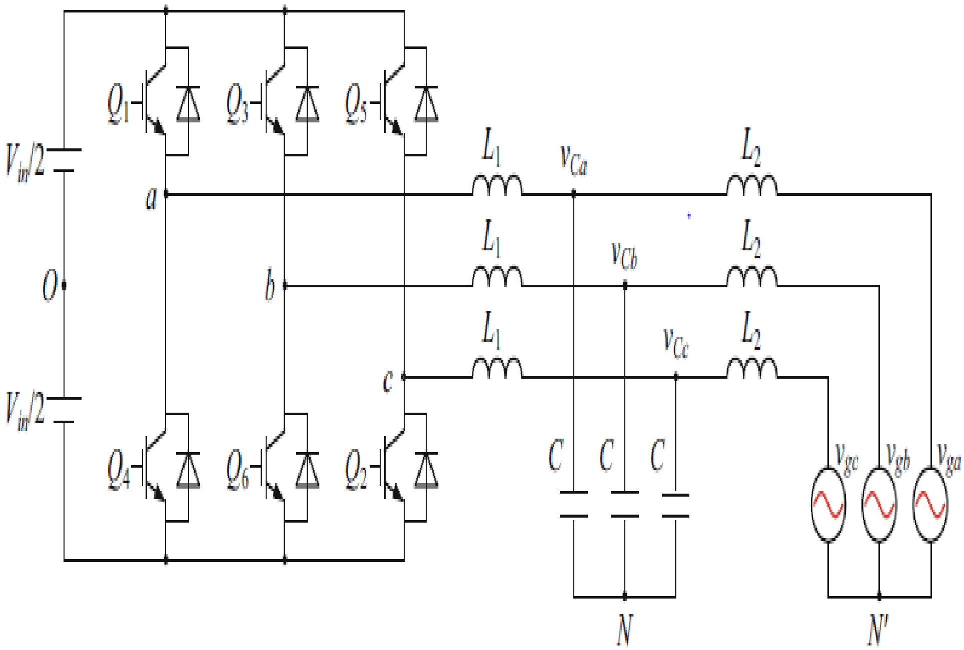

Figure 3-16: Grid connected converter with LCL filter [44]

From figure 3-16 V_{ao}, V_{bo}, and V_{co} are the three inverter output voltages with respect to midpoint O; i_{a1}, i_{b1}, and i_{c1} are the inverter-side current; V_{Ca}, V_{Cb}, $V_{Cc}$and i_{ca}, i_{cb}, and i_{Cc} are the filter capacitor voltage and current, respectively; i_{a2}, i_{b2}, and i_{c2} is the grid-side current. From Figure 3-16, inverter output voltages and grid voltage can be expressed as

$$\begin{cases} V_{ao} = L_1 \dfrac{di_{a1}}{dt} + V_{ca} \\ V_{bo} = L_1 \dfrac{di_{b1}}{dt} + V_{cb} \\ V_{co} = L_1 \dfrac{di_{c1}}{dt} + V_{Cc} \end{cases} \tag{3.76}$$

$$\begin{cases} V_{ga} = L_2 \dfrac{di_{a2}}{dt} - V_{ca} \\ V_{gb} = L_2 \dfrac{di_{b2}}{dt} - V_{cb} \\ V_{gc} = L_2 \dfrac{di_{c2}}{dt} + V_{Cc} \end{cases} \tag{3.77}$$

From the above equations the inverter and grid currents can be expressed as

$$\begin{cases} \dfrac{di_{a1}}{dt} = \dfrac{1}{L_1}\left[V_{ao} - V_{ca}\right] \\ \dfrac{di_{b1}}{dt} = \dfrac{1}{L_1}\left[V_{bo} - V_{cb}\right] \\ \dfrac{di_{c1}}{dt} = \dfrac{1}{L_1}\left[V_{co} - V_{Cc}\right] \end{cases} \tag{3.78}$$

$$\begin{cases} \dfrac{di_{a2}}{dt} = \dfrac{1}{L_2}\left[V_{ga} + V_{ca}\right] \\ \dfrac{di_{b2}}{dt} = \dfrac{1}{L_2}\left[V_{gb} + V_{cb}\right] \\ \dfrac{di_{c2}}{dt} = \dfrac{1}{L_1}\left[V_{gc} + V_{Cc}\right] \end{cases} \tag{3.79}$$

The three-phase filter capacitor voltages can be expressed as

$$V_{ca} = \frac{1}{c}\int i_{ca} dt \tag{3.80}$$

$$V_{cb} = \frac{1}{c}\int i_{cb} dt \tag{3.81}$$

$$V_{Cc} = \frac{1}{c}\int i_{Cc} dt \tag{3.82}$$

Where, $i_{ca} = i_{a1} - i_{a2}$, $i_{cb} = i_{b1} - i_{b2}$, $i_{Cc} = i_{c1} - i_{c2}$

Thus, the model of the grid side system is represented in Figure 3-17.

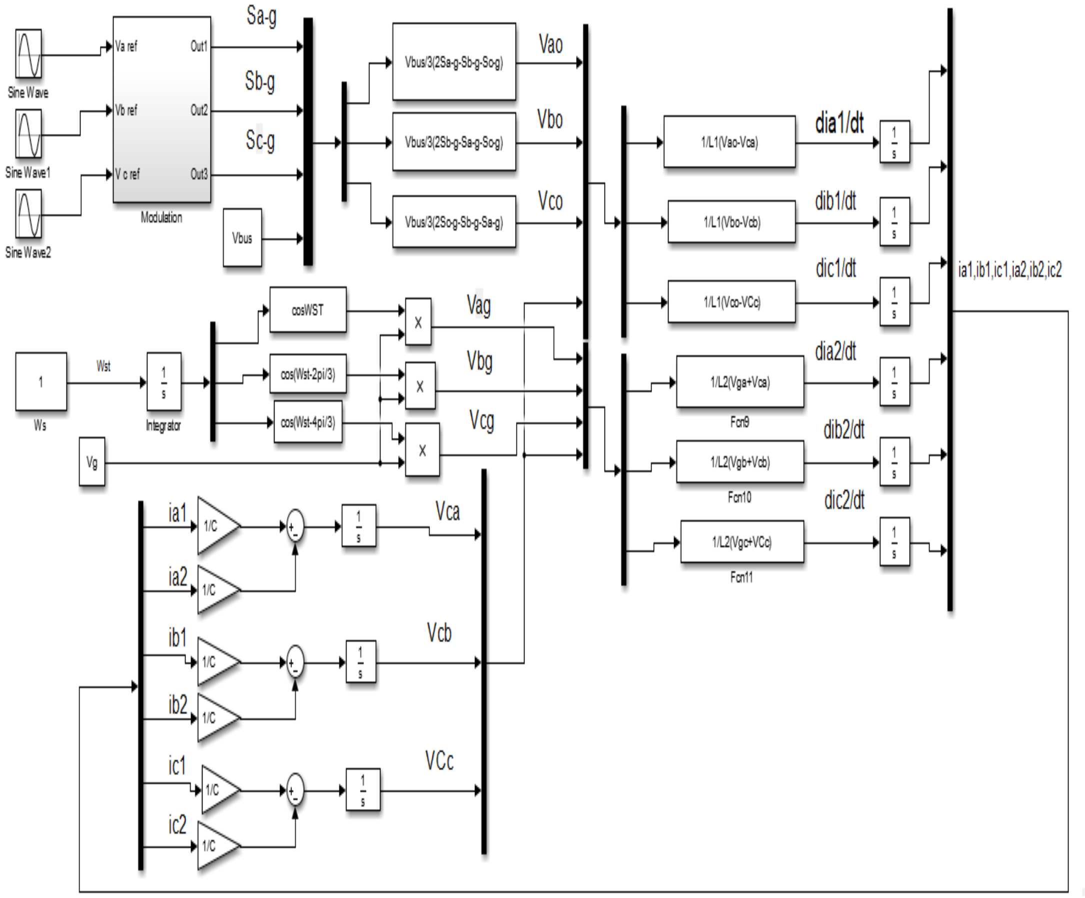

Figure 3-17: SIMULNK model of grid side converter, filter and grid voltage

3.4.4. DC Link Model

The DC part of the back-to-back converter is typically called the DC link, it tries to maintain a constant voltage in its terminals. It is the linkage between the grid side and machine side converters. Figure 3-18 shows a possible simplified model of a DC link. It is composed of a capacitor in parallel with a high resistance. In order to derive the model of the DC link, the DC bus voltage must be calculated.

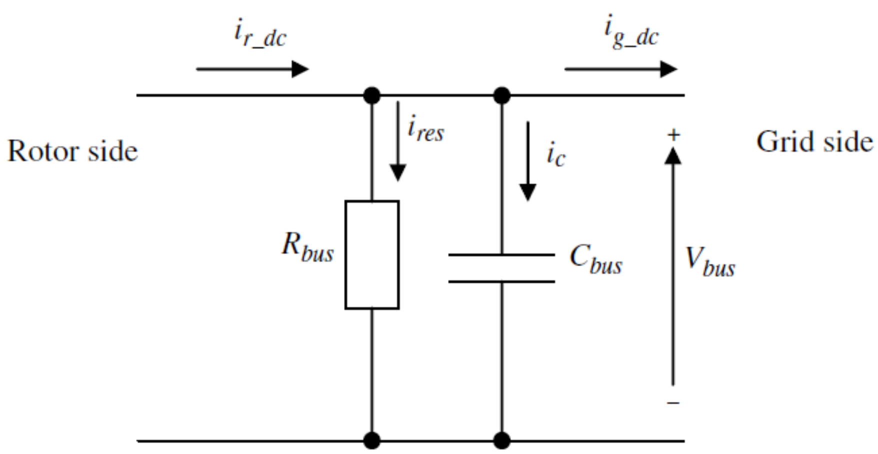

Figure 3-18: DC link system.

$$V_{bus} = \frac{1}{C_{bus}} \int i_c dt \tag{3.83}$$

The current through the capacitor can be found as

$$i_c = i_{r\text{-}dc} + i_{g\text{-}dc} - I_{res} \tag{3.84}$$

where

I_{res} = current through the resistance (A)

i_{g-dc} = DC current flowing from the DC link to the grid (A)

i_{r-dc} = DC current flowing from the rotor to the DC link (A)

The current through the resistance is $i_{res} = \frac{V_{bus}}{R_{bus}}$

On the other hand, the DC currents can be calculated as follows from the output AC currents of the converters:

$$i_{g\text{-}dc} = S_{a\text{-}g} i_{a2} + S_{b\text{-}g} i_{b2} + S_{c\text{-}g} i_{c2} \tag{3.85}$$

$$i_{r\text{-}dc} = S_{a\text{-}r} i_{a1} + S_{b\text{-}r} i_{b1} + S_{c\text{-}r} i_{c1} \tag{3.86}$$

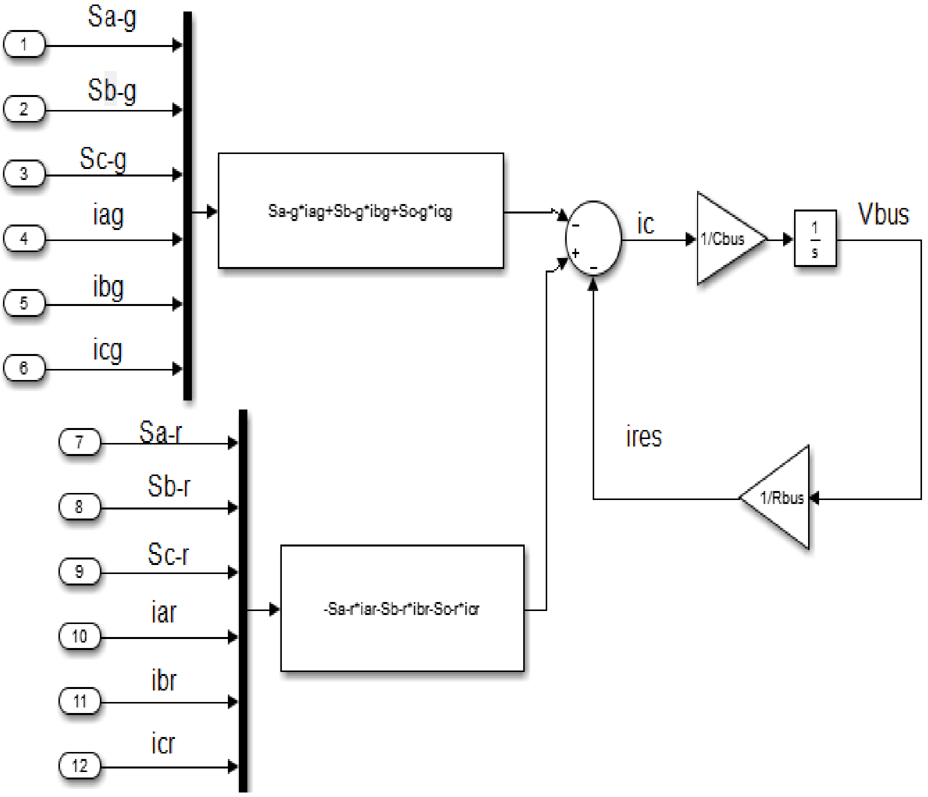

Figure 3-19: DC link model.

The current through the capacitor in figure 3-19 depends on the switching function of the grid side converter, rotor side converter DC output current and grid side AC output current.

3.5. Filter design

3.5.1. Design of LCL Filter

The first step is the design of the filter inductance. This should be designed carefully because a large inductance value attenuate higher frequencies and limit current ripples. On the other hand, it brings many disadvantages, such as greater inductor size, a decrease in the converter's dynamics and a smaller range of operation. The operation range is limited through the maximum reachable voltage drop across the inductance. It is dependent indirectly on the DC-link voltage. Thus, in order to achieve a large current through the inductance, a high DC-link voltage level or low input inductance is needed.

An AC-DC-AC converter is connected to the grid through an AC filter (e.g., L or LCL). The inductance allows current control by the voltage drop on itself. In order to obtain better reduction of current ripples, the LCL filter can be selected. The advantage of using an L filter as opposed to an LCL filter is the simple design concept. The disadvantage is that, for a specific amount of attenuation required at a switching frequency, a larger overall value of inductance is needed. The larger the inductance, the greater is the voltage drop across it thereby requiring a larger converter output voltage and the required minimum DC-link voltage.

For the LCL filter to fulfill the grid codes, or recommended practices for example, IEEE 519-1992 a variety of optimization criteria exist, such as minimum costs, low losses, smaller weight. However, it is a complex task because many parameters influence this process, for example, DC-link voltage level, phase current, modulation method, modulation index, switching frequency, fundamental frequency, and resonance frequency.

The purpose of the AC filter is to reduce higher harmonics distortion caused by switching process of a power electronics devices. The filtration capability of LCL filters are significantly higher than simple L filter. LCL filters allows to reduce volume of the filter and assures more effective higher harmonics current filtration in respect to L filter.

In the industrial grids, L-filters are usually applied. In applications where grid current harmonics should be attenuated significantly to achieve compliance with the grid standards, LCL-filters are more advantageous than L-filters.

The main advantages of LCL filter are

- Low grid current distortion,
- Reactive power production.

The input inductor has to be designed carefully because low inductance will give a high current ripple and will make the design more depending on the line impedance. The high value of inductance will give a low current ripple, but simultaneously reduce the operation range of the rectifier. The voltage drop across the inductance has influence for the line current. This voltage drop is controlled by the input voltage of the PWM rectifier but maximal value is limited by the DC-link voltage. Consequently, a high current (high power) through the inductance requires either a high DC-link voltage or a low inductance (low impedance).

The starting point for the design procedure is usually assumptions of the converter's rated power, grid, and switching frequencies. Those parameters allow the calculation of base values (base impedance Z_b, capacitance C_b and inductance L_b) as calculated in the next sections. The aim of the input filters (L_1) is to reduce the high harmonics at the grid side. The filter design procedure should take into account following aspects: power rating, line and switching frequency.

Step-1: Base impedance Z_b , base capacitance C_b and inductance L_b are defined by equation (3.87) and (3.89) in order to represent the filter components as percentages of the base values.

$$Z_b = \frac{V_n{}^2}{P_n}$$
$$L_b = \frac{Z_b}{\omega_n}$$
$$C_b = \frac{1}{\omega_n Z_b} \tag{3.87}$$

where $\omega_n = 2\pi * 5$, V_n^2 is nominal line to line converter voltage.

$$Z_b = \frac{690^2}{1.5*10^6} = 0.3174\Omega; L_b = \frac{0.3174}{100\pi} = 0.001\text{H} = 1\text{mH}; C_b = \frac{1}{100\pi * 0.3174} = 0.010029\text{F} = 10029\mu\text{F}$$

Step-2: Converter side inductance L_1 calculation

In manufacturer manual, the rating of the Grid side converter is given as 365 kVA. Taking the grid side voltage, assuming unity power factor and neglecting converter losses, then the Nominal RMS converter phase current (I_n) can be calculated as:

$$I_n = \frac{P_n}{\sqrt{3}V_n} = \frac{365*10^3}{\sqrt{3}*690} = 305\text{A} \tag{3.88}$$

Based on the IEEE 519-1992 [46] limitations and the assumption that peak ripples must not exceed 10% of the grid current. In this way,

$$I_{P\text{-}P,rip} = \sqrt{2} * 10\% * 305 = 43.1335 \tag{3.89}$$

By assuming the RMS converter voltage is equivalent with the grid rms voltage:

$$L_1 = \frac{mU_{dc}}{8\sqrt{3}f_{sw}I_{p\text{-}p,rip}},$$

$$m = \frac{2\sqrt{2}U_p}{U_{dc}} \tag{3.90}$$

Where f_{sw} is a switching frequency and 5kHz is used in this study

U_p is the converter RMS voltage = 690/√3

$$L_1 = \frac{2\sqrt{2}U_p}{8\sqrt{3}f_{sw}I_{p\text{-}p,ripp}} = \frac{2*\sqrt{2}*690/\sqrt{3}}{8\sqrt{3}*5000*0.1*305\sqrt{2}} = 0.21769mH$$

On the other hand, the maximum ripple current $I_{max,rip}$ can be selected between 10 and 25 % of nominal phase current I_n and the limit of L_1 that has to be fulfilled is given [47] as;

$$L_c \geq \frac{U_{dc}}{6f_{sw}\, I_{max,rip}} \gg \frac{Ug\sqrt{2}}{6f_{sw}\, I_{max,rip}} \tag{3.91}$$

In this regard, by assuming that $I_{max,rip} = 0.20(20\%)$, Then maximum converter side ripple current can be calculated as:

$$I_{max},_{rip} = \sqrt{2} * 0.20 * 305 = 86.27A$$

Accordingly,

$$L_c \geq \frac{690 * \sqrt{2}}{6 * 5000 * 86.27} = 0.21769mH$$

This value is used in this study for converter side filter.

Step-3: Filter capacitance (C) calculation

The filter capacitance should be less than 5 % of the base capacitance C_b [46]. For this study, if the assumption of the 4 %, i.e, the filter capacitance can be derived from:

$$C_{ref} = 0.04C_b$$

$$C = C_{ref} C_b = C_{ref} \frac{1}{\omega_n Z_b} = 0.04 \frac{1}{100\pi * 0.3174} = 0.000401F = 401\mu F \tag{3.92}$$

Step-4: Grid side inductance L_2 calculation

The main objective of a grid side filter is to damp the current harmonics injected to the grid. Typically, the converter-side inductance L_1 is larger than the grid-side inductance L_2 in order to attenuate most of the current ripple. In this case, a split factor r, given by
[48];

$$r_a = \frac{L_2}{L_1} \tag{3.93}$$

The ripple attenuation is described as:

$$\frac{I_g(h_{sw})}{I_p(h_{sw})} = \frac{1}{\left|1 + r(1 - 4\pi^2) L_c C f^2{}_{sw}\right|} \tag{3.93}$$

where $I_{g(h_{sw})}$ is the grid higher harmonics current and $I_{p(h_{sw})}$ is the converter higher harmonics current.

The split factor can be calculated as:

$$r_a = \left| \frac{1 - H_A}{H_A (1 - L_1 C \omega_{sw}{}^2} \right| \tag{3.94}$$

where, H_A is the harmonics attenuation of the phase current. The voltage disturbances given by IEEE 519-1992 is 5 % for the THD and below 3 % for each individual frequency. Moreover, according to IEEE 519-1992 and EN 50160 the THD factor can be calculated as:

$$THD_{ind} = \sqrt{\sum_{h=2}^{40} u^2(h)} * 100\%$$
$$THD_{IEEE} = \sqrt{\sum_{h=2}^{50} u^2(h)} * 100\% \tag{3.95}$$

In this study, $H_A = 0.05$ has been chosen. Then, r_a, can be found as:

$$r_a = \left| \frac{1 - 0.05}{0.05(1 - 0.000377 * 401 * 10^{-6} * [2\pi * 5000]^2} \right| = 0.1282$$

Then

$$L_2 = r_a L_1 = 0.1282 * 0.2177$$
$$= 0.0279mH$$

3.5. Three-level neutral point clamped grid side voltage source converter model

Multilevel voltage source converter topologies allow the handling of high power with standard components (semiconductors and drivers) and smaller filters, enabling operation to higher voltage levels. This is achieved by arranging a higher number of switches than in the classical two-level converters, configuring more complicated converter topologies. In general, the increased number of switching devices provides extra degrees of freedom, which are also used to improve the performance and quality of the output power and voltage. The trend of using voltage source converters (VSCs) with increasing converter output voltage and power, the restriction of the classical two-level converter imposed by the voltage rating of the semiconductors and the need to use series connected semiconductors, has led to the development of multilevel topologies. Although the most suitable multilevel VSC topologies for the doubly-fed induction generator-based wind turbine is the three-level neutral point clamped converter (3L-NPC).

The three-level neutral point clamped multilevel converter (Figure 3-20) is a VSC from the family of diode clamped multilevel converters. It generates output phase voltage waveforms (V_{ao}, V_{bo}, V_{co}) comprising three switching levels of amplitude $\left(0, {}^{V_{bus}}/_{2}, V_{bus}\right)$. These voltages are created on the AC side by switching the controlled switches $\left(S_{a1}, S'_{a1}, S_{a2}, S'_{a2}, S_{b1}, S'_{b1}, S_{b2}, S'_{b2}, S_{c1}, S'_{c1}, S_{c2}, S'_{c2}\right)$ connecting the DC bus to the AC output. The DC bus is created by two DC sources ($C_1$and C_2 capacitors in practical cases), providing a neutral point Z. This topology connects clamping diode $\left(D_a, D'_a, D_b, D'_b, D_c, D'_c,\right)$ from the neutral point to each arm (a, b, c) to achieve the medium voltage level ${}^{V_{bus}}/_{2}$.

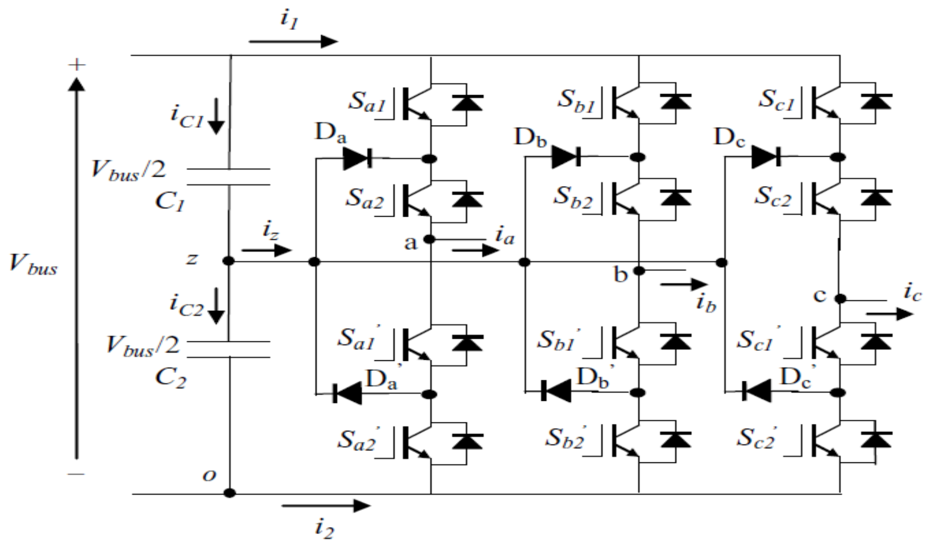

Figure 3-20: Three-level-NPC VSC topology

To perform a bidirectional flow of the current through the converter, each controlled switch is accompanied by one diode in antiparallel, as done in two-level converters. The switching states of the converter at each phase are restricted in such a way that each switch presents its complementary switch. Thus, in order to avoid non permitted states that would result in improper operation of the converter, the following switching status is imposed:

$$\begin{cases} S_{a1} + S'_{a1} = 1 \text{ and } S_{a2} + S'_{a2} = 1 \\ S_{b1} + S'_{b1} = 1 \text{ and } S_{b2} + S'_{b2} = 1 \\ S_{c1} + S'_{c1} = 1 \text{ and } S_{c2} + S'_{c2} = 1 \end{cases} \tag{3.96}$$

The commutation of the converter in normal operation produces a current flow through the neutral point Z, of different characteristics depending on the operating conditions. This current flow makes the DC bus capacitors (C_1 and C_2) charge and discharge. In general, with a finite value of the capacitors, this converter requires a special modulation algorithm that achieves DC bus voltage balance.

The output AC voltages of the converter referred to as the zero of the DC bus can be expressed as follows:

$$\begin{cases} V_{ao} = S_{a1}V_{c1} + S_{a2}V_{c2} \\ V_{bo} = S_{b1}V_{c1} + S_{a2}V_{c2} \\ V_{co} = S_{c1}V_{c1} + S_{a2}V_{c2} \end{cases} \tag{3.97}$$

From expressions (3.71) - (3.72) derived for the two-level converter, but valid also for Three-level-NPC VSC topology, combined with expressions (3.95) - (3.97), the output AC voltage expressions are calculated depending on the order commands:

$$\begin{cases} V_{an} = \frac{V_{c1}}{3}(2S_{a1} - S_{b1} - S_{c1}) + \frac{V_{c2}}{3}(S_{a2} - S_{b2} - S_{c2}) \\ V_{bn} = \frac{V_{c1}}{3}(2S_{b1} - S_{a1} - S_{c1}) + \frac{V_{c2}}{3}(S_{b2} - S_{a2} - S_{c2}) \\ V_{cn} = \frac{V_{c1}}{3}(2S_{c1} - S_{b1} - S_{a1}) + \frac{V_{c2}}{3}(S_{c2} - S_{b2} - S_{a2}) \end{cases} \tag{3.98}$$

The voltages of the capacitors in general are not necessarily exactly equal. On the other hand, the currents flowing through the DC bus capacitors can be calculated first by deducing the currents:

$$i_1 = S_{a1}i_a + S_{d1}i_b + S_{c1}i_c \tag{3.99}$$

$$i_2 = (S_{a2} - S_{a1})i_a + (S_{b2} - S_{b1})i_b + (S_{c2} - S_{c1})i_c \quad (3.100)$$

$$i_Z = -(i_1 + i_2) = -(S_{a1}i_a + S_{b1}i_b + S_{c1}i_c) \quad (3.101)$$

Thus, depending on the state of the switches, the output phase current (i_a, i_b, i_c) determine the current though the capacitors as follows:

$$i_{c1} = -i_1 = -S_{a1}i_a - S_{d1}i_b - S_{c1}i_c \quad (3.102)$$

$$i_{c2} = i_2 = -S_{a2}i_a - S_{b2}i_b - S_{c2}i_c \quad (3.103)$$

The capacitor C1 and C2 are charged and discharged depending on the switching function and the output AC currents.

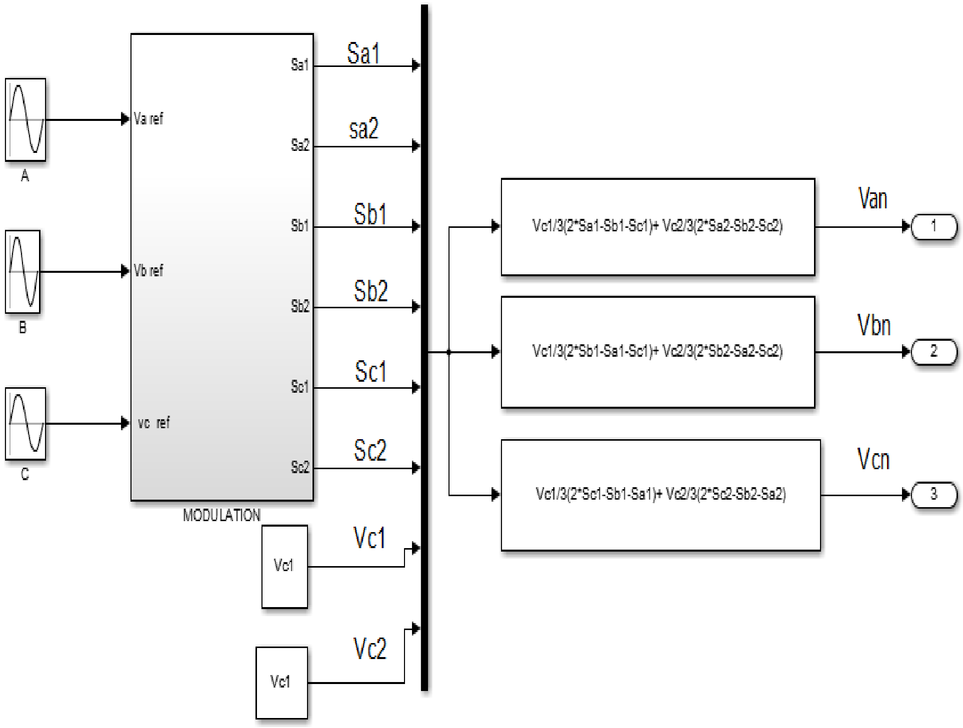

Figure 3-21: SIMULNK model of 3L-NPC VSC

Figure 3-21 shows the schematic block diagram of the three-level neutral point clamped converter model. Modeling of filter and grid for three level NPC voltage source converter are similar to that of two-level voltage source converter as seen in previous section, the only difference is the modeling of the converters.

3.6. **αβ Model of** Grid side converter with LCL-filter

By applying the space vector notation to the abc modeling equations (3.76) and (3.77), it is possible to represent the electric equations in αβ components, the resulting equations yields;

$$V_{\alpha O} = L1\frac{di_{\alpha 1}}{dt} + V_{c\alpha}$$
$$V_{\beta O} = L1\frac{di_{\beta 1}}{dt} + V_{c\beta} \qquad (3.104)$$

$$\begin{cases} V_{\alpha g} = L2\dfrac{di_{\alpha 2}}{dt} - V_{c\alpha} \\ V_{\beta g} = L2\dfrac{di_{\beta 2}}{dt}0 - V_{c\beta} \end{cases} \qquad 3.105)$$

Or in a compact version, referred to a stationary reference frame,

$$\begin{cases} V_o^s = L_1\frac{di_1^s}{dt} + V_c^s \\ V_g^s = L_2\frac{di_2^s}{dt} - V_c^s \end{cases} \qquad (3.106)$$

Where

$$\begin{cases} V_o^s = V_{\alpha O} + jV_{\beta o} \\ V_g^s = V_{\alpha g} + jV_{\beta g} \end{cases} \qquad (3.107)$$

3.7. dq Model

In a similar way, by multiplying Equation (3.99) by $e^{-j\theta}$, from the $\alpha\beta$ expressions the dq expressions are also derived as:

$$\begin{cases} V_{d0} = L_1\dfrac{di_{da1}}{dt} + V_{cd} - j\omega L_1 i_{qa1} \\ V_{q0} = L_1\dfrac{di_{da1}}{dt} + V_{cq} + j\omega L_1 i_{da1} \end{cases}$$

(3.108)

$$\begin{cases} V_{dg} = L_2\dfrac{di_{da2}}{dt} - V_{cd} - j\omega L_2 i_{qa2} \\ V_{qg} = L_2\dfrac{di_{da2}}{dt} - V_{cq} + j\omega L_2 i_{da2} \end{cases} \qquad (3.109)$$

These last two expressions are the dq equations of the electric system, referred to a reference frame dq rotating at speed ω. In order to decouple and further simplify the system, typically the synchronous angular speed ω_a is chosen equal to the angular speed of the grid voltage ω_s, and the d axis of the rotating frame is aligned with the grid voltage space vector V_g^a. This choice corresponds to one of the most important requirements, in order to perform the vector control technique. The super index of the space vectors is omitted, but both reference frames ($\alpha\beta$ and dq) are represented. The resulting dq components of the grid voltage yield:

$$\begin{cases} V_{dg} = \left|V_g{}^a\right| \\ V_{qg} = 0 \end{cases} \tag{3.110}$$

This grid voltage alignment not only slightly simplifies the voltage equations of the system, but also reduces the active and reactive power computations.

$$\begin{cases} P_g = \frac{3}{2}(V_{dg}i_{dg} + V_{qg}i_{qg}) = \frac{3}{2}\left|V_g{}^a i_{dg}\right| \\ Q_g = \frac{3}{2}(V_{qg}i_{dg} - V_{dg}i_{qg}) = -\frac{3}{2}\left|V_g{}^a i_{qg}\right| \end{cases} \tag{3.111}$$

The voltage terms of these last two expressions are constant under ideal conditions; this means that a decoupled relationship between the current dq components and active and reactive powers has been obtained. Thus, the i_{dg}current is responsible for the P_g value, while the i_{qg} current is responsible for the $Q_g$value.

3.8. Grid-side converter control

The inverter is connected to the grid with LCL filter. It is positioned after the DC bus and has two basic functions: the first one is to maintain constant DC bus voltage whatever the magnitude and direction of power flow through it, second to maintain a stable power factor at the connection point to the power grid. The basic control principles of the grid side converters are implemented by measure abc voltages of the grid and transformed form three phase to two phases in the dq reference frame. In this section, a vector control-based schema is studied. This control technique is widely extended among the control strategies for grid connected converters. It provides good performance characteristics with reasonably simple implementation requirements. The vector control technique follows the philosophy of representing the system that is going to be controlled-in our case the grid side system-in a space vector form represented, reasonably good decoupled control of currents and power is achieved.

3.8.1. Grid voltage-oriented vector control

The vector control method is based on a synchronously rotating, stator flux-oriented d-q reference frame, which means that the d-axis is aligned with the vector of the grid voltage and the q component is zero. The grid side converter is in charge of controlling part of the power flow of the doubly fed induction generator (DFIG). The power generated by the wind turbine is partially delivered though the rotor of the DFIG. This power flow that goes through the rotor flows also through the DC link capacitor and finally is transmitted by the converter to the grid. The block diagram of the grid side system, together with a schematic of its control block diagram, is given in Figure 3-22. In this section two-level voltage source converter (VSC) topology is presented. Generally, from a vector control point of view, using three-level-NPC or two-level converter topology the same procedure is followed [49]. In order to keep DC bus voltage and the reactive power of the gird constant and at the required rang, as illustrated in figure 3-22, currents and voltages of the grid $(i_{ag,} i_{bg,} i_{cg})$, $(V_{ag,} V_{bg,} V_{cg})$ are measured and transform to rotating reference frame, as well as the voltage of the DC bus (V_{bus}) are measured and compared to the DC bus voltage reference V_{bus}^{*} and set reactive power reference Q_g^{*} , finally pulses are generated by the modulator to the converter switches or transistors to open or close accordingly [50].

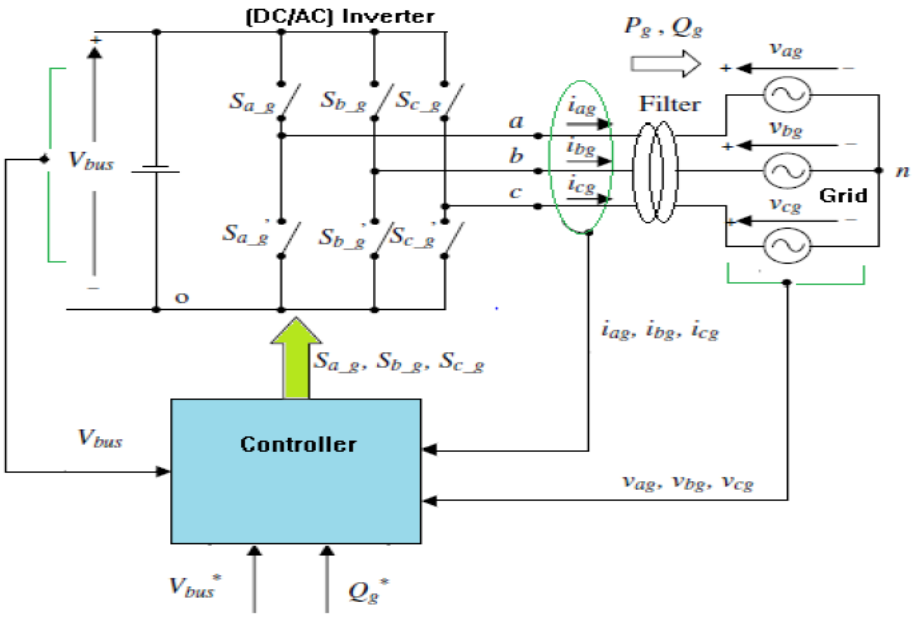

Figure 3-22: Grid Side Control [51]

The pulses for the controlled switches $(S_{a-g}, S_{b-g}, S_{c-g})$ of the two level-VSC, that is, the output voltage of the converter, are generated in order to control the DC bus voltage (V_{bus}) of the DC link and the reactive power exchanged with the grid (Q_g). This is done, in general, according to a closed loop control law. The typical vector control method used in the grid side converter is grid voltage-oriented vector control (GVOVC). On the other hand, control of V_{bus} is necessary since, the DC link is mainly formed by a capacitor. Thus, the active power flow through the rotor must cross the DC link and then it must be transmitted to the grid. Therefore, by only controlling the V_{bus} variable to a constant value, this active power flow through the converters is ensured, together with a guarantee that both grid and rotor side converters have available the required DC voltage to work properly. In a similar way, one variable that can also be controlled with this schema is the reactive power exchange with the grid (Q_g). Since, in general, a sensor-less strategy is not typically adopted, for control the magnitudes that must be measured are the grid side current and voltage, together with the DC link voltage.

The grid voltage-oriented vector control (GVOVC) block diagram is shown in figure 3-23 in more details. From the V_{bus} and Q_g reference, it creates pulses for the controlled switches $(S_{a-g}, S_{b-g}, S_{c-g})$. Thus, the modulator creates the pulses $S_{a-g}, S_{b-g}, S_{c-g}$ from the abc voltage references (V_{af}^*, V_{bf}^*, and V_{cf}^*) for the grid side converter. The modulator can be based on any of the schemas presented in the next section in this chapter for two-level and three-level NPC VSC converter. In this work the grid side converter are analysis by using different pulse width modulation, the abc voltage are first transformed in dq coordinates $(V_{df}^*, V_{qf}^*,)$, then transformed to αβ coordinates $(V_{\alpha f}^*, V_{\beta f}^*)$, and finally generate the abc voltage references. Then, the dq voltage references $(V_{df}^*, V_{qf}^*,)$ are independently created by the dq current $(i_{dg}^*, i_{qg}^*,)$ controllers.

Figure 3-23 indicates that by modifying V_{df}, i_{dg} is mainly modified; while by modifying V_{qf}, i_{qg} is mainly modified. There is also one coupling term in each equation that is best considered in the control as a feed-forward term (at the output of the current controllers), for better performance in the dynamic responses:

$$\begin{cases} e_{df} = -\omega_s L_f i_{qg} \\ e_{df} = \omega_s L_f i_{qg} \end{cases} \tag{3.112}$$

The current references (i_{dg}^*, i_{qg}^*) are totally decoupled from the active and reactive powers. Thus, i_{dg}^* control implies P_g control, while i_{qg}^* control implies Q_g control. The constant terms needed are easily deduced form Equations (3.106):

$$\begin{cases} K_{Pg} = \dfrac{1}{\frac{3}{2} V_{dg}} \\ K_{Qg} = \dfrac{1}{\frac{3}{2} V_{dg}} \end{cases} \tag{3.113}$$

As mentioned before, the power P_g reference is created by the V_{bus} regulator. Indirectly, by this loop, active power flow through the back-to-back converter is ensured. Finally, for voltage and current coordinate transformations and to estimate the angle of the grid voltage

, the angle of the grid voltage is needed(θ_g). In general, this angle is estimated by a phase locked loop (PLL).

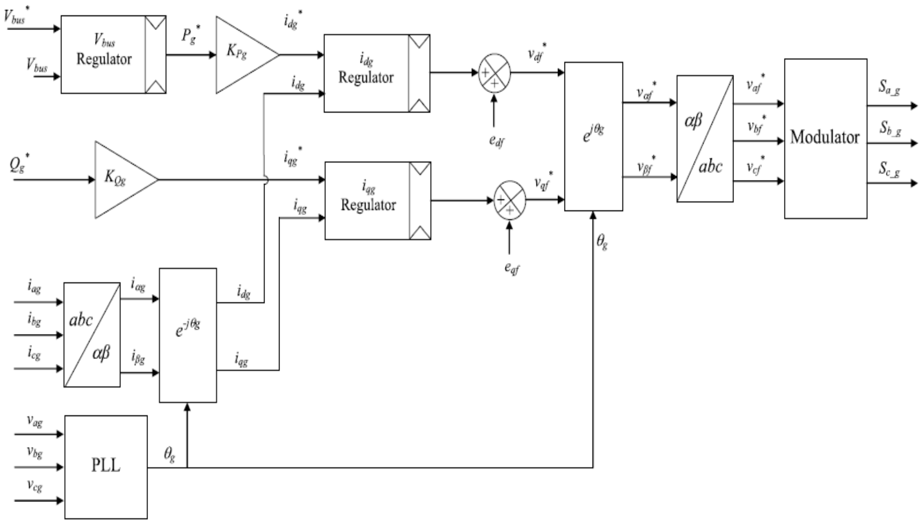

Figure 3-23: Grid voltage-oriented vector control (GVOVC) block diagram [51]

The presented PLL is synchronized by using the dq coordinates of the voltage with which it is required to be synchronized. Thus, the d component of the grid voltage (V_{dg}) must be aligned with the d rotating reference frame; this means that the estimated θ_g must be modified until the q component of the voltage V_{qg}) is zero. At that moment, it can be said that the rotating reference frame dq and the grid voltage space vector are synchronized and aligned to the d axis.

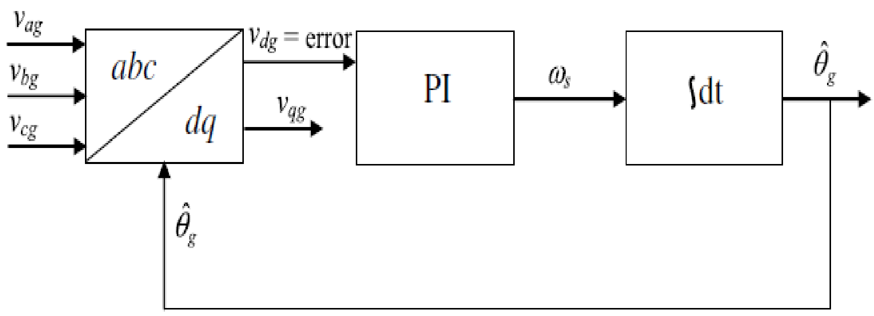

Figure 3-24: PLL structure block diagram

The closed loop PLL structure is illustrated in Figure 3.25. It takes the input abc voltages and transforms them into dq coordinates by using its own estimated Q_g angle. Then the calculated d component is passed through a PI controller which is tuned by Ziegler Nichols tuned technique, modifying the estimated angular speed until the d component is made zero; this means that the synchronization process has been stabilized.

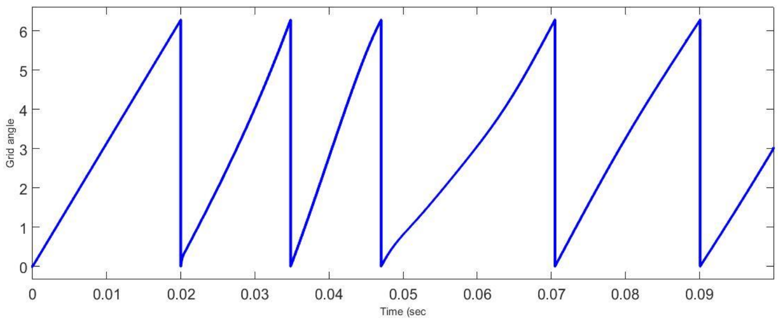

Figure 3-25: estimated grid angle

3.8.2. Designing a proportional-integral (PI) controller

A PI (proportional-Integral) controller has been defined for DFIG rotor circuit for output power to closely track and follow the reference. Designing a PI controller gain parameters and applying them into a system like wind power energy conversions system (WECS) is very important. The controller can play a greater role in attenuating the signal to the desired value with minimization of error and optimization of the process output. Even though PID control is by far the most common way of using feedback in natural and man-made systems, most controllers do not use derivative action. That is why a PI control is selected in this study for tuning the machine parameters. This section describes a fundamental concept of a PI controller for the DFIG connected with the grid and the back to back PWM converter used in the system for optimal power flow to ensure stable and improved power quality. Based on Ziegler Nichols tuned technique the value of Kp and k_i are calculated.

The PI control in mathematical expression is given as:

$$\text{Output(t)} = k_p e(t) + k_i \int_0^t e(\tau) d(\tau) \tag{3.116}$$

Taking the Laplace transform:

$$\text{Output(t)} = \left[k_p + k_i \frac{1}{s}\right] e(t) \tag{3.117}$$

e(t) = Set Reference Value – Actual Calculated Value

The steady state and transient simulation models developed in MATLAB/Simulink would analyze the performance of DFIG and its power controller using two different orientation frames (d-axis and q axis). The Q axis of the grid voltage, V_q will be zero while, the d-axis of the grid voltage, V_d will be a constant. The real and reactive power of a grid -side converter under such reference in equation (3.113) is regulated by the currents, i_{dg} and i_{qg} respectively. The inner or current control loop is applied in real and reactive power flow control in the stator and rotor part of the machine and the voltage (outer) control loop can be designed and used for controlling the DC link voltage between two back to back converters for stable power flow to the grid through the converters. The voltage error is produced by comparing the actual dc voltage with the reference dc voltage. The voltage error is processed through a PI controller to keep constant dc voltage. In relates to the PI controller, a reference current signal i_{gd} is produced and q-axis current part i_{gq} is set as zero, to maintain unity power factor at the grid.

$$i_{dg}^{*} = \left(k_{p1} + \frac{k_{i1}}{s}\right)(V_{dc}^{*} - V_{dc}) \tag{3.118}$$

The dq axis drive voltage signals are generated through equations (a). The control signal for grid converter are obtained by transformation this dq axis voltage.

$$V_{d} = \left(k_{p2} + \frac{k_{i2}}{s}\right)\left(i_{dg}^{*} - i_{dg}\right) \tag{3.119}$$

$$V_{q} = \left(k_{p3} + \frac{k_{i3}}{s}\right)\left(i_{qg}^{*} - i_{qg}\right) \tag{3.120}$$

The value of K_p and K_i are calculated Based on Ziegler Nichols tuning technique.

3.9. Pulse width modulation techniques

The order commands for the controlled semiconductors of the two-level converter can be generated according to different laws called “Modulation.” This section presents some of the most commonly used modulation techniques.

1. Sinusoidal pulse width modulation (PWM) technique
2. Third Harmonic Injection Pulse Width Modulation (THIPWM)
3. Space vector modulation (SVM) technique

The modulations are used for two-level converter and in addition to this Space vector modulation (SVM) technique are used for three level neutral point clamped converter, eliminating in the notation of the order commands $\left(S_{a-g}, S_{b-g}, S_{c-g}\right)$ the sub-indexes referring to the gird: Sa, Sb, and Sc. The modulation technique can be applied at both the rotor and grid side converters.

3.9.1. Sinusoidal Pulse Width Modulation (PWM)

This modulation is a widely extended modulation technique among voltage sourced converters. From the V_{bus} and Q_g reference in GVOVC, it creates abc voltage references (V_{af}^{*}, V_{bf}^{*}, and V_{cf}^{*}). Three sinusoidal reference signals at the frequency of the desired output but displaced from each other by 120 degree are compared with a triangular carrier waveform of suitably frequency to creates the pulses $S_{a-g}, S_{b-g}, S_{c-g}$. The resulting switching signals from each comparator are used to drive the inverter switches of the corresponding leg. The switching signals for each inverter leg are complementary. This technique creates the output voltage according to the following law:

$S_j = 1$if $V_j^* > V_{tri}$ with $j = a, b, c$

Where

V_a^*, V_b^*, V_c^* = Reference voltages for each phase

V_{tri} = Triangular signal

The relationships between the amplitudes and frequencies of the signals need the following indexes:

1. Frequency Modulation Index(m_f). The relationship between the frequency of the triangular signal and the reference signal can be expressed as

$$m_f = \frac{f_{tri}}{f_{ref}} \tag{3.121}$$

In general, in order to create a good quality output voltage, m_f should be a high number. However, since the imposed frequency of the triangular signal (f_{tri}) determines the switching frequency of the switches of the converter. As the frequency f_{tri} gets high (switching frequency of switches), the group of harmonics can be displaced further away from the fundamental frequency. This is advantageous in obtaining good quality voltage and current at the output of the converter; however, this increases power losses in the switches. Therefore, when it comes to choosing a value for m_f, it is necessary to find a compromise between the quality of the voltage created and the power losses in the converter.

2. Amplitude Modulation Index(m_a). The relationship between the amplitude of the reference signal and the triangular signal can be expressed as

$$m_a = \frac{V_{ref}}{V_{tri}} \tag{3.122}$$

Under ideal conditions, the amplitude relationship between the fundamental component of the achieved output voltage and the DC bus voltage is given by the amplitude modulation index as follows:

$$\langle V_{an} \rangle 1 = m_a \frac{V_{bus}}{2} \text{ if } m_a<1 \tag{3.123}$$

The schematic block diagram for the implementation is shown in Figure 3-24. The maximum achievable fundamental voltage without over-modulation ($m_a \leq 1$) is $V_{bus}/2$.

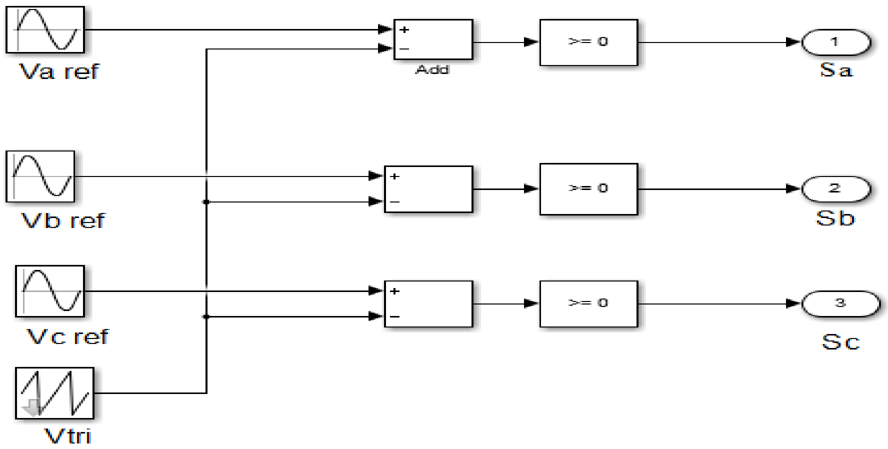

Figure 3-26: SIMULNK model of SPWM

3.9.2. Third Harmonic Injection Pulse Width Modulation

Sinusoidal PWM is easy to understand and easly implementation but it is not able to fully occupy the available DC bus supply voltage. Due to such problem, third harmonic injection pulse width modulation (THIPWM) came in light. This method helps inverter in its performance enhancement. The sine PWM method approaches less of maximum achievable output voltage. Hence, by simply adding third harmonic signal in low frequency sinusoidal reference signal, we can achieve the amplitude increase in output voltage waveform.

Similar to SPWM the method of modulation can also be applied in third harmonic PWM method. In THIPWM, addition of third harmonic means that, in one cycle of sinusoidal wave, three cycles of harmonic should complete. The third harmonic injection to reference signal wave is shown in Figure 3-28. It is impressive that, the result of addition of the third and fundamental harmonic is less in amplitude than fundamental harmonic. On other side, the reference signal occupies two maxima at $\theta = {}^{\pi}/_{3}$ and $\theta = 2\pi$ equals to 1.

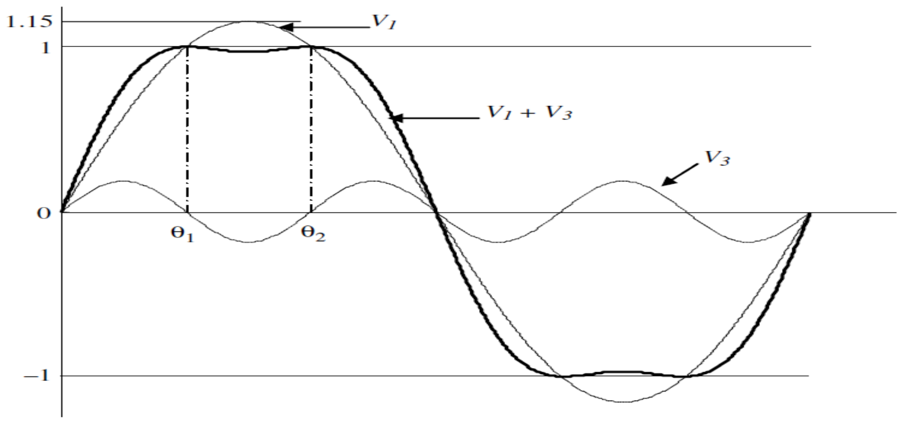

Figure 3-27: Third harmonic injection to the reference signal

The fundamental harmonic and third harmonic equations can be written as

$$V_1 = V_{1max} \sin\theta \tag{3.124}$$

$$V_1 = V_{1max} \sin\left(\frac{\pi}{3}\right)$$

Hence at $\theta = {}^{\pi}/_{3}$, ${}^{V_{bus}}/_{2}$ is the voltage taken by the first harmonic of line to neutral output voltage. Now, the equations can be written as

$$\frac{V_{bus}}{2} = V_{1max} \sin\left(\frac{\pi}{3}\right)$$

Which yields,

$$V_{1max} = \frac{V_{bus}}{2}(0.86) = \frac{V_{bus}}{1.732} \tag{3.125}$$

In this case, the amplitude modulation index is still defined as in Equation (3.126); however, since the reference is composed of the addition of two signals (fundamental component and injected third harmonic), m_a is referred only to the fundamental component:

$$m_a = \frac{|V_1^*|}{|V_{tri}|} \tag{3.126}$$

Third harmonic injection increase the amplitude of the fundamental output voltage by 15% more than sinusoidal PWM. The schematic block diagram for implementation on MATLAB is shown in Figure 3-28. The output voltage waveform for each phase with third harmonic content can be written as

$$V_{1max} \sin(\omega t) + V_{3max} \sin(3\omega t)$$

$$V_{1max} \sin\left(\omega t - \frac{2\pi}{3}\right) + V_{3max} \sin(3\omega t)$$

$$V_{1max} \sin\left(\omega t + \frac{2\pi}{3}\right) + V_{3max} \sin(3\omega t)$$

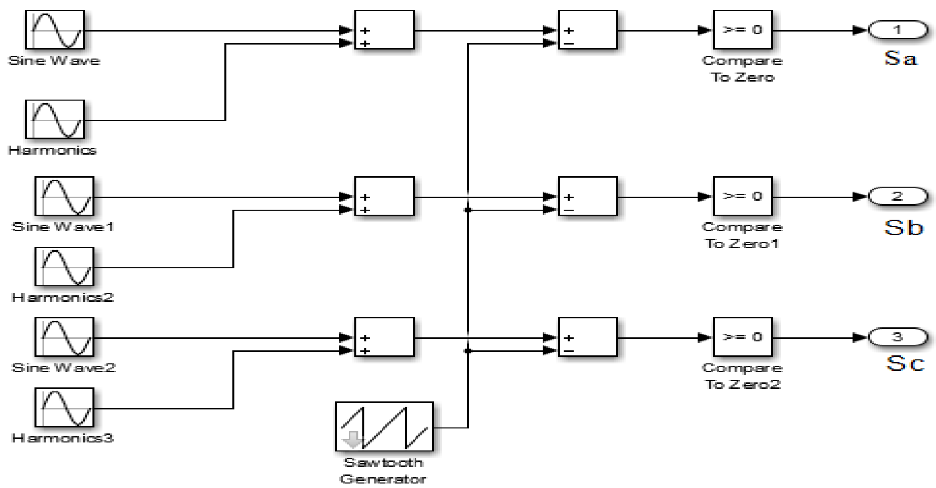

Figure 3-28: Third harmonic pulse generation model.

3.10.3. Modeling of Space vector modulation for two level inverters (AC/DC/AC)

Modeling of Space vector modulation for two level converters (AC/DC/AC) is one of the preferred real-time modulation techniques and widely used for digital control of voltage source converters. It generates the output converter voltage, based on the space vector representation principle. As an alternative to the PWM method seen in the previous sections, with SVM the pulses for the controlled switches of the converters are generated by a slightly different philosophy. The biggest difference from other PWM methods is that the SVPWM uses a vector as a reference. This gives the advantage of a better overview of the system. Therefore, as seen in pervious section, the two-level converter provides eight different output voltage combinations on the AC side (V_0, V_1, V_2, V_3, V_4, V_5, V_6, V_7) that can be represented in a space vector diagram as shown below in Figure 2.21. The region in the plane covered by the voltage vector disposition is a hexagon divided into six different.

3.9.3.1. Reference Vector

The reference vector is represented in a αβ-plane. This is a two-dimensional plane transformed from a three-dimensional plane containing the vectors of the three phases. The switches being ON or OFF is determined by the location of the reference vector on this αβ-plane.

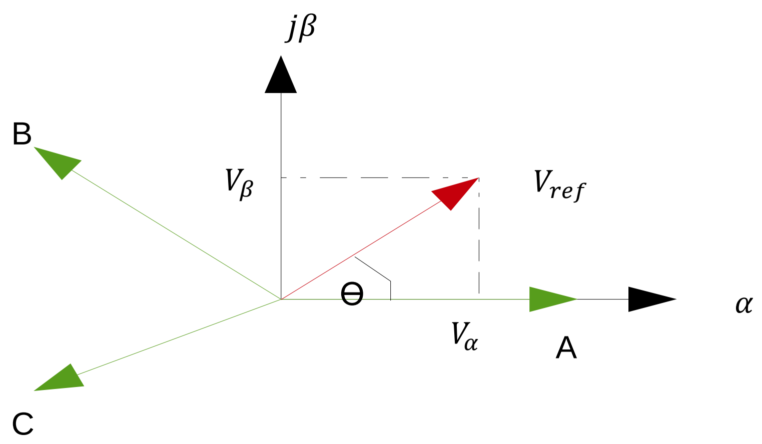

3-29: The reference vector in the two- and three-dimensional plane

Table 3.4 shows that the switches can be ON or OFF, meaning 1 or 0. The switches$\left(S_{a-g}, S_{b-g}, S_{c-g}\right)$ are the upper switches and if these are 1 (separately or together) it turns the upper inverter leg ON and the terminal voltage (V_{ao}, V_{bo}, V_{co}) is positive ($+V_{bus}$). If the upper switches are zero, then the terminal voltage is zero). The lower switches are complementary to the upper switches, so the only possible combinations are the switching states: 000, 001, 010, 011, 100, 110, 110, 111. This means that there are 8 possible switching states, for which two of them are zero switching states and six of them are active switching states. These are represented by active ($V_1 - V_6$) and zero ($V_0$and V_7) vectors. The zero vectors are placed in the axis origin (Figure 3-30).

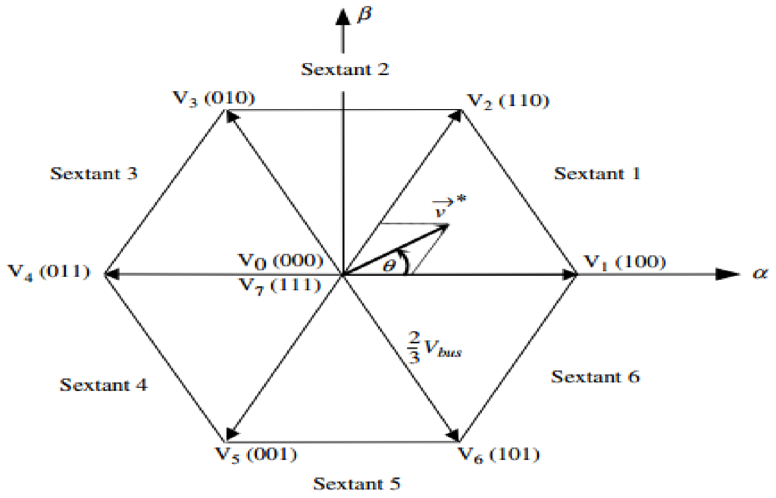

Figure 3-30: Space vector in different sectors

It is assumed that the three-phase system is balanced:

$$V_{aO} + V_{bO} + V_{cO} = 0 \tag{3.127}$$

These are the instantaneous phase voltages:

$$\begin{cases} V_{ao} = V\sin(\theta t) \\ V_{bo} = V\sin(\theta t + \frac{2\pi}{3}) \\ V_{co} = V\sin(\theta t + \frac{4\pi}{3}) \end{cases} \tag{3.128}$$

When the three phase voltages are applied to an AC machine a rotating flux is created. This flux is represented as one rotating voltage vector. The magnitude and angle of this vector can be calculated with Clark's Transformation:

$$V_{ref} = V_\alpha + jV_\beta = \frac{2}{3}(V_a + aV_b + a^2V_c) \tag{3.129}$$

$$a = e^{j\frac{2\pi}{3}}$$

The magnitude and angle (determining in which sector the reference vector is in) of the reference vector is:

$$|V_{ref}| = \sqrt{V_\alpha{}^2 + V_\beta{}^2} \tag{3.130}$$

The reference voltage can then be expresses as:

$$V_\alpha + jV_\beta = \frac{2}{3}(V_a + e^{j\frac{2\pi}{3}}V_b + e^{-j\frac{2\pi}{3}}V_c) \tag{3.131}$$

Inserting the phase shifted values for V_a, V_b and V_C, gives

$$V_\alpha + jV_\beta = \frac{2}{3}(V_a + \cos(\frac{2\pi}{3})V_b + \cos(\frac{2\pi}{3})V_c) + j\frac{2}{3}(V_a + \sin(\frac{2\pi}{3})V_b - \sin(\frac{2\pi}{3})V_c \quad (3.132)$$

The voltage vectors on the alpha and beta axis can then be described as:

$$\begin{bmatrix} V_\alpha \\ V_\beta \end{bmatrix} = \frac{2}{3} * \begin{bmatrix} 1 & \cos(\frac{2\pi}{3}) & \cos(\frac{2\pi}{3}) \\ 0 & \sin(\frac{2\pi}{3}) & -\sin(\frac{2\pi}{3}) \end{bmatrix} * \begin{bmatrix} V_a \\ V_b \\ V_c \end{bmatrix} = \frac{2}{3} * \begin{bmatrix} 1 & -\frac{1}{2} & -\frac{1}{2} \\ 0 & \frac{\sqrt{3}}{2} & -\frac{\sqrt{3}}{2} \end{bmatrix} * \begin{bmatrix} V_a \\ V_b \\ V_c \end{bmatrix} \quad (3.133)$$

$$V_\alpha = \frac{2}{3}(V_a - \frac{1}{2}V_b - \frac{1}{2}V_c) \quad (3.134)$$

$$V_\beta = \frac{2}{3}(\frac{\sqrt{3}}{2}V_b - \frac{\sqrt{3}}{2}V_c \quad (3.135)$$

Having calculated V_α, V_β, V_{ref} and the reference angle in this step is taken. The next step is to calculate the duration time for each vector $V_1 - V_6$.

3.9.3.2. Time Duration

V_{ref} can be found with two active and one zero vector. For sector 1 (0 to $\frac{\pi}{3}$): V_{ref} can be located with V_0 , V_1 and V_2 . V_{ref} in terms of the duration time can be considered as:

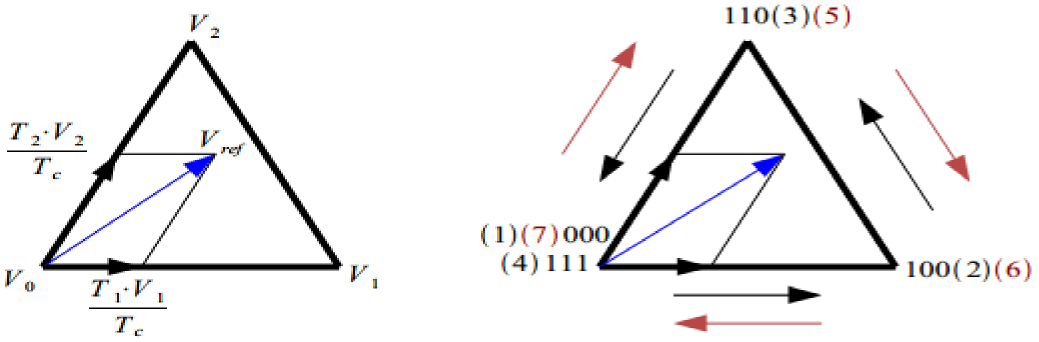

Figure 3-31: Space vector diagram for Sector 1 (a) described with the duty cycle for each vector (b) described with it switching states

The general calculation to receive the duty times in the rest of the sectors is given by:

$$T_1 = T_c * a * \sin\left(\frac{\pi}{3} - \theta + \frac{n-1}{3} * \pi\right) = T_C * a * \left[\sin(\frac{n}{3}\pi)\cos(\theta) - \cos(\frac{n}{3}\pi)\sin(\theta)\right] \quad (3.136)$$

$$T_2 = T_c * a * \sin\left(\theta - \frac{n-1}{3} * \pi\right) = T_C * a * \left[-\cos(\theta)\sin\left(\frac{n-1}{3}\pi\right) + \sin(\theta)\cos(\frac{n-1}{3}\pi)\right] \quad (3.137)$$

$$T_0 = T_c - T_1 - T_2 \quad (3.138)$$

Choosing n as the number of the sector (n = 1,2,3,4,5,6) the calculations for the time duration in each sector can be calculated.

$$V_{ref} * T_c = V_1 * \frac{T_1}{T_c} + V_2 * \frac{T_2}{T_c} + V_0 * \frac{T_0}{T_c}$$

$$V_{ref} = V_1 T_1 + V_2 T_2 + V_0 T_0 \quad (3.139)$$

The total cycle is given by:

$$T_C = T_1 + T_2 + T_0 \quad (3.140)$$

The position of V_{ref}, V_1, V_2 and V_0 can be described with its magnitude and angle:

$$V_{ref} = V_{ref} * r^{j0} \quad (3.141)$$

$$V_1 = \frac{2}{3} * V_{bus} * e^{j\frac{\pi}{3}} \quad (3.142)$$

$$V_0 = 0$$

$$T_C * V_{ref} * \begin{pmatrix} \cos\theta \\ \sin\theta \end{pmatrix} = T_1 * \frac{2}{3} * V_{bus} * \begin{pmatrix} 1 \\ 0 \end{pmatrix} + T_2 * \frac{2}{3} * V_{bus} * \begin{pmatrix} \cos(\frac{\pi}{3}) \\ \sin(\frac{\pi}{3}) \end{pmatrix} \quad (3.143)$$

Dividing these in real and imaginary parts simplifies the calculation for each duration time:

Real part: $T_C * V_{ref} * \cos(\theta) = T_1 * \frac{2}{3} * V_{bus} + T_2 * \frac{1}{3} * V_{bus}$

Imaginary part: $T_C * V_{ref} * \sin(\theta) = T_2 * \frac{1}{\sqrt{3}} * V_{bus}$

T_1 and T_2 is then given by:

$$T_1 = T_c * \frac{\sqrt{3} * V_{ref}}{V_{bus}} * \sin\left(\frac{\pi}{3} - \theta\right) = T_c * a * \sin\left(\frac{\pi}{3} - \theta\right) \quad (3.144)$$

$$T_2 = T_c * \frac{\sqrt{3} * V_{ref}}{V_{bus}} * \sin(\theta) = T_c * a * \sin(\theta) \quad (3.145)$$

Where $a = \frac{\sqrt{3} * V_{ref}}{V_{bus}}$ is modulation index.

3.9.3.3. Switching Time

Duty cycle for each sector there are 7 switching states for each cycle. It always starts and ends with a zero vector. This also means that there is no extra switching state needed when changing the sector. The uneven numbers travel counter clockwise in each sector and the even sectors travel clockwise. For sector 1 it goes through these switching states: 000 – 100 – 110 – 111 – 110 – 100 - 000, one round and then back again. This is during the time T_c and it has to be divided amongst the 7 switching states, three of them being zero vectors.

$$T_c = \frac{T_0}{4} + \frac{T_1}{2} + \frac{T_0}{2} + \frac{T_2}{2} + \frac{T_1}{2} + \frac{T_0}{4} \quad (3.146)$$

This can be calculated for all the sectors (Figure 3-27). There are different kinds of waveforms: center aligned and edge aligned. Edge align waveforms makes it easier when comparing with the carrier wave, but the center aligned has the advantage of reducing the harmonics and also reducing noise. Following the pattern for each sector results in a ON/OFF waveform for each sector and phase. Each switch has it switching information depending on where the reference vector is located. For Sector 1, the switch is ON between $\mathrm{T_0}/_4$ and $\mathrm{T_c} - \mathrm{T_0}/_4$ in the first phase, between $\mathrm{T_0}/_4 + \mathrm{T_1}/_2$ and $\mathrm{T_c} - (\mathrm{T_0}/_4 + \mathrm{T_1}/_2)$ for the second phase and so on. For the switch to know that it should be switched ON at these specific times requires a timer that can give this information.

3.10. Space Vector Pulse Width Modulation for three-level converters

Figure 3-32 shows a three-level neutral point clamped inverter. It contains 12 switching devices and also supplied with two capacitors connected in series. Both are charged with $\mathrm{V_{DC}}$. The point between these capacitors is the DC-voltage neutral point. Each phase leg consists of 4 series-connected switching devices (IGBT's) and two clamping diodes. This diode is used to clamp the six middle switches potential to the DC-link point at Z. Specific combinations of the twelve switches gives the three-level output voltage.

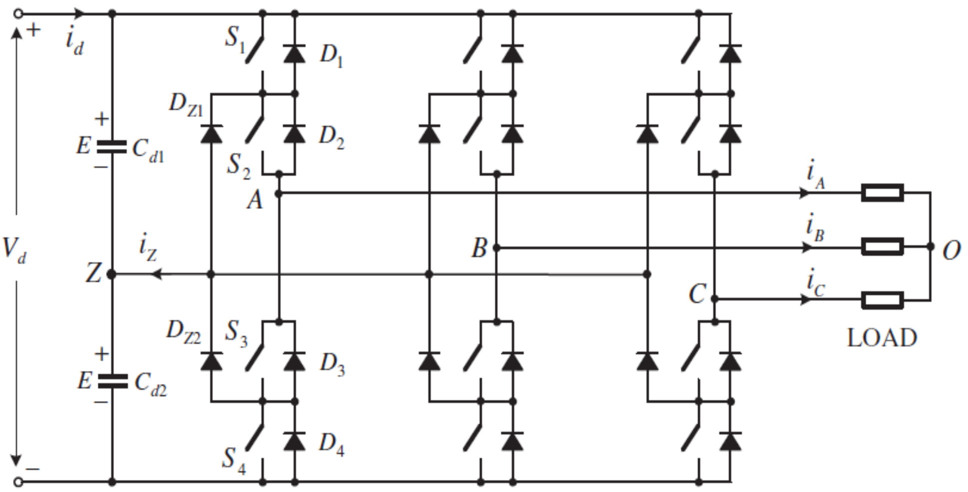

Figure 3-32: Three-level, three-phase neutral point clamped inverter

The four switches in one phase leg can only be turned on two at a time and so be connected to the DC-link point's p, o, and n. These are represented with the switching states P, O and N. This means that three voltage levels can be created using O as the reference. The advantages of three-level converters instead of two-level:

- Higher levels mean that the output waveform resembles the sinusoidal waveform more. This also means that the harmonic distortion is decreased.
- Smaller voltage levels are used. This means smaller voltage change, which means reduced stress on the motor bearings.

- The clamping diodes limits the voltage across the OFF-state switching devices to one capacitor voltage level (half of the DC-link voltage). This reduces the voltage, so medium rated semiconductor devices can be used for high-voltage level application.

3.10.1. Switching state

The operating status of the switches in the NPC inverter can be represented by switching states shown in Table 3.4. Switching state "P" denotes that the upper two switches in leg A are on and the inverter terminal voltage V_{AZ}, which is the voltage at terminal Z with respect to the neutral point Z, is $+E$, whereas "N" indicates that the lower two switches conduct, leading to $V_{AZ} = -E$.

Table 3-4: definition of switching states

Switching state	Device Switching Status (Phase A)				Inverter terminal Voltage (V_{AZ})
	S_1	S_2	S_3	S_4	
P	ON	ON	OFF	OFF	$+E$
O	OF	ON	ON	OFF	0
N	OFF	OFF	ON	ON	$-E$

Switching state "o" signifies that the inner two switches S_2 and S_3 are on and V_{AZ} is clamped to zero through the clamping diodes. Depending on the direction of load current i_A, one of the two clamping diodes is turned on. For instance, a positive load current $(i_A > 0)$ forces D_{Z1} to turn on, and the terminal A is connected to the neutral point Z through the conduction of D_{Z1} and S_2. It can be observed from Table 3.4 that switches S_1 and S_3 operate in a complementary manner. With one switched on, the other must be off. Similarly, S_2 and S_4 are a complementary pair as well. For a three-level three-phase inverter there are 27 switching states. These states represent the connection to the different DC-link points. The generated inverter output phase voltage can be expressed as follows:

$$\begin{cases} V_{AZ} = (2S_1 - S_1 - S_1) + (2S_2 - S_2 - S_2) \\ V_{BZ} = (2S_1 - S_1 - S_1) + (2S_2 - S_2 - S_2) \\ V_{CZ} = (2S_1 - S_1 - S_1) + (2S_2 - S_2 - S_2) \end{cases} \tag{3.147}$$

These are the line-to-neutral voltages. To receive the line-to-line voltage:

$$\begin{cases} V_{AB} = V_{AZ} - V_{BZ} \\ V_{BC} = V_{BZ} - V_{CZ} \\ V_{CA} = V_{CZ} - V_{AZ} \end{cases} \tag{3.148}$$

There is requested to generate five levels of outputs, so the three-level can be created. These levels are $2E, E, 0, -E$ and $-\ 2E$ (for the line-to-line voltage).

As for the two-level inverter the reference vector is given with the help from three voltage vectors. For the three-level converter each sector also is divided into 4 regions, specifying the output even more. Based on the magnitude the voltage vectors and switching states can be defined in table 3.5:

Table 3-5: Voltage vectors and switching states

<table>
<tr><th colspan="2">Space Vector</th><th colspan="2">Switching State</th><th>Voltage Vector Classification</th><th>Vector Magnitude</th></tr>
<tr><td colspan="2">$\overrightarrow{V_0}$</td><td colspan="2">$PPP, OOO. NNN$</td><td>Zero vector</td><td>0</td></tr>
<tr><td rowspan="3">$\overrightarrow{V_1}$</td><td></td><td>P-type</td><td>N-type</td><td rowspan="13">Small vector</td><td rowspan="13">$\frac{1}{3}V_d$</td></tr>
<tr><td>$\overrightarrow{V_{1P}}$</td><td>POO</td><td></td></tr>
<tr><td>$\overrightarrow{V_{1N}}$</td><td></td><td>ONN</td></tr>
<tr><td rowspan="2">$\overrightarrow{V_2}$</td><td>$\overrightarrow{V_{2P}}$</td><td>POO</td><td></td></tr>
<tr><td>$\overrightarrow{V_{2N}}$</td><td></td><td>OON</td></tr>
<tr><td rowspan="2">$\overrightarrow{V_3}$</td><td>$\overrightarrow{V_{3P}}$</td><td>OPO</td><td></td></tr>
<tr><td>$\overrightarrow{V_{3N}}$</td><td></td><td>NON</td></tr>
<tr><td rowspan="2">$\overrightarrow{V_4}$</td><td>$\overrightarrow{V_{4P}}$</td><td>OPP</td><td></td></tr>
<tr><td>$\overrightarrow{V_{4N}}$</td><td></td><td>NOO</td></tr>
<tr><td rowspan="2">$\overrightarrow{V_5}$</td><td>$\overrightarrow{V_{5P}}$</td><td>OOP</td><td></td></tr>
<tr><td>$\overrightarrow{V_{5N}}$</td><td></td><td>NNO</td></tr>
<tr><td rowspan="2">$\overrightarrow{V_6}$</td><td>$\overrightarrow{V_{6P}}$</td><td>POP</td><td></td></tr>
<tr><td>$\overrightarrow{V_{6N}}$</td><td></td><td>ONO</td></tr>
<tr><td colspan="2">$\overrightarrow{V_7}$</td><td colspan="2">POP</td><td rowspan="5"></td><td rowspan="5">$\frac{\sqrt{3}}{3}V_d$</td></tr>
<tr><td colspan="2">$\overrightarrow{V_8}$</td><td colspan="2">OPN</td></tr>
<tr><td colspan="2">$\overrightarrow{V_9}$</td><td colspan="2">NPO</td></tr>
<tr><td colspan="2">$\overrightarrow{V_{10}}$</td><td colspan="2">NOP</td></tr>
<tr><td colspan="2">$\overrightarrow{V_{11}}$</td><td colspan="2">ONP</td></tr>
</table>

$\overrightarrow{V_{12}}$	PNO	Medium vector	
$\overrightarrow{V_{13}}$	PNN	Large vector	$\frac{2}{3}V_d$
$\overrightarrow{V_{14}}$	PPN		
$\overrightarrow{V_{15}}$	NPN		
$\overrightarrow{V_{16}}$	NPP		
$\overrightarrow{V_{17}}$	NNP		
$\overrightarrow{V_{18}}$	PNP		

The inverter has a total of 27 valid combinations of switching states. As listed in Table 3.5, these three-phase switching states are represented by three letters for the inverter phases $A, B,$ and C. The 27 switching states listed in the table correspond to 19 voltage vectors, based on their magnitude (length), the voltage vectors can be divided into four groups:

- Zero vector $(\overrightarrow{V_0})$**,** representing three switching states [PPP], [OOO], and [NNN]. The magnitude of $\overrightarrow{V_0}$ is zero;
- Small vectors $(\overrightarrow{V_0}$ to $\overrightarrow{V_6})$, all having a magnitude of $\frac{1}{3}V_d$. Each small vector has two switching states, one containing [P] and the other containing [N], and therefore can be further classified into a P- or N-type small vector;
- Medium vectors $(\overrightarrow{V_7}$ to $\overrightarrow{V_{12}})$**,** whose magnitude is $\frac{\sqrt{3}}{3}V_d$; and
- Large vectors $(\overrightarrow{V_{13}}$ to $\overrightarrow{V_{18}})$, all having a magnitude of $\frac{2}{3}V_d$.

3.10.2. Time duration (Dwell Time Calculation)

To facilitate the dwell time calculation, the space vector diagram can be divided into six triangular sectors (I to VI), each of which can be further divided into four triangular regions (1 to 4) as illustrated in Figure 3-33. The switching states of all the vectors are also shown in the figure. Similar to the SVM algorithm for the two-level converter, the SVM for the three level NPC converter is also based on “volt-second balancing” principle, that is, the product of the reference voltage $\overrightarrow{V_{ref}}$ and sampling period T_s equals the sum of the voltage multiplied by the time interval of chosen space vectors. In the NPC inverter, the reference vector $\overrightarrow{V_{ref}}$ can be synthesized by three nearest stationary vectors.

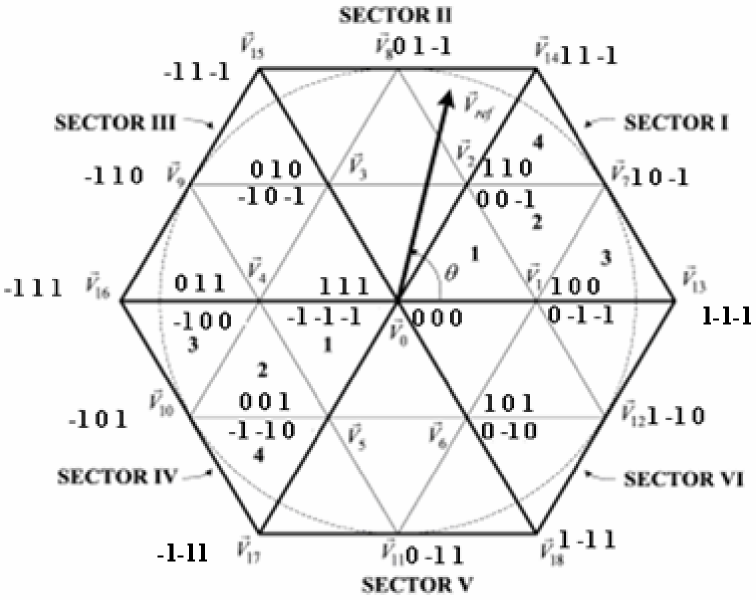

Figure 3-33: Division of sectors and regions [52]

For instance, when $\overrightarrow{V_{ref}}$, falls into region 2 of sector I as shown in Fig. 3-33. the three nearest vectors are $\overrightarrow{V_1}$, $\overrightarrow{V_2}$, and $\overrightarrow{V_7}$, from which

$$\overrightarrow{V_{ref}} T_s = \overrightarrow{V_1} T_a + \overrightarrow{V_7} T_b + \overrightarrow{V_2} T_c$$

$$T_s = T_a + T_b + T_c \tag{3.149}$$

Where $T_a, T_b,$ and T_c are the dwell times for $\overrightarrow{V_1}$, $\overrightarrow{V_7}$, and $\overrightarrow{V_2}$, respectively Note that $\overrightarrow{V_{ref}}$ can also be synthesized by other space vectors instead of the "nearest three." However, it will cause higher harmonic distortion in the inverter output voltage, which is undesirable in most cases.

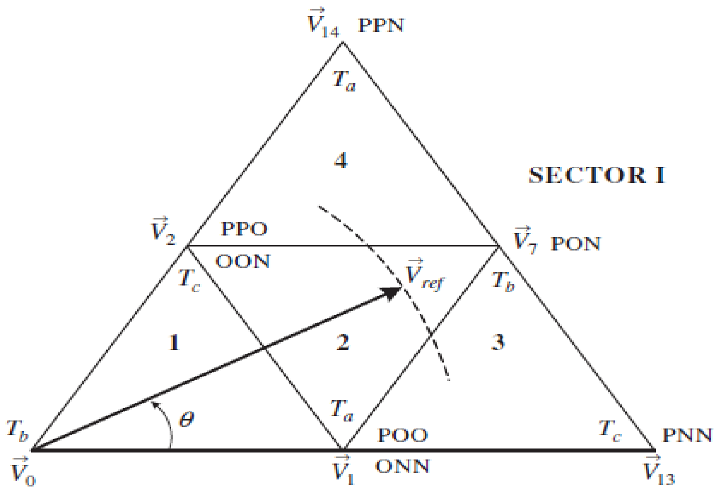

Figure 3-34: Voltage vectors and their dwell times

The voltage vectors $\overrightarrow{V_1}$, $\overrightarrow{V_2}$, $\overrightarrow{V_7}$, and $\overrightarrow{V_{ref}}$ in Fig 3-34. can be expressed as

$$\overrightarrow{V_1} = \frac{1}{3}V_d, \overrightarrow{V_2} = \frac{1}{3}V_d e^{\frac{j\pi}{3}},\ \overrightarrow{V_7} = \frac{\sqrt{3}}{3}V_d e^{\frac{j\pi}{6}}, \overrightarrow{V_{ref}} = V_{ref}e^{j\theta} \tag{3.150}$$

Substituting (3.150) into (3.149) yields

$$V_{ref}e^{j\theta}T_s = \frac{1}{3}V_d T_a + \frac{\sqrt{3}}{3}V_d e^{\frac{j\pi}{6}}T_b + \frac{1}{3}V_d e^{\frac{j\pi}{3}}T_c$$

For which

$$V_{ref}(\cos\theta + j\sin\theta)T_s = \frac{1}{3}V_d T_a + \frac{\sqrt{3}}{3}V_d\left(\cos\frac{\pi}{6} + j\sin\frac{\pi}{6}\right)T_b + \frac{1}{3}V_d\left(\cos\frac{\pi}{3} + j\sin\frac{\pi}{3}\right)T_c \tag{3.151}$$

Splitting equation (3.118) into the real and imaginary parts gives

$$\begin{cases} \text{Re: } T_a + \frac{3}{2}T_b + \frac{1}{2}T_c = 3\frac{V_{ref}}{V_d}(\cos\theta)T_s \\ \text{Im: } \frac{\sqrt{3}}{2}T_b + \frac{\sqrt{3}}{2}T_c = 3\frac{V_{ref}}{V_d}(\sin\theta)T_s \end{cases} \tag{3.152}$$

By solve equation (3.152) with the equation for total time, $T_s = T_a + T_b + T_c$ for dwell times

$$\begin{cases} T_a = T_s[1 - 2m_a\sin\theta] \\ T_b = T_s\left[2m_a\sin\left(\frac{\pi}{3} + \theta\right) - 1\right] \\ T_c = T_s\left[1 - 2m_a\sin\left(\frac{\pi}{3} - \theta\right)\right] \end{cases} \text{for } 0 \leq \theta < \frac{\pi}{3} \tag{3.153}$$

Where ma is the modulation index, defined by

$$m_a = \sqrt{3}\frac{V_{ref}}{V_d} \tag{3.154}$$

Table 3-6: Dwell time calculation for (V_ref) in sector I

Region	Ta		Tb		Tc	
1	$\overrightarrow{V_1}$	$T_s\left[2m_a\sin\left(\frac{\pi}{3} - \theta\right)\right]$	$\overrightarrow{V_0}$	$T_s\left[1 - 2m_a\sin\left(\frac{\pi}{3} + \theta\right)\right]$	$\overrightarrow{V_2}$	$T_s[2m_a\sin(\theta)]$
2	$\overrightarrow{V_1}$	$T_s[1 - 2m_a\sin\theta]$	$\overrightarrow{V_7}$	$T_s\left[2m_a\sin\left(\frac{\pi}{3} + \theta\right) - 1\right]$	$\overrightarrow{V_2}$	$T_s\left[1 - 2m_a\sin\left(\frac{\pi}{3} - \theta\right)\right]$
3	$\overrightarrow{V_1}$	$T_s\left[2 - 2m_a\sin\left(\frac{\pi}{3} + \theta\right)\right]$	$\overrightarrow{V_7}$	$T_s[2m_a\sin(\theta)]$	$\overrightarrow{V_{13}}$	$T_s\left[2m_a\sin\left(\frac{\pi}{3} - \theta\right) - 1\right]$
4	$\overrightarrow{V_{14}}$	$T_s[2m_a\sin(\theta) - 1]$	$\overrightarrow{V_7}$	$T_s\left[2m_a\sin\left(\frac{\pi}{3} - \theta\right)\right]$	$\overrightarrow{V_2}$	$T_s\left[2 - 2m_a\sin\left(\frac{\pi}{3} + \theta\right)\right]$

Table 3.6 gives the equations for the calculation of dwell times for $\overrightarrow{V_{ref}}$ in sector I. The maximum length of the reference vector $\overrightarrow{V_{ref}}$ corresponds to the radius of the largest circle that can be inscribed within the hexagon of Fig 3-34. which happens to be the length of the medium voltage vectors

$$\overrightarrow{V_{ref}}, \max = \sqrt{3}\,{}^{V_d}/_{3} \tag{3.155}$$

Substituting $\overrightarrow{V_{ref}}$, max into (3.121) yields the maximum modulation index

$$m_{a,max} = \sqrt{3}\frac{V_{ref,max}}{V_d} = 1 \tag{3.156}$$

from which the range of m_a is

$0 \leq m_a \leq 1$

The equations in Table 3.6 can also be used to calculate the dwell times when $\overrightarrow{V_{ref}}$ is in other sectors (II to VI) provided that a multiple of ${}^{\pi}/_{3}$ is subtracted from the actual angular displacement θ such that the modified angle falls into the range between zero and ${}^{\pi}/_{3}$ for use in the equations.

3.11. Overall system software simulation modeling and design

3.11.1. MATLAB/SIMULINK model

The simulation results are given for the DFIG for the following specification: Number of pole = 2, Rated power = 1.5MW, Rated voltage = 690V, Frequency [F] = 50 Hz, rated speed 1500rpm.

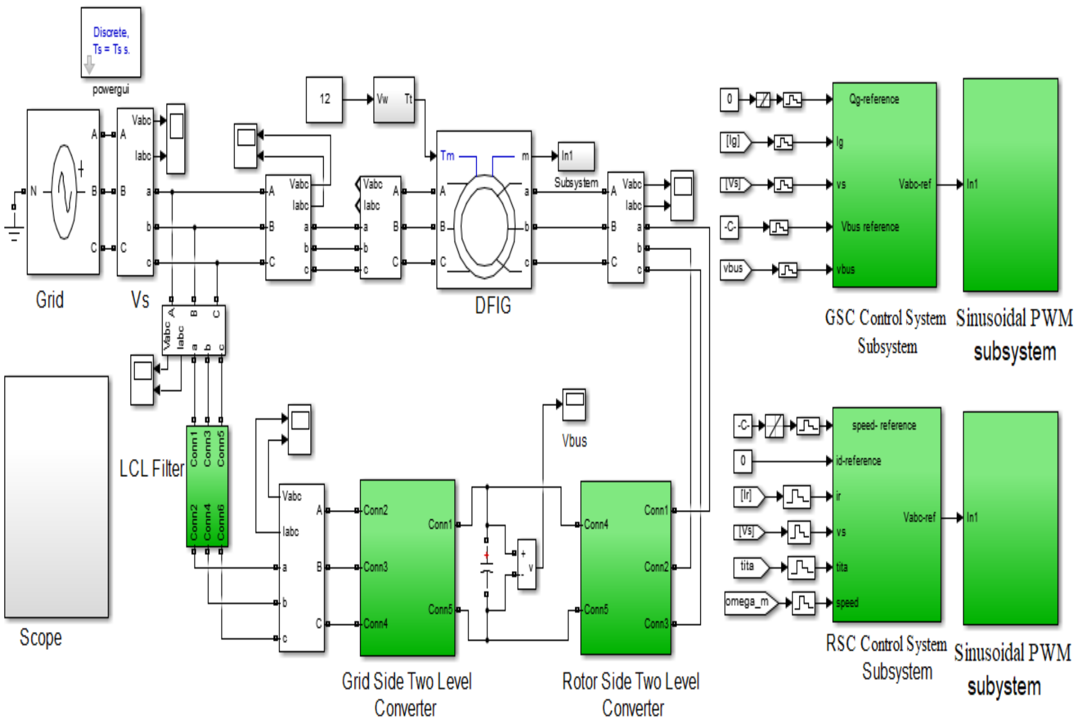

Figure 3-35: Simulink model of a DFIG using back-to-back converter with SPWM

The above Figure 3-35 shows the complete MATLAB / SIMULINK model of a DFIG using back-to-back converter with sinusoidal pulse width modulation control. Its subsystem model shown in Figure.A1, Figure.A2, and Figure.A3(Appendix).

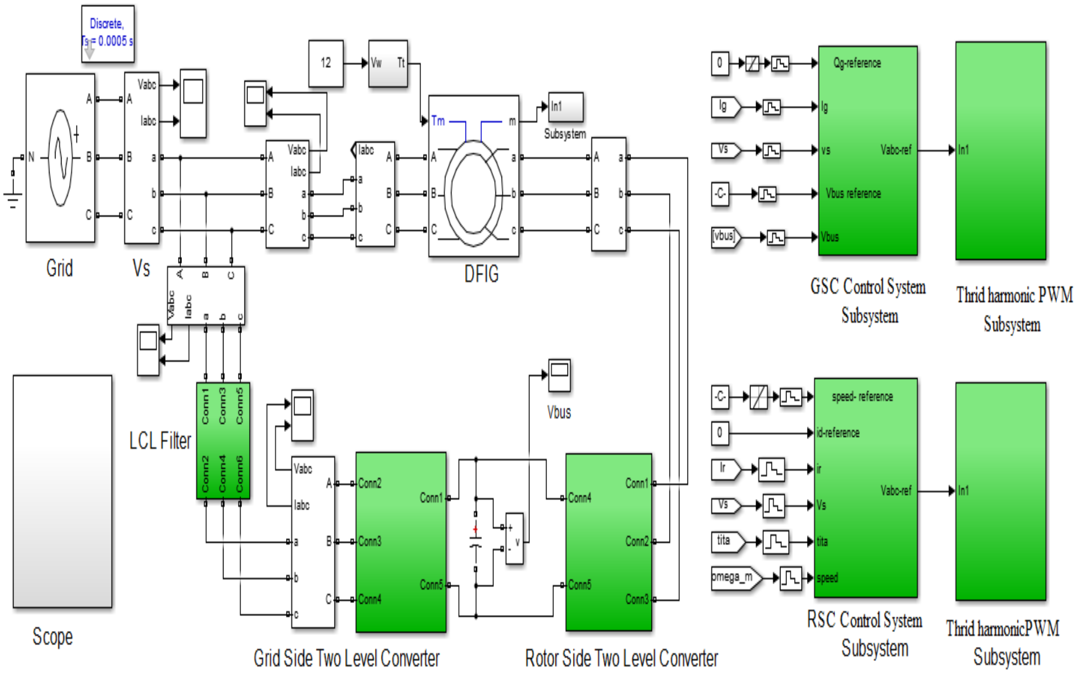

Figure 3-36: Simulink model of a DFIG using back-to-back converter with THIPWM

Figure 3-36 shows the complete MATLAB / SIMULINK model of a DFIG using back-to-back converter with third harmonics injected pulse width modulation control. Its subsystem model shown in Figure.A1, Figure.A2, and Figure.A4(Appendix).

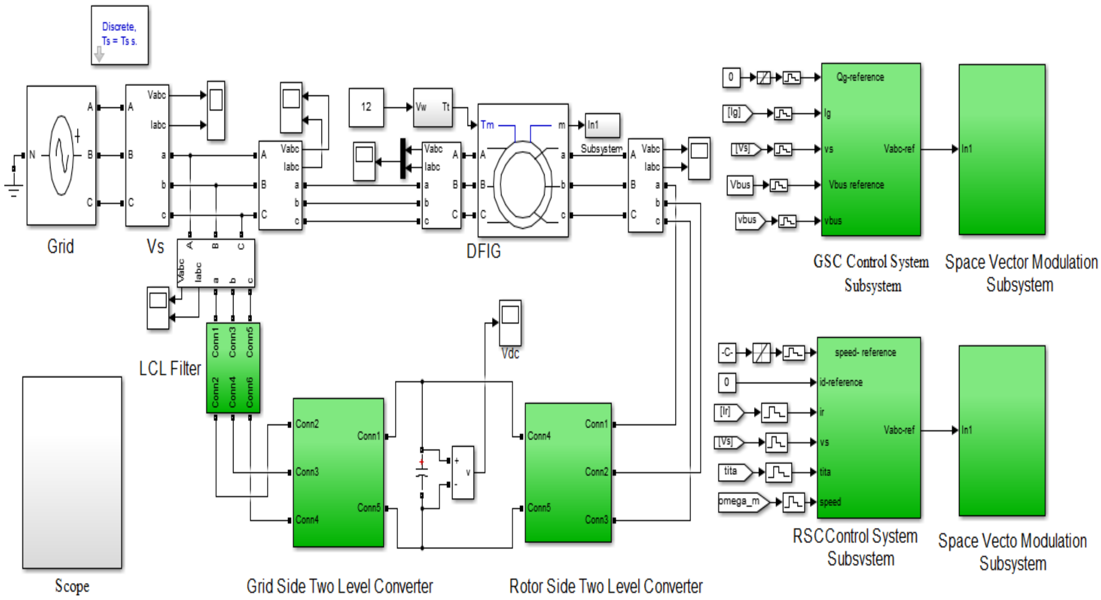

Figure 3-37: Simulink model of a DFIG using two level back-to-back converter with SVPWM

Figure 3-37 indicate the complete MATLAB / SIMULINK model of a DFIG using back-to-back converter with space vector pulse width modulation control. Its subsystem model shown in Figure.A1, Figure.A2, and Figure.A5(Appendix).

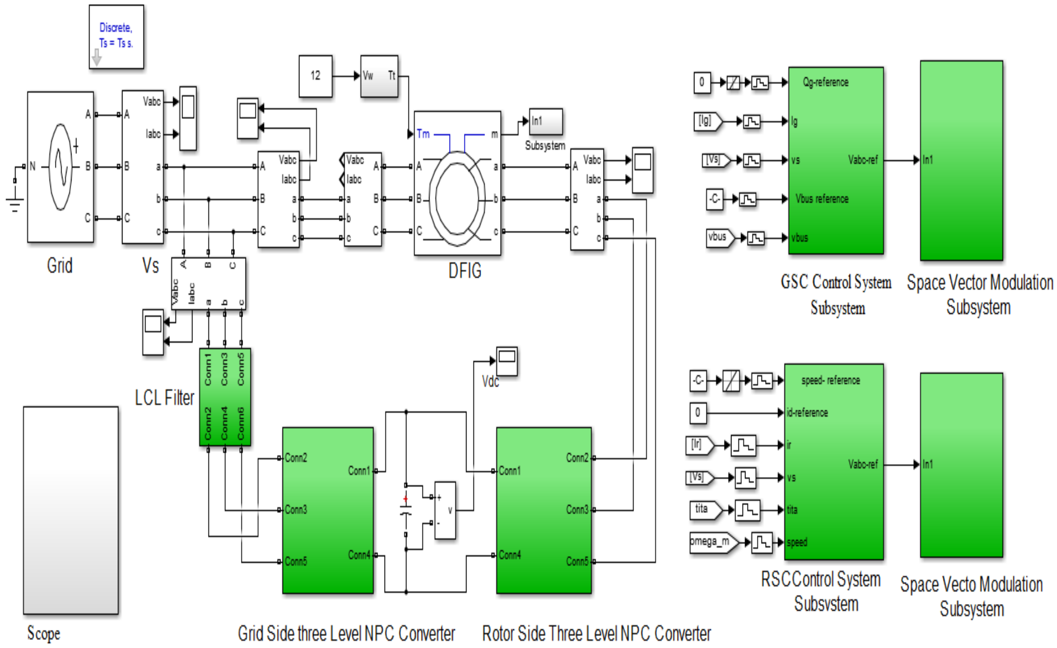

Figure 3-38: Simulink model of a DFIG using three level NPC back-to-back converter with SVPWM

Figure 3-38 shows the complete MATLAB / SIMULINK model of a DFIG using three level NPC back-to-back converter with space vector pulse width modulation control. Its subsystem model shown in Figure.A1, Figure.A2, and Figure.A6(Appendix).

CHAPTER FOUR

4. RESULT AND DISCUSSIONS

4.1. MATLAB Simulation results

4.1.1. Dynamic Simulation Results

Based on the above modelling concepts and applying them in the embedded MATLAB Simulink, the results obtained are discussed in this section. The DFIG with 690 stator line to line voltage, 50 Hz frequency together with other necessary real parameters obtained through numerical analysis and nameplates are used.

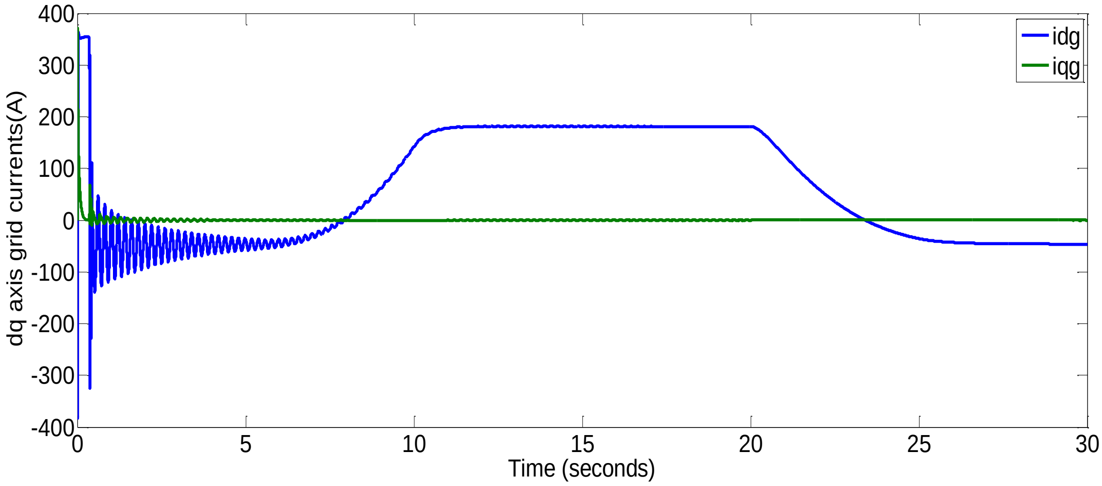

Figure 4-1: Simulation results of dq currents at the grid side (load currents)

It can be observed from the response of Figure 4-1 that change in dc voltage reference and /or the wind speed change requires a change of current to maintain an active power balance. Hence, we can see a change in load current maintaining the active power almost constant. However, the change in references gives some transients in the active power as well, which is reflected in the d-component of current. It can be seen that the effect of transient is not present in the reactive power or q-component of current. Hence the decoupled control of active and reactive power is also ensured. The PI controller performs well in tracking the reference input.

Effect of Change in reactive power

In this case, the dc voltage reference value is held at reference value. The system is initially operating with a reactive power reference of 1KVAR. At t = 10s, the reactive power reference is reversed to 100KVAR at the grid side whereas the reference at the stator side held 0. The responses of the system are shown in Figure 4-2 below.

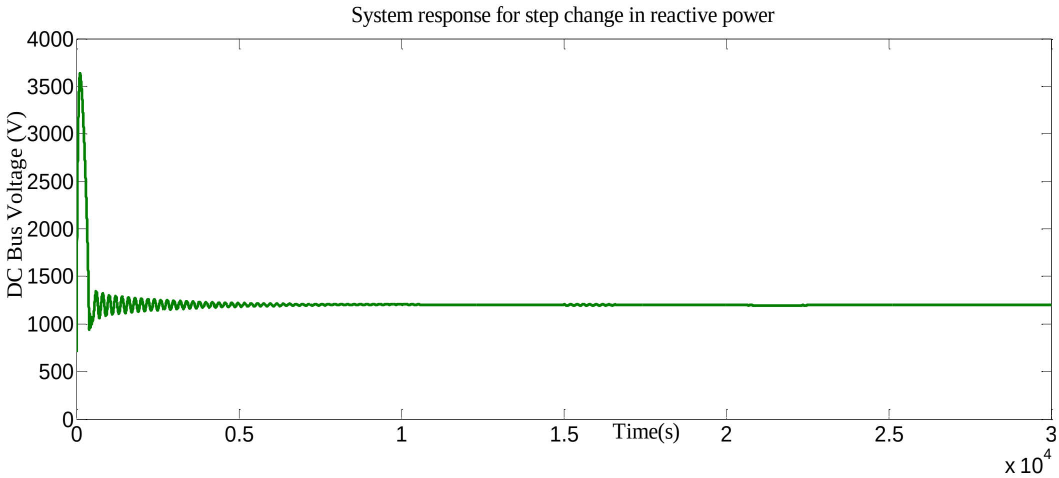

Figure 4-2: The responses of the system for reactive power change

There is a very small ripple in dc voltage during the transient in reactive power, which is again reflected in the q-current reference as shown in Figure 4-3 below.

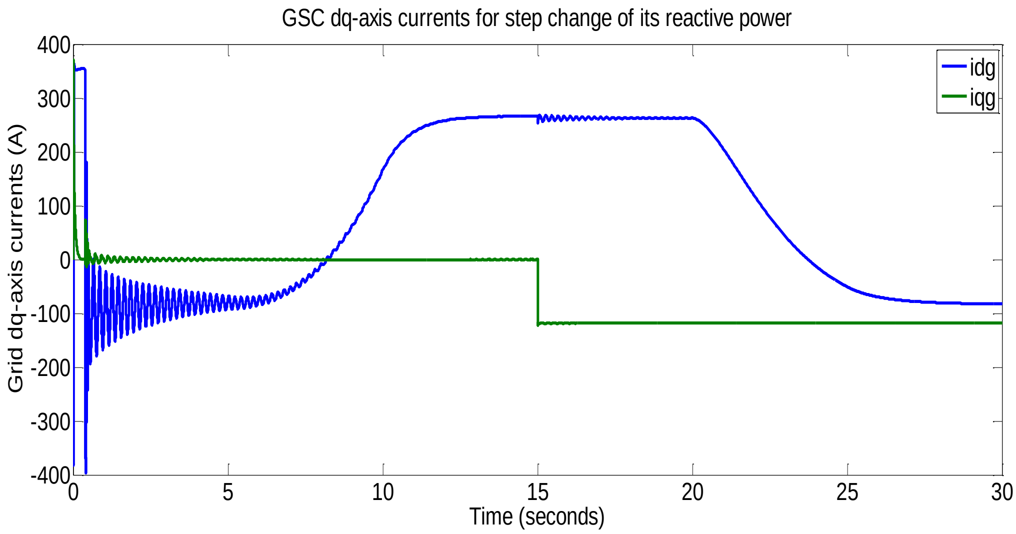

Figure 4-3: q-axis current reference results

The active power is maintained at the reference value constantly. The change in reactive power is reflected in the change of q-component of current, whereas the d-component remains constant, showing the decoupling of the d and q axis components.

Change in active power load (output active power)

In this case, with the dc voltage reference set as it is, and the reactive power references set at 0 and active power reference set at its point, the load at receiving end is changed from 0 to 200A at time t=5 secs and the result is shown in Figure 4-4.

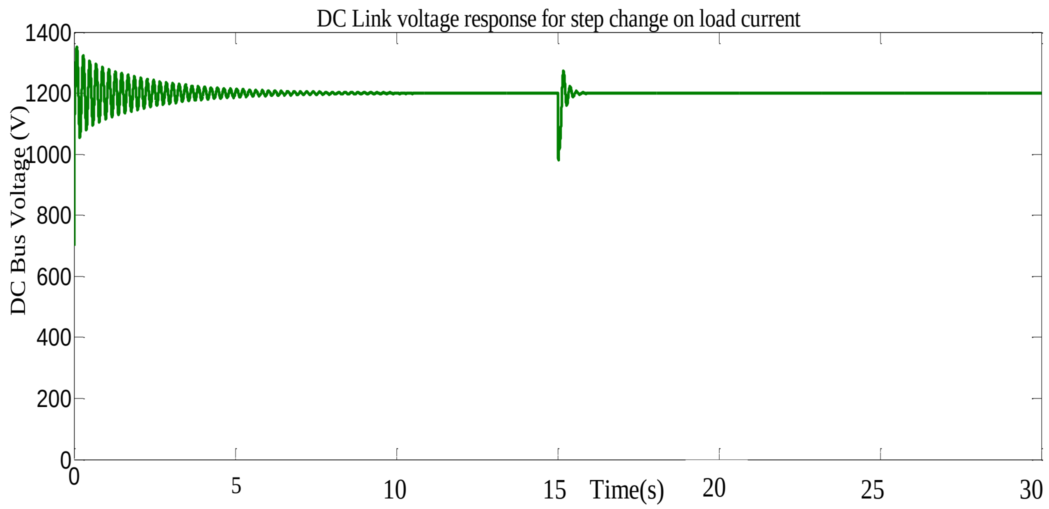

Figure 4-4: DC link voltage response to active power change.

The change in active power is reflected in d-component of current and the load current magnitude and direction shown in Figure 4-5 below.

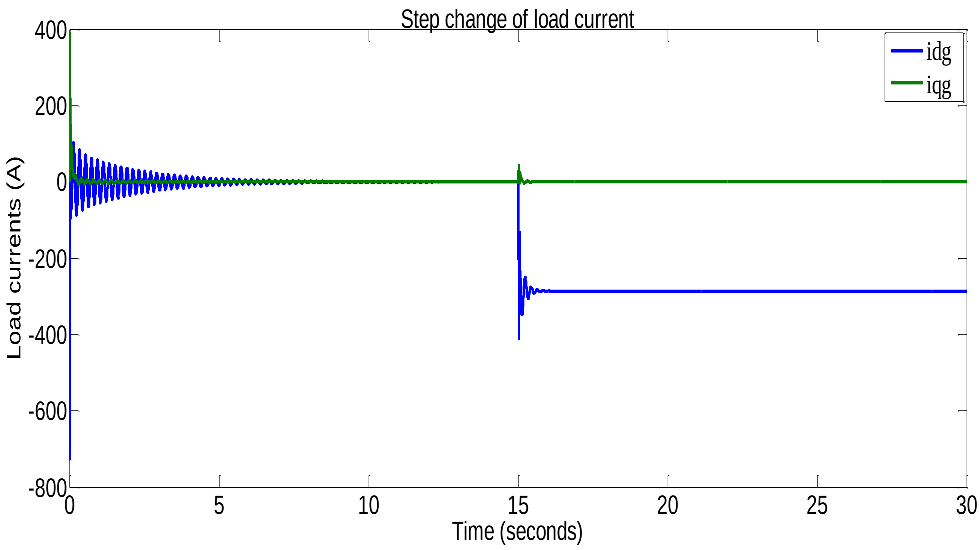

Figure 4-5: Change of active power reflection on d-component of current

Because of the decoupling, almost no effect is observed in the control of reactive power. The step change causes transients in dc voltage, but, the step change in active power (load current) causes a much higher transient than that with the change in reactive power.

4.1.2. Simulation result of two-level converter with SPWM

The SPWM technique treats each modulating voltage as a separate entity that is compared to the common carrier triangular waveform (V_{car}). A three-phase voltage set (V_{aref}, V_{bref} and V_{cref}) is compared in three separate comparators with a common triangular carrier waveform of fixed amplitude as shown in the figure 4-6. The output of the comparators form the control signals for the three legs of the inverter composed of the switch pairs

$(S_1, S_4), (S_3, S_6),$ and (S_5, S_2), respectively. From these switching signals and the DC bus voltage, phase voltage and phase-to-neutral voltages as shown in figure 4-7 and 4-8 are obtained. Among different modulation type SPWM is selected to analysis the existing DFIG based wind turbine. From equation (3.113), the reactive and active power are related to i_{dg} and i_{qg}respectively. So, the change in active power and reactive power are realized by the change in i_{dg} and i_{qg}.

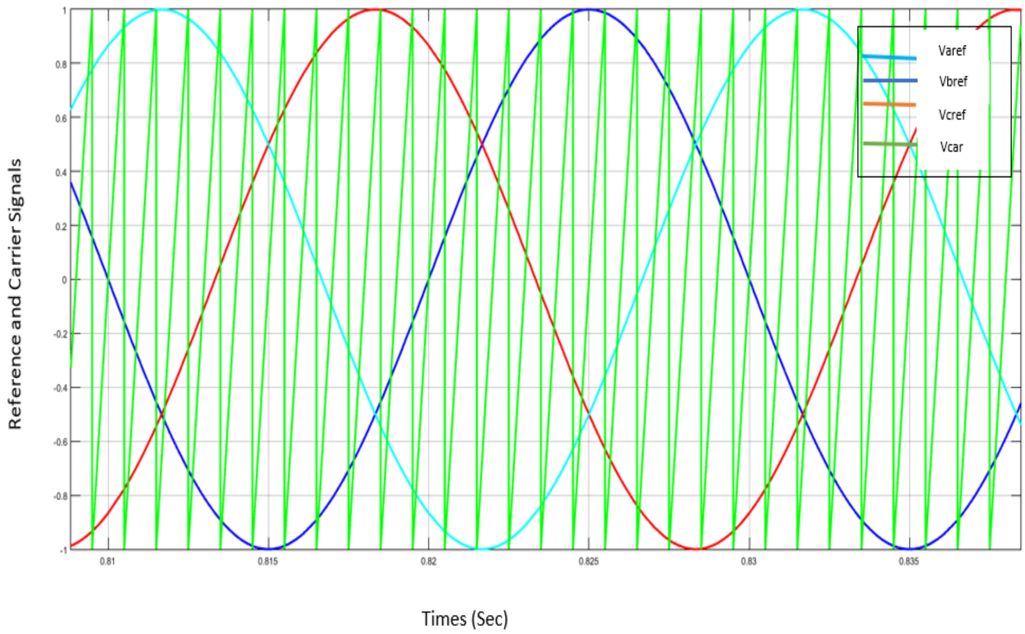

Figure 4-6: Modulating reference signal with triangular signal for SPWM

Figure 4-6 shows the three reference signal voltages (V_a^*, V_b^* , V_c^*) and the triangular signal (V_{car}). The modulation signal is displaced in the time domain by 120° by varies between 0 and 1 and the carrier signal remains constant.

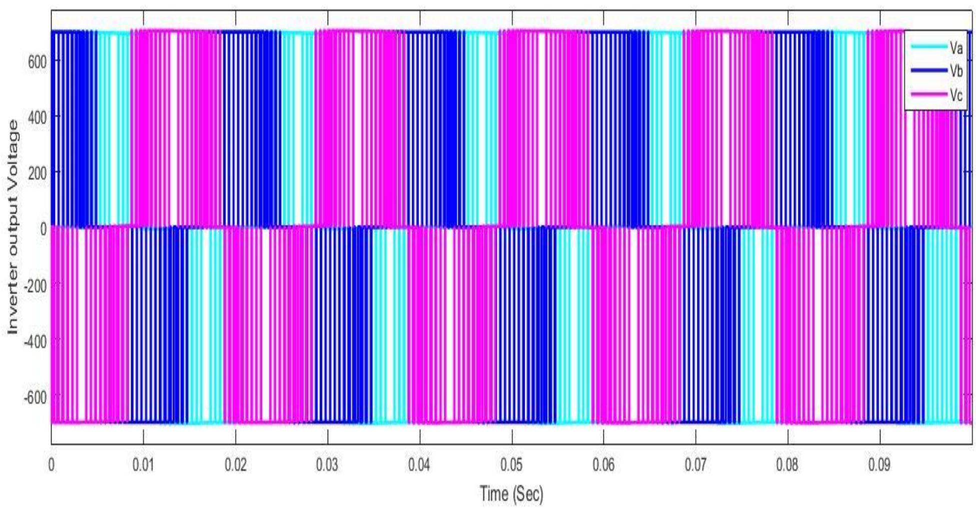

Figure 4-7: Response of Phase voltage for three phase two-level converter

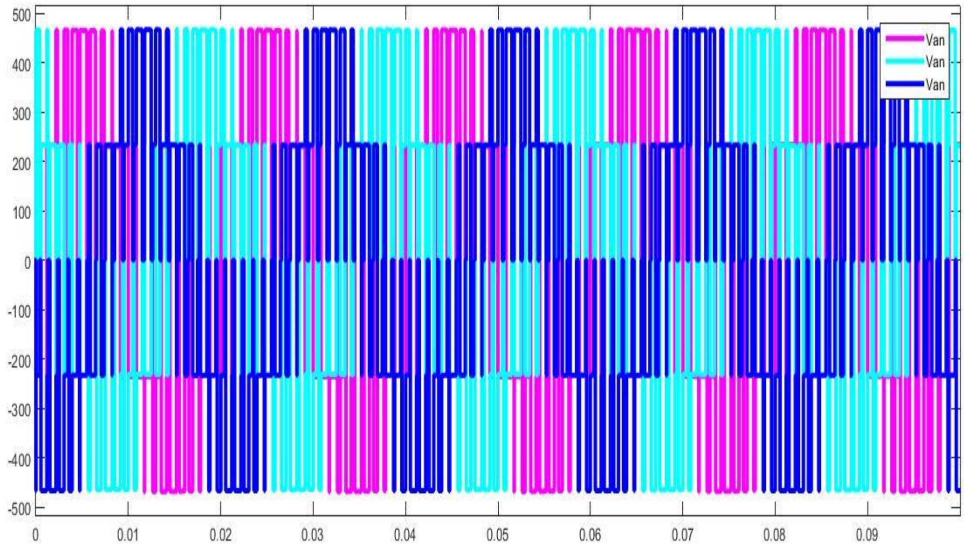

Figure 4-8: Response of Phase to neutral voltage for three phase two-level converter

Figure 4-7 and 4-8 shows the phase output voltage and Phase to neutral voltage of two-level inverter respectively which is generated based on the switching instant signal in each leg of the inverters. The gate pulse for each converter legs are generated based on comparing the reference signal with the triangular signal using SPWM modulation method.

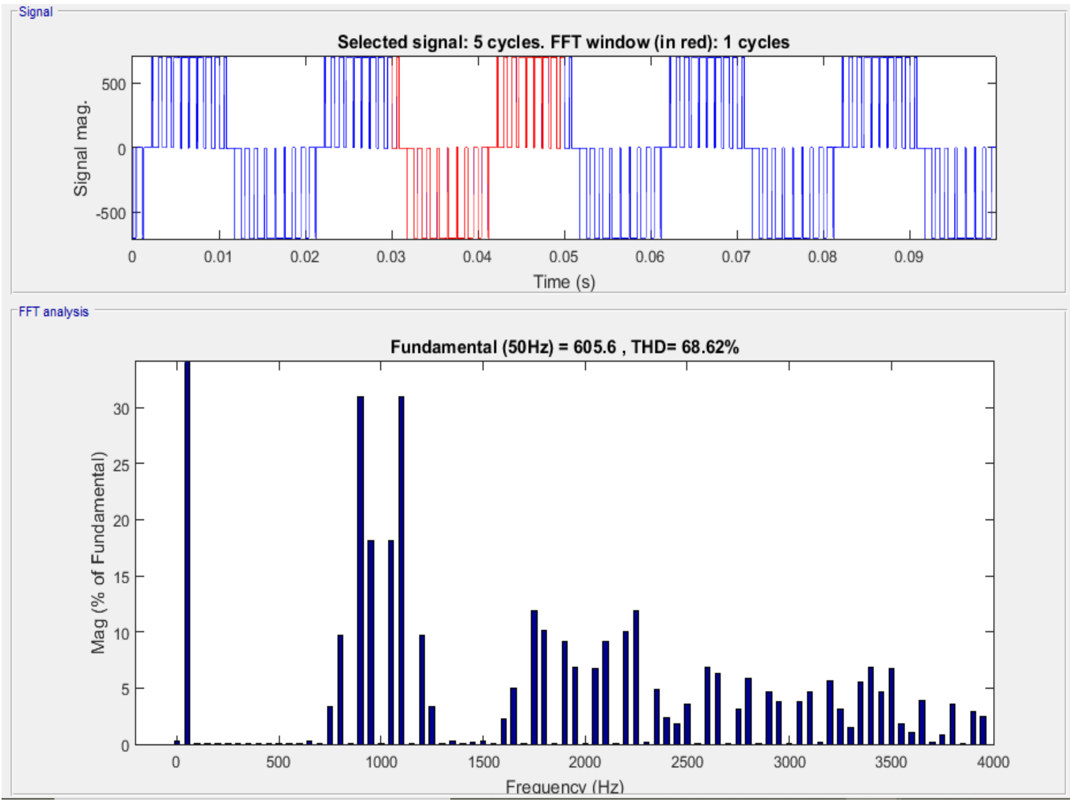

Figure 4-9: FFT analysis of phase voltage

4.1.3. Simulation result of two-level converter with THIPWM

Third-harmonic injection PWM has been used to improve the SPWM technique by adding a third harmonic to the modulation signal. It follows the same SPWM implementation. The difference between third-harmonic and sinusoidal PWM is that the reference of the third harmonic includes third harmonic components as shown in Figure 4-10. This increased the amplitude of fundamental output voltage by 15% more than SPWM.

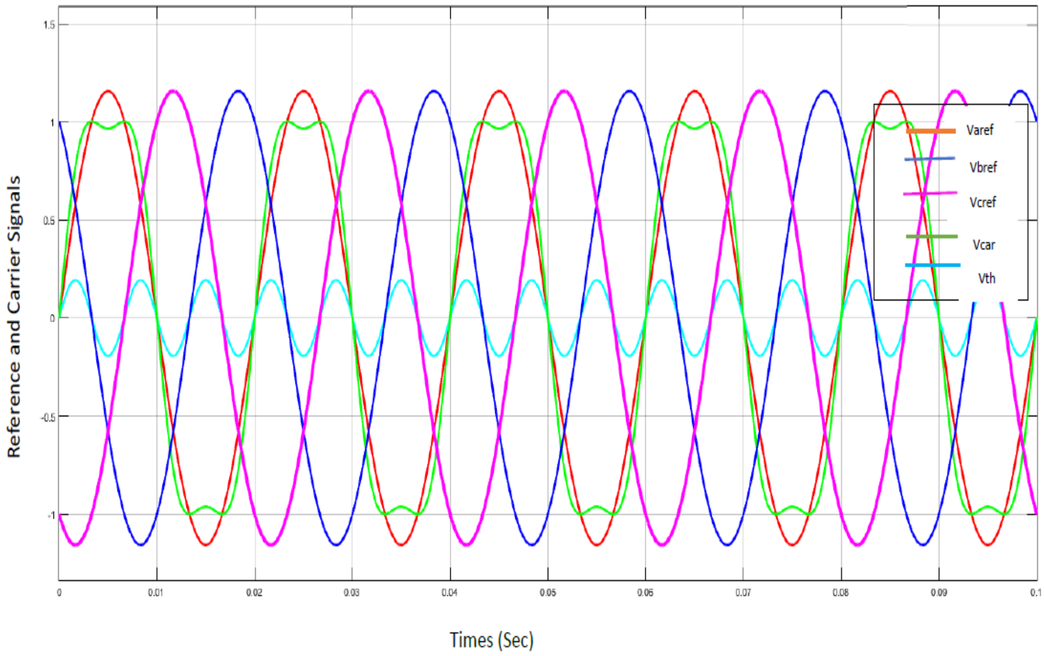

Figure 4-10: Third harmonic injection to the reference signal

THIPWM techniques are applied to two level converters by comparing reference waveform signal with the triangle carrier signal and this technique have higher utilization of the DC-bus voltage and reduction in the total harmonic distortion (THD) of the waveform of output voltages as shown in figure 4-13, compared with the SPWM technique.

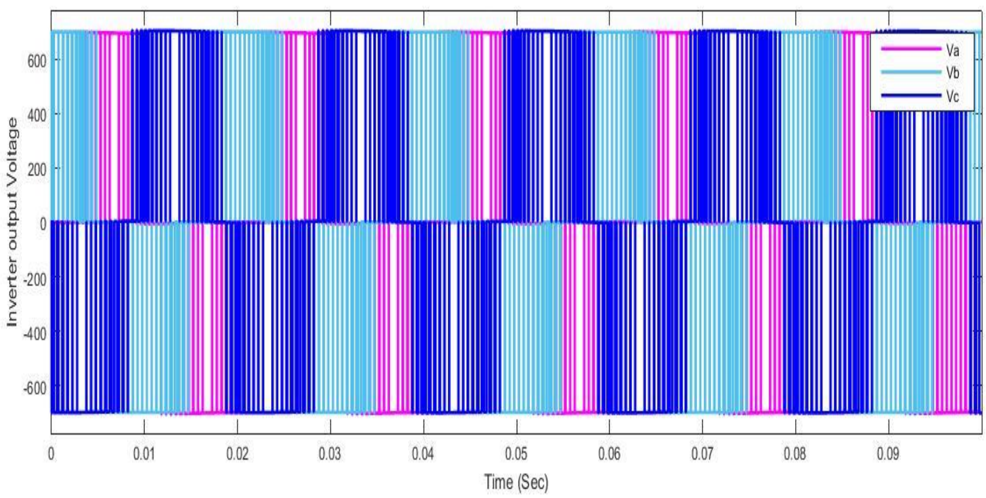

Figure 4-11: Response of inverter phase voltage

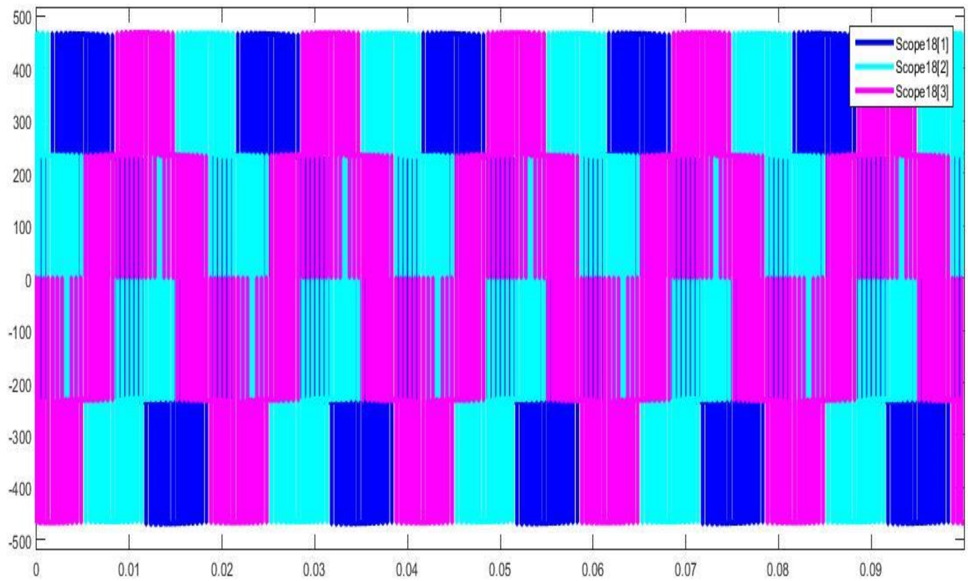

Figure 4-12: Response of Phase to neutral voltage for three phase two-level converter

Figure 4-11 shows the three phase AC output voltage and figure 4-12 shows the phase to neutral voltage of two-level inverter using THIPWM, which is generated based on the switching instant signal in each leg of the inverters. The gate pulse for each converter legs are generated based on comparing the reference signal with the triangular signal.

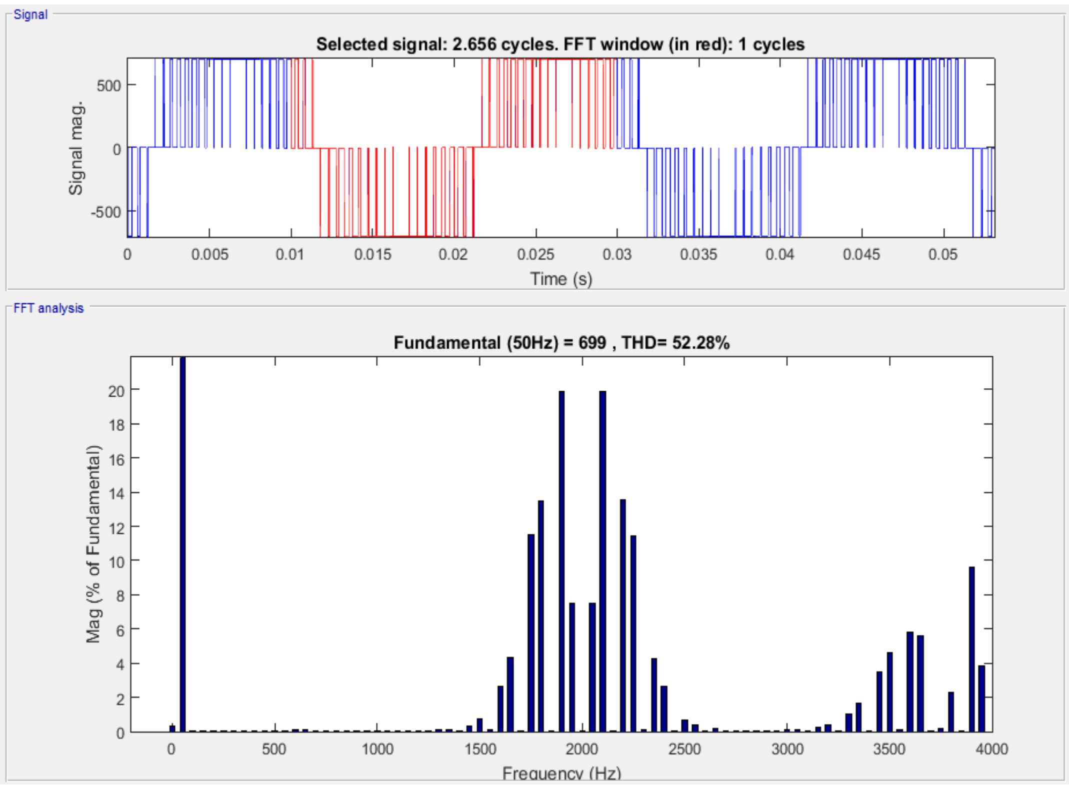

Figure 4-13: FFT analysis of phase voltage

From figure 4-13 the THD value of the output inverter voltage using THIPWM is reduced as compared with SPWM and the fundamental output voltage value is increased.

4.1.4. Three Phase Two-Level Inverter by Using SVPWM Algorithm

Figure 4-15: shows phase output voltage for three phase two level inverter by using SVPWM algorithm (see appendices A MATLAB files for SVPWM and Figure A5: MATLAB Simulink subsystem model of SVPWM for two level converters).

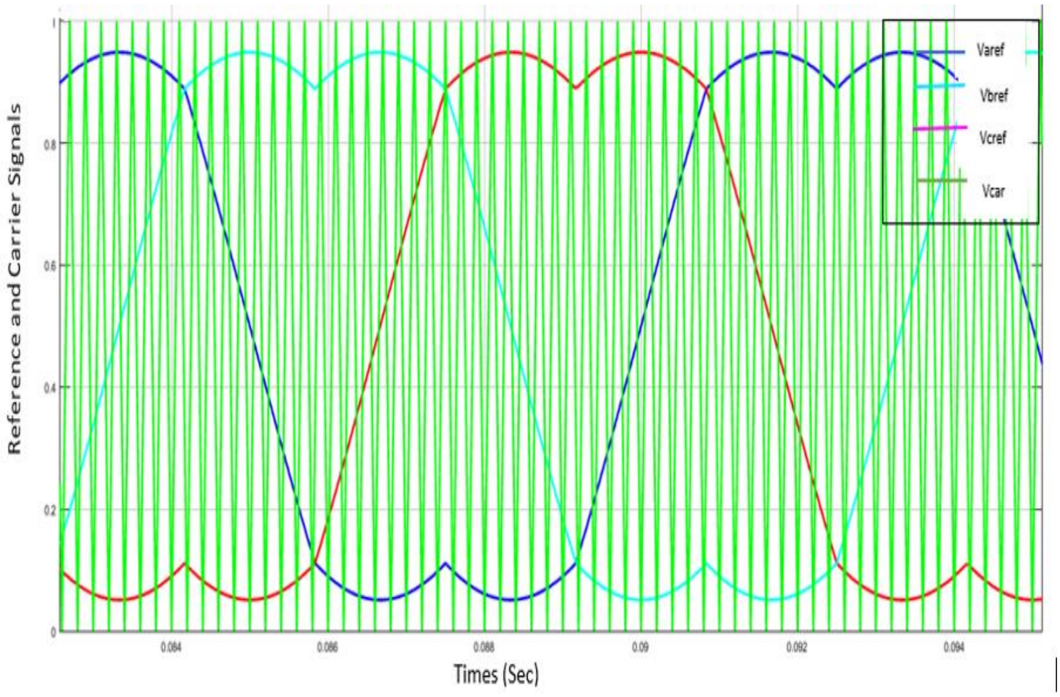

Figure 4-14: Modulating reference signal with triangular signal for SVM

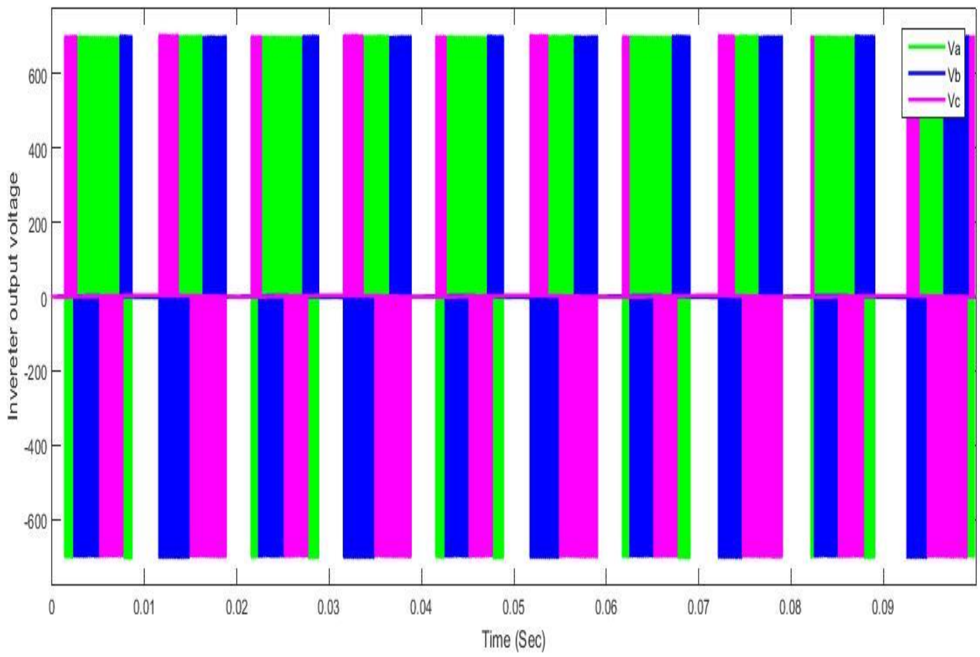

Figure 4-15: Phase output voltage by using SVPWM algorithm

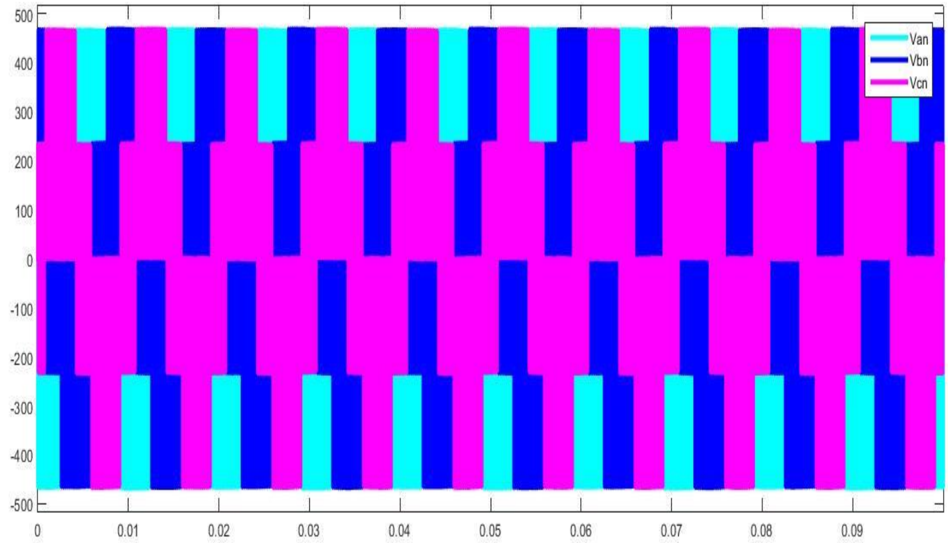

Figure 4-16: Response of Phase to neutral voltage for three phase two-level inverter

As indicated from Figure 4-15 and Figure 4-16, it can be seen that the fundamental phase and phase to neutral voltage amplitude using SVM is similar with THIPWM, but higher than the value found using SPWM and better dc bus voltage utilization. The performance of the farm enhanced due to the reduction of harmonic filters size.

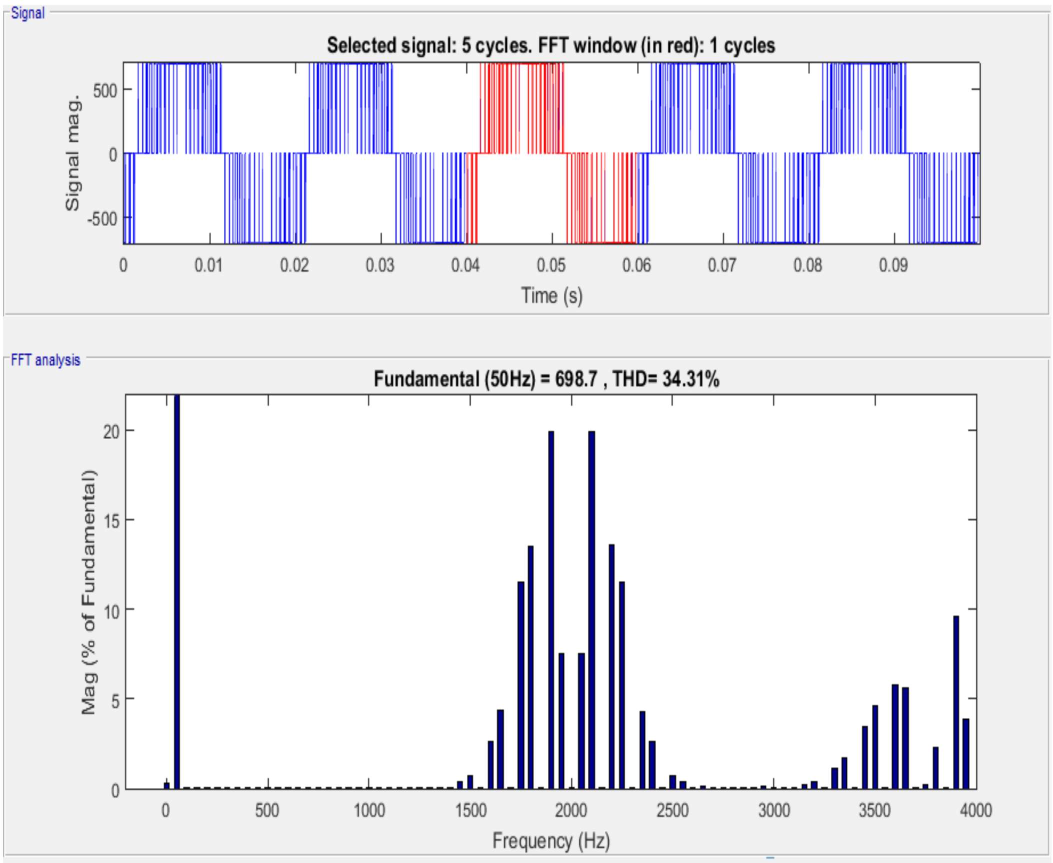

Figure 4-17: FFT analysis of phase voltage

4.1.5. Three Phase Three-Level NPC converter by Using SVPWM Algorithm

Figure 4-18: shows phase output voltage for three phase three level inverter by using SVPWM algorithm (see appendices B MATLAB files for SVPWM and Figure A6: MATLAB Simulink subsystem model of SVPWM for three level converters).

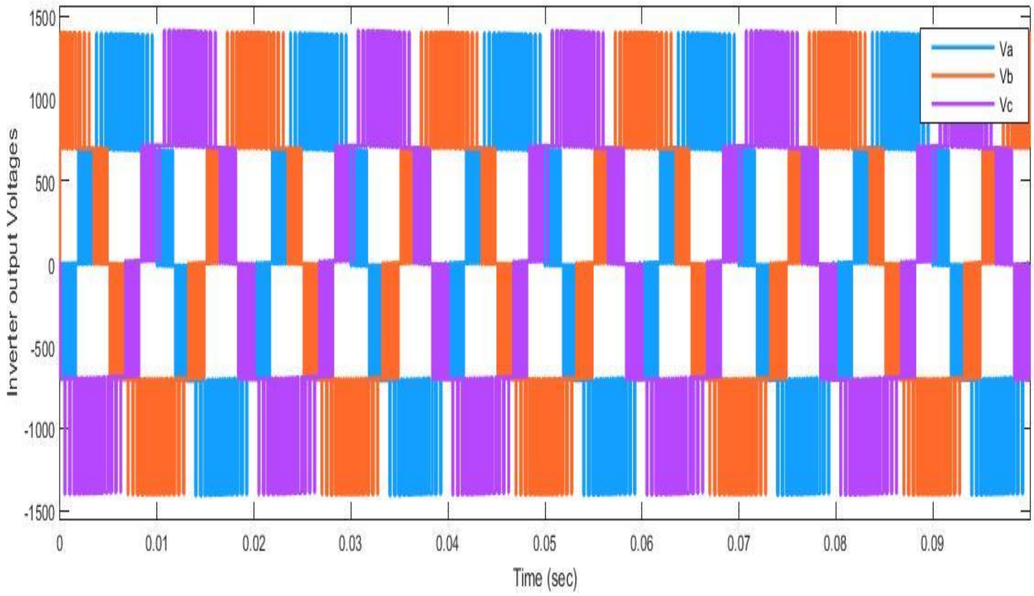

Figure 4-18: The output phase voltage for three phase three-level NPC inverter

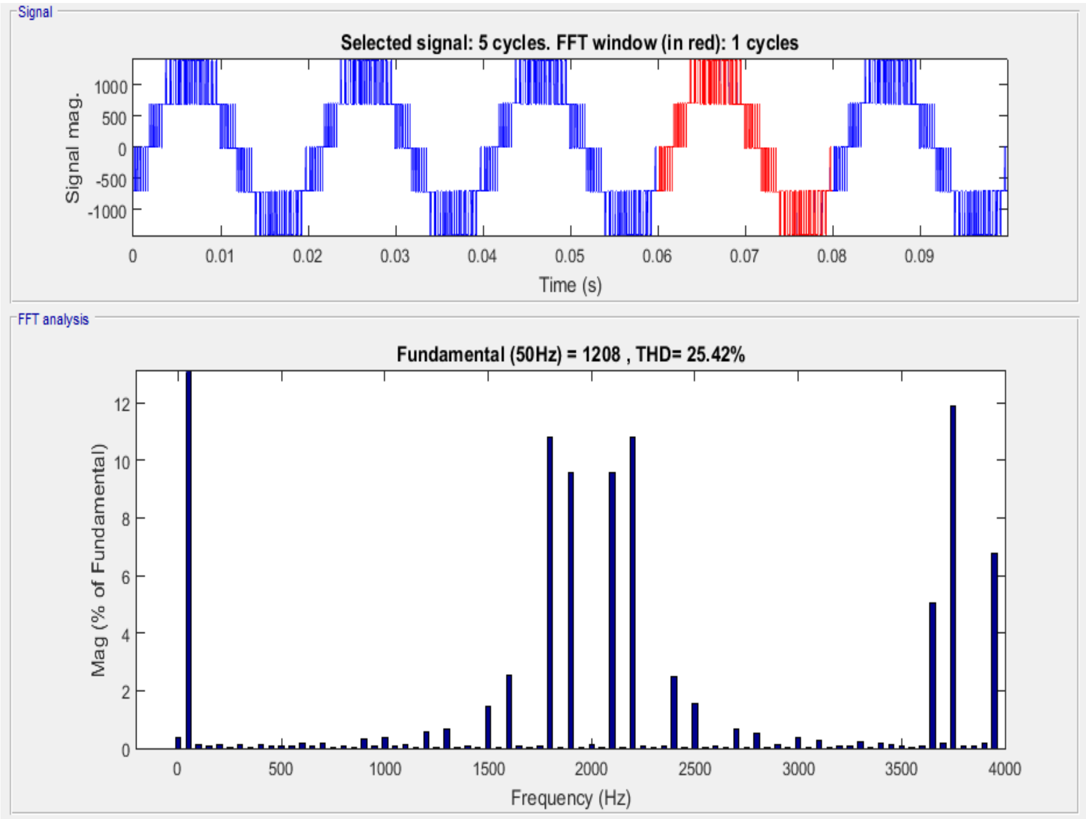

Figure 4-19: FFT analysis of phase voltage

Table 4-1: Comparisons between different converter topology with SPWM, THIPWM and SVPWM techniques.

Technique	**SPWM**		**THIPWM**		**SVM**	
Converter Topology	Output Phase voltage (peak) volt	THD (%)	Output Phase voltage (peak) volt	THD (%)	Output Phase voltage (peak) volt	THD (%)
Two level converters	605.6	68.62	699	52.28	698.7	34.31
Three level NPC converter					1208	25.42

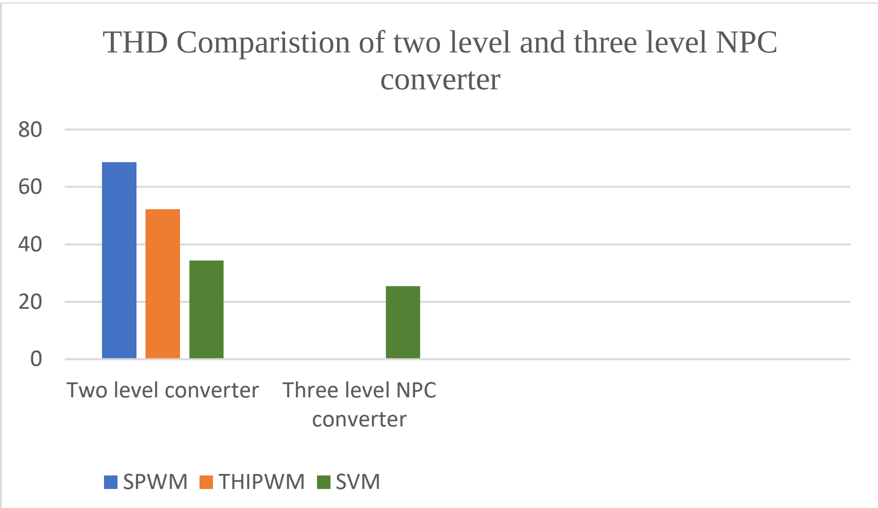

Figure 4-20: Graphical representation of different converter topology with SPWM, THIPWM and SVPWM techniques.

Table 4.1 and figure 4-20 indicate the comparison of two-level converter with different PWM techniques such as SPWM, THIPWM, and SVM and three level converters with SVM in a grid connected wind power system. SPWM method has less DC bus utilization and higher THD than the other PWM method. To minimize this higher THD value with in the international standard limit STD 519, a large size filter is required to connect the converter in to the grid. This can increase the cost of the filter used in the DFIG based wind energy conversion system and reduce the performance and efficiency of the overall wind farm system. Among various modulation techniques, SVM is the proposed PWM method to have better DC bus utilization and reduce the THD value. AS seen from the simulation result, THD value in SVM is reduced compared to SPWM and THIPWM in two level and three level NPC converter topology. The required filter size in order to reduce THD obtained using SVM method in the grid side converter is much reduced as compared to the two PWM technique.

4.1.6. Grid voltage with Harmonic Analysis

The steady state output of voltage THD values are analyzed using FFT analysis from MATLAB. The simulation is done at the selected PCC of 690V bus bar system. Three phases waveform output of voltage at 690V bus bar system is shown below.

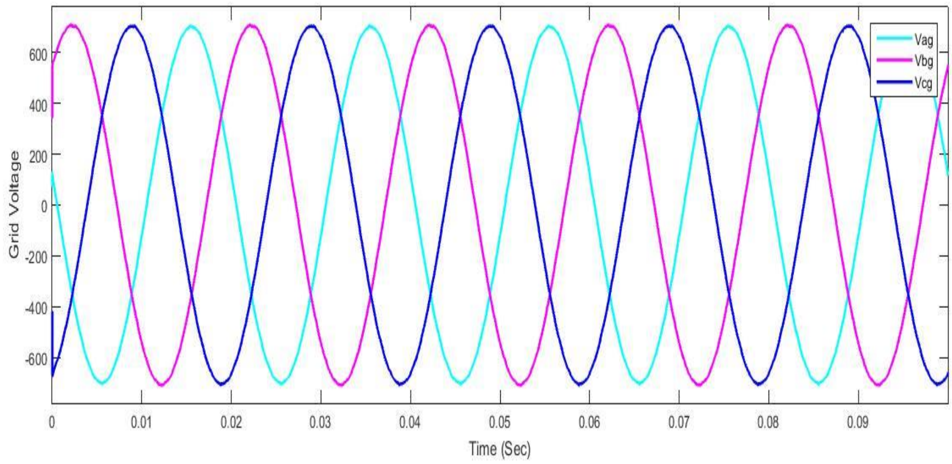

Figure 4-21: Grid side phase voltage after LCL filter in SPWM

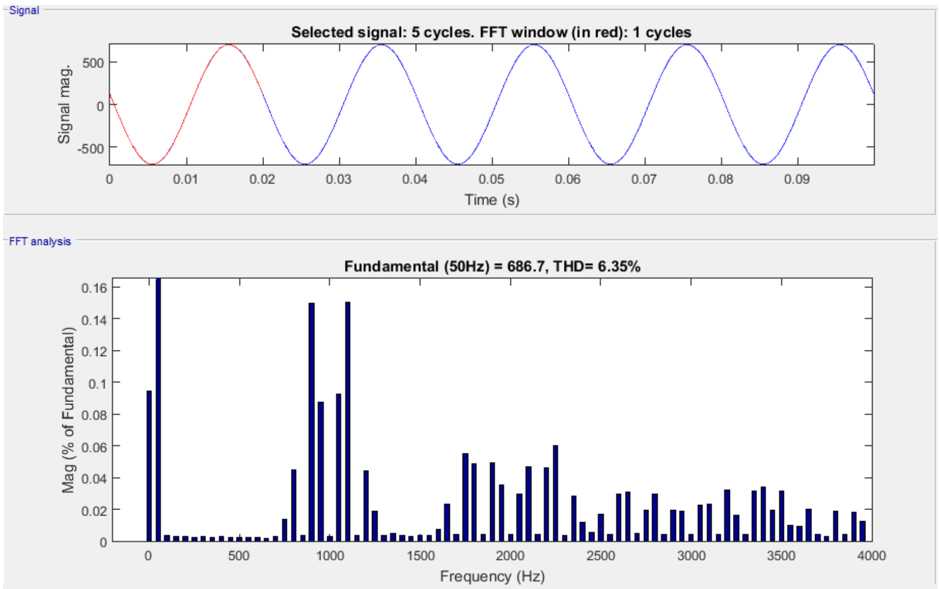

Figure 4-22: FFT analysis of phase voltage

Figure 4-22: shows the THD value found from the MATLAB/Simulink. As compared to the IEEE power quality standard and guideline, this result is found to be not within permissible limit. As indicated in the FFT analysis the THD value using SVM is 6.35 %, which is less than 5% is also validated with respect to IEEE standard. The harmonic filters used in the wind farm have large size to cancel the amount of harmonic voltage values displayed.

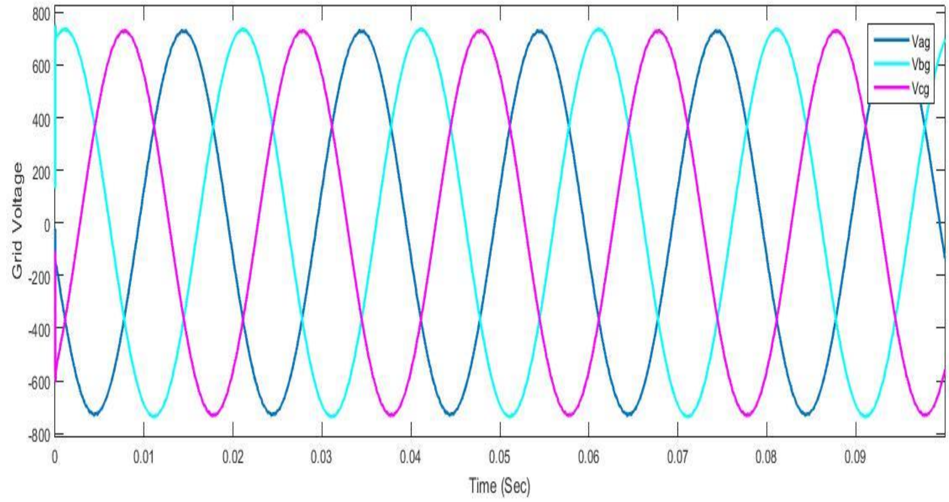

Figure 4-23: Grid side phase voltage after LCL filter in THIPWM

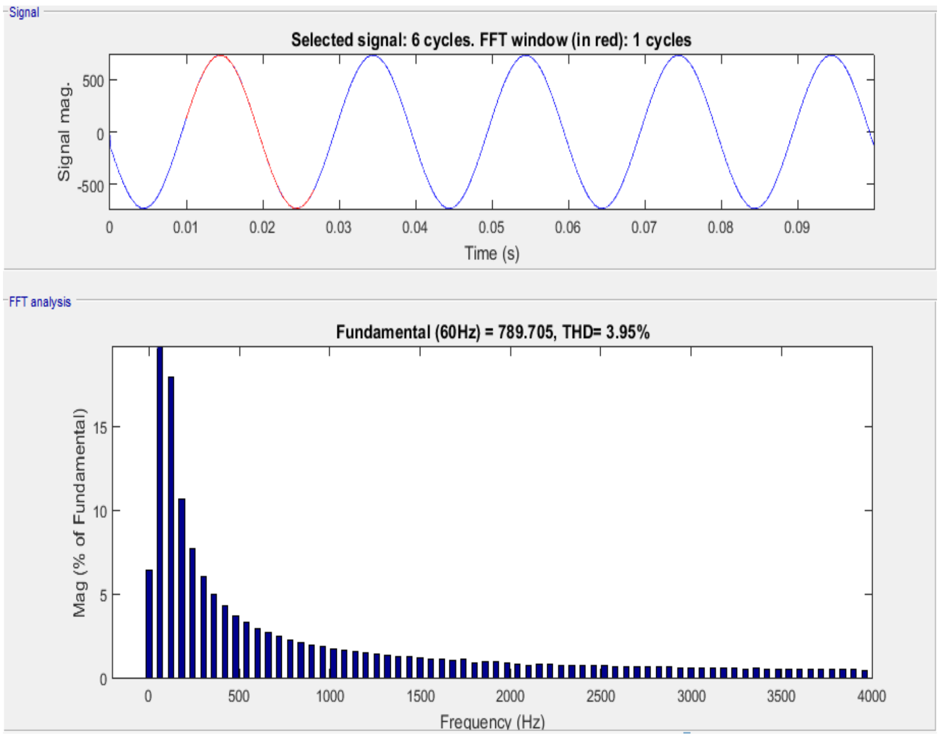

Figure 4-24: Harmonic analysis for THIPWM

Figure 4-24: shows the THD value found from the MATLAB/Simulink. As compared to the IEEE power quality standard and guideline, this result is found to be within permissible limit. As indicated in the FFT analysis the THD value using SVM is 3.95 %, which is less than 5% is also validated with respect to IEEE standard.

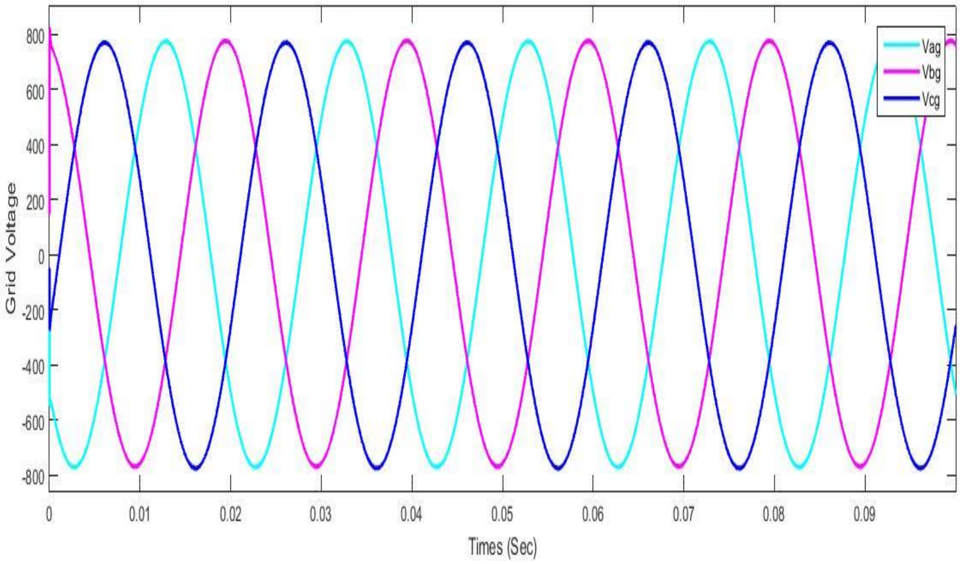

Figure 4-25: Grid side phase voltage after LCL filter in SVM

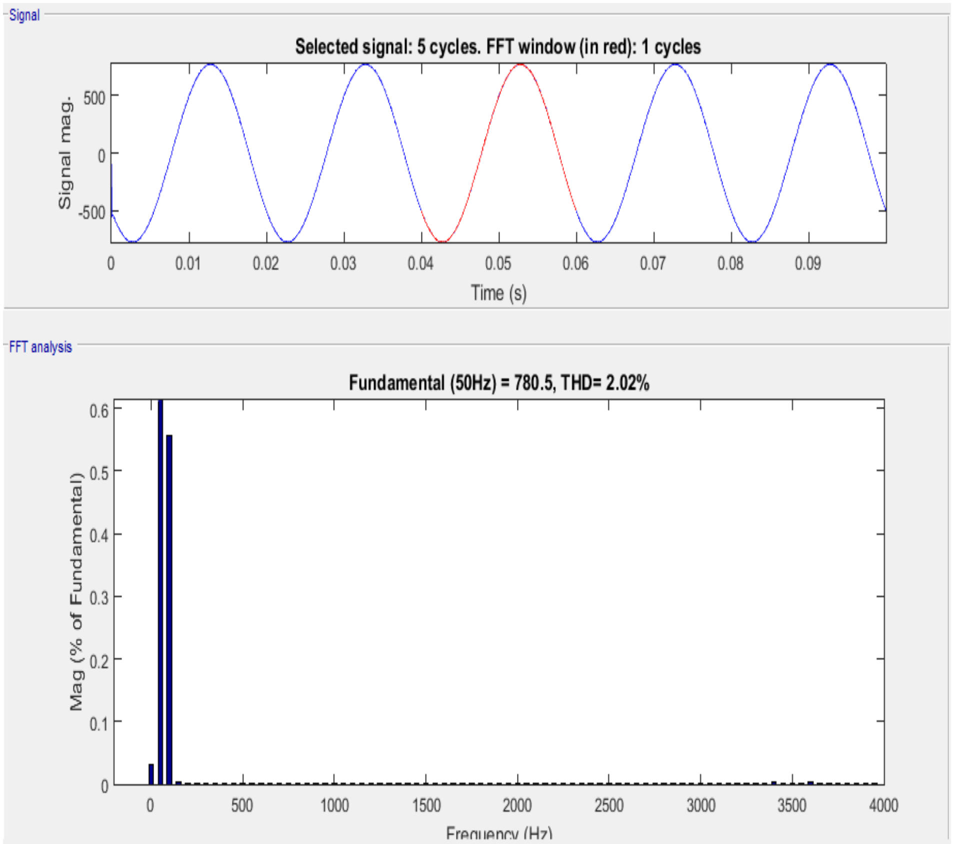

Figure 4-26: Harmonic analysis for SVM

Figure 4-26: indicates the THD value found from the MATLAB/Simulink. As compared to the IEEE power quality standard and guideline, this result is found to be within permissible limit. As indicated in the FFT analysis the THD value using SVM is 2.02%, which is less than 5% is also validated with respect to IEEE standard.

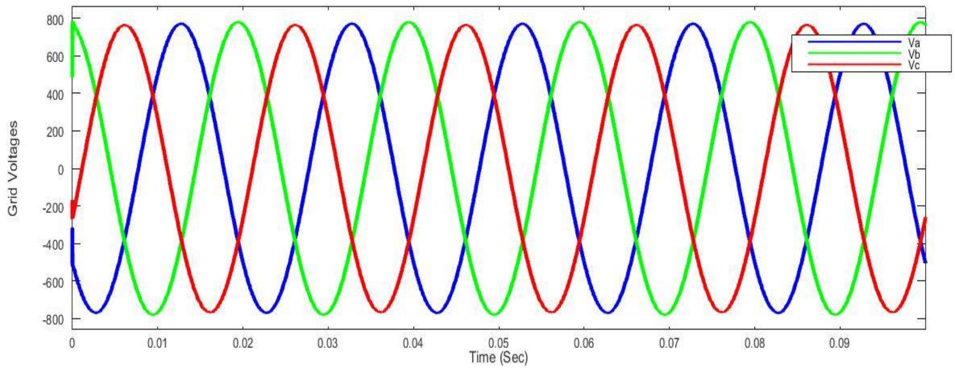

Figure 4-27: Grid side phase voltage after LCL filter in SVM

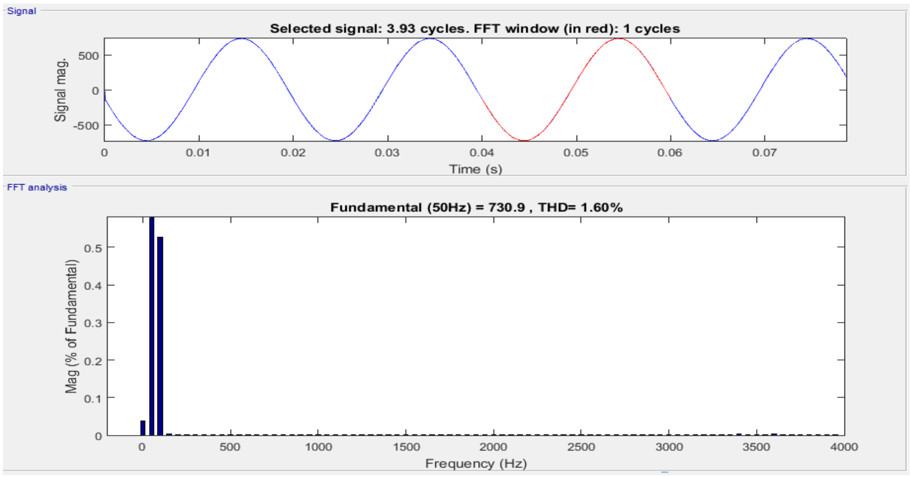

Figure 4-28: Grid side voltage after LCL filter in SVM

Figure 4-28: shows the THD value found from the MATLAB/Simulink. As compared to the IEEE power quality standard and guideline, this result is found to be within permissible limit. As indicated in the FFT analysis the THD value using SVM is 1.60%, which is less than 5% is also validated with respect to IEEE standard.

ANSI/IEEE 519 Voltage Distortion limits:

This standard predominantly lays out limits for Total Harmonic Distortion and Individual Harmonic Distortion for voltage distortions at different voltage levels in the power system. The limits and requirements to be met using such a standard are shown in table 4.2.

Table 4-2: ANSI/IEEE 519 Voltage Distortion Limits:

Bus Voltage	Individual harmonics distortion, %	Voltage THD, %
V<69 kV	3.0	5.0
69≤V<161 kV	1.5	2.5
V≥161 kV	1.0	1.5

Table 4-3: Comparison of different converter topologies

S.NO	Topology	THD (%)
1	Two level grid connected converter with SPWM	6.35
2	Two level grid connected converter with THIPWM	3.95
3	Two level grid connected converter with SVM	2.02
4	Three level NPC grid connected converter with SVM	1.60

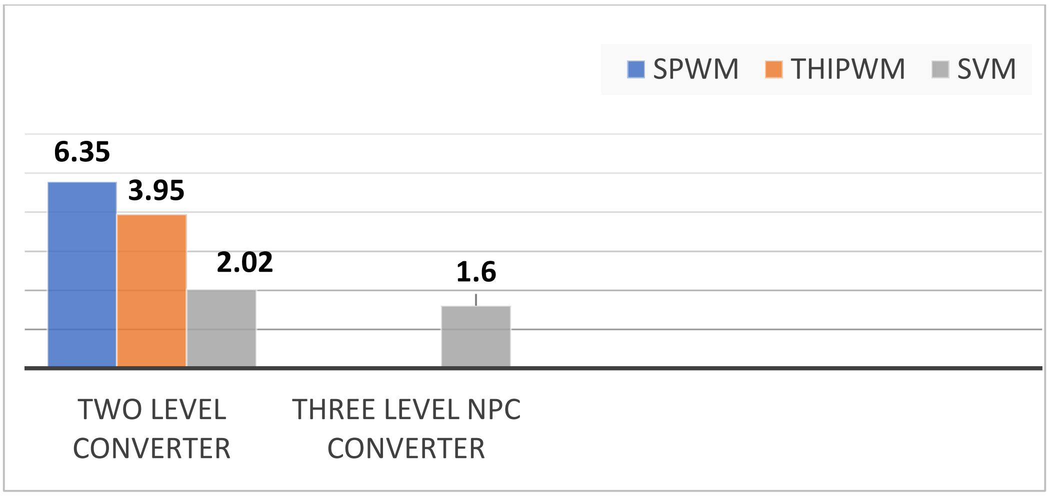

Figure 4-29: Graphical representation of different converter topology with SPWM, THIPWM and SVPWM techniques.

From table 4-3 and figure 4-29, it shows that the fundamental voltage level at each rotor speed operation is almost at the same value when using two-level converter with THIPWM or SVM methods. It means that give very less influence to the generation of harmonic distortion. The three-level NPC converter produced lower voltage THD than the two-level converter using SVM with maximum different about 0.42%.

For all cases except two level converters with SPWM, the voltage THD at the low voltage grid of the DFIG based WT during the entire rotor speed operation points are still lower than 5% limit required by the standard IEEE STD-519. It can be concluded that for the DFIG based WT system studied in this thesis, using either two-level converter or three-level NPC converter using SVM produced acceptable low level of voltage THD at low voltage grid for the entire rotor speed operations.

CHAPTER FIVE

5. CONCLUSION AND RECOMMENDATION

5.1. Conclusion

In this thesis, the performances of doubly fed induction generator (DFIG) based wind turbine (WT) during steady state and dynamics operation in two alternative scenarios, namely using different PWM types and different converter topologies have been studied. The performance criteria include the voltage total harmonic distortion in the grid side converter, the converter power losses and decoupled control of active and reactive powers.

The study focuses on the development of back-to-back converter in terms of its topologies design and switching schemes. Two different converter topologies, namely two-level converter which is the commonly used topology for DFIG and three-level NPC converter which is known to having better performances have been selected.

In many semiconductor switching devices available nowadays, insulated gate bipolar transistor (IGBT) has been chosen since it has a capability of self-commutated and commonly used in converter for wind turbine application. Dependent on their availability in the market and commutation voltage, IGBT class for the two-level converter and three-level NPC converter have been chosen.

A detailed simulation model of a DFIG-based wind turbine system is developed for the 1.5 MW wind turbine connected to the power grid. All of the primary components are modelled including DFIG and back-to-back converter. In this thesis, the modelling and control of a doubly-fed induction generator-based wind turbine-generator system have been considered. More specifically, the modelling of different components, the control strategies for the back-to-back converter have been studied and analyzed in detail. As a basis of the research, the model of a wind turbine-generator system equipped with a doubly-fed induction generator was developed in a MATLAB/Simulink. Two control schemes were implemented in the wind turbine system, which are, the machine-side converter control and grid-side converter control. The objective of the vector-control scheme for the grid-side converter controller is used to maintain constant voltage across the capacitor and produce a unity power factor operation of the grid.

As seen from the simulation results, the performance of two level and three level NPC converter-based vector controlled DFIG is investigated under steady state operation conditions. The main focus of this thesis is to use wind energy with minimal harmonic distortion levels and the filter L_1 in the inverter side is reduced by 0.3265mH and L_2 in the grid side reduced by 0.285mH used in ADAMA II wind farm. A two-level converter in the grid side using SPWM, THIPWM and SVM technique is capable to maintain voltage THD levels to 6.35%, 3.95% and 2.02% at rated wind speed conditions of 12 m/s respectively. A three level NPC converter is capable to maintain THD levels at normal wind speeds at 1.60%. This paper investigates on dynamic modeling of DFIG based WECS. The main contribution in the proposed model is to simulate the internationally well adopted DFIG grid interconnection using different converter topology with SPWM, THIPWM and SVM techniques and to achieve the IEEE 519 criteria of THD which is less than 5%. So DFIG using SVPWM topology is best suited for practical implementation and dynamic response analysis of DFIG for decoupled control of active and reactive powers.

5.2. Recommendations for Future Work

In this thesis work, as it can be said in the conclusion section, there obtained best results. However, still there are some limitations that need additional investigations for further research directions.

- ❖ Direct torque control and direct power control should be considered, because of the advantages of no current regulators, no coordinate transformations and specific modulations, and no current control loops.
- ❖ Matrix converters are another interesting topic because of their ac to ac transformation ability.
- ❖ The transient behaviors of the DFIG-based wind turbine system under disturbances of grid failures should be studied.
- ❖ The laboratory set-up for the DFIG and the back-to-back has not been conducted due to lack facilities. For best validation of simulation results, this can be taken into account in further works.
- ❖ The results presented in this thesis were obtained only from simulation environment. It is recommended verifying the results through experimental evaluation to check their applicability in the real world. Regarding the cost evaluation, since the cost of electrical components vary dependent on manufacturer, it is also necessary to have the cos.t comparison from other different manufacturers.

Reference

[1] M. Tazil, V. Kumar, R.C. Bansal, S. Kong, Z.Y. Dong, W. Freitas, and H.D. Mathur (2010) "Three-Phase Doubly Fed Induction Generators: An Overview," IEEE Transaction on Electronic Power, vol. 4, pp 75–89.

[2] W. Xu L., "Torque and Reactive Power Control of a Doubly Fed Induction Generators," 2013.

[3] Petersson, A, Analysis, Modeling and control of Doubly-Fed generators for wind turbine, Goteborg.: halmers University, 2005.

[4] G. Abad, J. Lo´pez and M. A. Rodri'guez, "Doubly Fed Induction Machine: Modeling and Control for Wind Energy Generation," First Edi.,2011, IEEE Press and John Wiley and Sons Ltd.

[5] Zarei, M.E, and Asaei, B. "Combined Vector Control and Direct Power Control Methods for DFIG Under Normal and Unbalanced and Distorted Grid Voltage Conditions," Proc. of the 4th power elec., drive sys. and techno. conf. (PEDSTC), Tehran, Iran, 13–14 Feb. 2013; pp. 107–112.

[6] Raja Ram Kumar, Sunil Kumar, and Alok Yadav, "Comparison of PWM Techniques and Inverter Performance," IOSR Journal of Electrical and Electronics Engineering (IOSR-JEEE), ISSN: 2278-1676 Volume 4, Issue 1 (Jan. - Feb. 2013), PP 18-22.

[7] H. Salehfar, "DSP-Based Implementation of Vector Control of Induction Motor Drives,"Taylor & Francis Group, LLC, 2005.

[8] R.K. Pongiannan, and N. Yadaiah, "FPGA Based Three Phase Sinusoidal PWM VVVF Controller," IEEE ICEES (International Conference on Electrical Energy Systems), pp. 34-39, 2011.

[9] A. Aktaibi, A. Rahman, and A. Razali, "A Critical Review of Modulation Techniques." Available from: http://necec.engr.mun.ca/ocs2010/viewpaper.php?id=13.

[10] K.V. Kumar, P.A. Michael, J.P. John and S.S. Kumar, "Simulation and Comparison of SPWM and SVPWM Control for Three Phase Inverter," Asian Research Publishing Network, Vol. 5, No. 7, pp. 61-74, July 2010.

[11] J.Y. Lee, and Y.Y. Sun, "A New SPWM Inverter with Minimum Filter Requirement," International Journal of Electronics, Vol. 64, No. 5, pp. 815-826, 2001.

[12] H. Quan, Z.Gang and C. Jie, Z. Wu, "Study of A Novel Over-modulation Technique Based on Space-Vector PWM," IEEE Computer Distributed Control and Intelligent Environmental Monitoring (CDCIEM), pp. 295-298, 2011.

[13] A.W. Leedy, and R.M. Nelms, "Harmonic Analysis of a Space Vector PWM Inverter using the Method of Multiple Pulses," IEEE Transactions on Industrial Electronics, Vol. 4, pp. 1182-1187, July 2006.

[14] K. Zhou and D. Wang, "Relationship Between Space-Vector Modulation and Three Phase Carrier Based PWM: A Comprehensive Analysis," IEEE Transactions on Industrial Electronics, Vol. 49, No. 1, pp. 186-196, February 2002.

[15] W.F. Zhang and Y.H. Yu, "Comparison of Three SVPWM Strategies," Journal of Electronic Science and Technology of China, Vol. 5, No. 3, pp. 283-287, September 2007.

[16] J. Holtz, "On Continuous Control of PWM Inverters in Over-modulation Range Including the Six-Step," IEEE Transactions on Power Electronics, Vol. 8, No. 4, pp. 546-553, 1993.

[17] D.C. Lee, "A Novel Over-modulation Technique for Space Vector PWM inverters," IEEE Transactions on Power Electronics, Vol. 13, No. 6, pp. 1144-1151, Nov. 1996.

[18] D.G. Holmes and T.A. Lipo, "Pulse Width Modulation for Power Converters," John Wiley & Sons, Inc. 2003.

[19] G.K. Dubey, "Fundamental of Electrical Drives", Narosa, 2011.

[20] L. Munteanu, A.L. Bratcu, N. Cutululis and E. Caenge, "Optimal Control of Wind Energy Systems" Advances in Industrial Control, 2008.

[21] A.A.K. Gupta, B.H. Bhushan and C.P. Samuel, "Generator Topologies with Power Electronics Converters for a Wind Energy Conversion System: A Review," 2011.

[22] M. Molinas, B. Naess, W. Gullvik and T. Undeland, "Cage Induction Generators for Wind Turbines with Power Electronics Converters in the Light of the New Grid Codes," EPE 2005.

[23] S.A. Shaheen, H.M. Hasanien and M.A. Badr, "Study on Doubly Fed Induction Generator Control," Proceedings, MEPCON, December.

[24] Juan Manuel Carrasco, Jan T. Bialasiewicz, and José Ignacio León, "Power-Electronic Systems for the Grid Integration of Renewable Energy Sources: A Survey" IEEE Transactions on Industrial Electronics, vol. 53, no. 4, August 2006.

[25] A. Nabae, I. Takahashi, and H. Akagi, "A new neutral-point-clamped PWM inverter," IEEE Trans. Ind. Appl., vol. IA-17, no. 5, pp. 518–523, Sep./Oct. 2009.

[26] Bin Wu, "High-Power Converters and AC Drives," A John Wiley & Sons, Inc., Publication, New York, NY, USA: Wiley, 2006.

[27] J. Rodriguez, S. Bernet, B. Wu, J. O. Pontt, and S. Kouro, “Multilevel voltage-source-converter.”

[28] M. H. Rashid, “Power Electronics, 2nd ed. Englewood Cliffs, NJ, USA: Prentice-Hall, 1993 Topologies for Industrial Medium-Voltage Drives,” IEEE Trans. Ind. Electron., vol. 54, no. 6, pp. 2930–2945, Dec. 2007.

[29] F. Z. Peng, “Z-Source Inverter,” IEEE Trans. Ind. Appl., vol. 39, no. 2, pp. 504–510, Mar/Apr 2003.

[30] M. H. Rashid, “Power electronics handbook: devices, circuits, and applications handbook, third edition, Butterworth-Heinemann publications, USA, 2011.

[31] Semikron, “Application Fields and Current Performance Limits for Power Semiconductors,” 07 December 2010.

[32] Jin Wang and Damoun Ahmadi, “A Precise and Practical Harmonic Elimination Method for Multilevel Inverters”, IEEE Transactions on Industry Applications, vol. 46, no. 2, pp. 857-865, Mar-Apr 2010.

[33] S. H. Hosseini, M. Ahmadi and S. Ghassem Zadeh, “Reducing the Output Harmonics of Cascaded H-Bridge Multilevel Inverter for Electric Vehicle Applications”, 8th International Conference on Electrical Engineering, Thailand, pp. 752-755, May 2011.

[34] A. K. Bhardwaj, “Modeling and Simulation of Dfig to Grid Connected Wind Power Generation,” No. 4, pp. 6–9, 2016.

[35] Saleh A. M. Saleh, “Wavelet Modulated DC-AC Power Inverters,” PhD Thesis, Memorial University of Newfoundland, April, 2007.

[36] Adel A. Ghandakly and Ziad H. Sbeiti, “A digital Optimal Controller for VSCF Wind Generators,” IEEE Industrial Application Society Annual Meeting, Vol. 2, p.1787–1792, October 2003.

[37] Ahmet M. Hava, Russel J. Kerkman, and Thomas A. Lipo, “A High Performance Generalized Discontinuous PWM Algorithm,” IEEE Applied Power Electronics Conference and Exposition, Vol. 2, pp. 886–894, 23.-27, February 1997.

[38] E. G. Marconi, “Grid Connected Doubly Fed Induction Generator Based Wind Turbine Under LVRT,” vol. 2, no. 1, pp. 45–48, 2014.

[39] BinWu, Yongqiang Lang, Navid Kouro, “Power Conversion and Control of Wind Energy Systems, 2011.”

[40] G. Abad, J. Lopez, M.A. Rodriguez, L. Marroyo, G. Iwanski, “Doubly Fed Induction Machine Modeling and Control for Wind Energy Generation” IEEE Press, John Wiley & Sons, INC., Publication, 2011.

[41] A.A.K. Gupta, B.H. Bhushan and C.P. Samuel, “Generator Topologies with Power Electronics Converters for a Wind Energy Conversion System: A Review”. 2011.

[42] Eduard Ned Mohan, Tore M. Undeland, and William P. Robbins, “Power Electronics: Converters, Applications, and Design,” 3rd Edition. Hoboken, NJ: John Wiley & Sons Inc., 2003.

[43] G. A. Raducu, “Control of Grid Side Inverter,” p. 40, 2008.

[44] Xiaoxu Fan, Yuegang Lv, Yan Bai and Daping Xu. “Hybrid System Modeling and Analysis for Power Grid Side Converter Modulated by SVPWM Technology of the Double-fed Induction Wind Power Generator”, Fourth International Conference on Natural Computation, pp. 143-148, October 2008.

[45] M. B. Tuka and R. Leidhold, “Modeling and Control of a Doubly Fed Induction Generator Using a Back-to-Back Converters in Grid Tied Wind Power System,” pp. 75–80, 2017.

[46] M. Liserre, F. Blaabjerg, and S. Hansen, “Design and control of an LCL-filter-based three-phase active rectifier,” IEEE. Trans. Industrial Applications, vol. 41, pp. 1281-1291, 2005.

[47] Kantar, Emre; Hava, Ahmet M., “Design of Grid Connected PWM Converters Considering Topology and PWM Methods for Low-Voltage Renewable Energy Applications,” Power Electronics Conference (IPEC-Hiroshima 2014 - ECCE-ASIA), 2014 International, vol., no., pp.2034, 2041, 18-21 May 2014.

[48] Y. Tang, P. C. Loh, P. Wang, F. H. Choo and F. Gao, “Exploring Inherent Damping Characteristics of LCL-Filters for Three-Phase Grid-Connected VSI,” IEEE Trans. Power Elec., vol. 27, no. 3, pp. 1433-1443, Mar. 2012.

[49] Moussa Reddak, Abdelmajid Berdai, Anass Gourma, Jamal Boukherouaa, “An Improved Control Strategy using RSC of the Wind Turbine Based on DFIG for Grid Harmonic Currents Mitigation,” International Journal of Renewable Energy Research, Vol.18,No.1,march 2018.

[50] Brahim Metidji, Nabil Taib, Lotfi Baghli, Toufik Rekioua and Seddik Bacha, “Low-Cost Direct Torque Control Algorithm for Induction Motor Without AC Phase Current Sensors,” IEEE transactions on power electronics, volume 27, pp 4132-4139, September 2012.

[51] M. Manuela, “Development of Hybridization Concept for Horizontal Axis Wind / Tidal Systems Using Functional Similarities and Advanced Real-Time Emulation Methods,” pp. 124–125, 2019.
[52] Abd Almula G. M. Gebreel, “Simulation and Implementation of Two level and Three-Level Inverters by Matlab And Rt-Lab,” pp.90-94, 2011.

APPENDIX

Appendix A: M-file for SVPWM for two level converters

M-file for Determine Valpha, Vbeta, and Angle teta:

```
function [Valpha, Vbeta, teta] = Clark (Va, Vb, Vc)
Valpha= Va-Vb/2-Vc/2;
Vbeta= (sqrt (3)/2) *(Vb-Vc);
teta= atan2(Vbeta, Valpha);
```

M-file for sector selection

```
function n = Sectror(teta)
   n=0;
if(teta>0)&&(teta<=pi/3)
   n=1;
end
if(teta>pi/3)&&(teta<=2*pi/3)
   n=2;
end
if(teta>2*pi/3)&&(teta<=pi)
   n=3;
end
if(teta<=0)&&(teta>-1*pi/3)
   n=6;
end
if(teta<=-1*pi/3)&&(teta>-2*pi/3)
   n=5;
end
if(teta<=-2*pi/3)&&(teta>-1*pi)
   n=4;
end
```

M-file for Determine Vref

```
function Vr = Vr(Valpha, Vbeta)
Vr=0;
Vr=sqrt(Valpha^2+Vbeta^2);
```

M-file for Determine angle

```
function phi = PHI(n, teta)
phi=0;
if(n==1)
   phi=teta;
end
if(n==2)
   phi=teta-pi/3;
end
if(n==3)
   phi=teta-2*pi/3;
end
if(n==6)
   phi=teta+pi/3;
end
if(n==5)
   phi=teta+2*pi/3;
end
if(n==4)
   phi=teta+pi;
end
```

M-file for Determine Dwell Time

```
function [T0, T1, T2] = Time(Vr,phi,Vdc, T)
a=Vr/Vdc;
T1=T*a*sin(pi/3-phi)/sin(pi/3);
T2=T*a*sin(phi)/sin(pi/3);
T0=T-T1-T2;
```

M-file for Determine gate signal and their sequences

```
function [S1, S3, S5] = Duty(T0, T1, T2, n)
S1=0;
S3=0;
S5=0;
if (n==1)
   S1=T1+T2+T0/2;
```

```
    S3=T2+T0/2;
    S5=T0/2;
end
if(n==2)
    S1=T1+T0/2;
    S3=T1+T2+T0/2;
    S5=T0/2;
end
if(n==3)
    S1=T0/2;
    S3=T1+T2+T0/2;
    S5=T2+T0/2;
end
if(n==4)
    S1=T0/2;
    S3=T1+T0/2;
    S5=T1+T2+T0/2;
end
if(n==5)
    S1=T2+T0/2;
    S3=T0/2;
    S5=T1+T2+T0/2;
end
if(n==6)
    S1=T1+T2+T0/2;
    S3=T0/2;
    S5=T1+T0/2;
end
```

Appendix B: M-file for space vector pulse width modulation for three level NPC converters

M-file for Determine Valpha, Vbeta, and Angle teta:

```
function [Valpha,Vbeta,deta] = fcn(VA,VB,VC)
Valpha=2/3*(VA-VB/2-VC/2);
Vbeta=2/3*(sqrt(3)/2*VB-sqrt(3)/2*VC);
```

```
deta=atan2(Vbeta,Valpha)
```

M-file for Determine Vref

```
function Vref = fcn(Valpha,Vbeta)
Vref=sqrt(Valpha^2+Vbeta^2)
```

M-file for sector selection

```
function n = SECTOR(deta)
n=0
if(deta>=0)&&(deta<pi/3)
   n=1;
end
if(deta>=pi/3)&&(deta<2*pi/3)
   n=2;
end
if(deta>=2*pi/3)&&(deta<pi)
   n=3;
end
if(deta>=-pi/3)&&(deta<0)
   n=6;
end
if(deta>=-2*pi/3)&&(deta<-pi/3)
   n=5;
end
if(deta>=-pi)&&(deta<-2*pi/3)
   n=4;
end
```

M-file for Determine angle

```
function phi = fcn(n,deta)
phi=0;
if(n==1)
   phi=deta;
end
if(n==2)
   phi=deta-pi/3;
end
```

```
if(n==3)
   phi=deta-2*pi/3;
end
if(n==6)
   phi=pi/3+deta;
end
if(n==5)
   phi=2*pi/3+deta;
end
if(n==4)
   phi=pi+deta;
end
function y = fcn(Vref,phi,VDC)
y=0;
m=Vref/(2/3*VDC);
m1=m*2/sqrt(3)*sin(pi/3-phi);
m2=m*2/sqrt(3)*sin(phi);
if(m1<0.5)&&(m2<0.5)&&(m1+m2<0.5)
   y=1;
end
if(m1<0.5)&&(m2<0.5)&&(m1+m2>0.5)
   y=2;
end
if(m1>0.5)
   y=4;
end
if(m2>0.5)
   y=3;
end
```

M-file for Determine Dwell Time

```
function [TA,TB,TC] = fcn(Vref,y,phi,UDC,Ts)
TA=0;
TB=0;
TC=0;
```

```
m=Vref/(2/3*UDC);
k=2/sqrt(3)*m*Ts;
if(y==1)
   TA=2*k*sin(pi/3-phi);
   TB=Ts-2*k*sin(pi/3+phi);
   TC=2*k*sin(phi);
end
if(y==2)
   TA=Ts-2*k*sin(phi);
   TB=2*k*sin(pi/3+phi)-Ts;
   TC=Ts-2*k*sin(pi/3-phi);
end
if(y==3)
   TA=2*k*sin(phi)-Ts;
   TB=2*k*sin(pi/3-phi);
   TC=2*Ts-2*k*sin(pi/3+phi);
end
if(y==4)
   TA=2*Ts-2*k*sin(pi/3+phi);
   TB=2*k*sin(phi);
   TC=2*k*sin(pi/3-phi)-Ts;
end
```

M-file for Determine gate signal and their sequences

```
function [S1A,S2A,S1B,S2B,S1C,S2C] = fcn(y,TA,TB,TC,TS)
S1A=0;
S2A=0;
S1B=0;
S2B=0;
S1C=0;
S2C=0;
if(y==1)
   S1A=TC/4+TA/4;
   S2A=TS/2;
   S1B=TC/4;
```

```
    S2B= TS/2-TA/4;
    S1C=0;
    S2C=TS/2-TA/4-TC/4;

end
if(y==2)
    S1A=TS/2-S2B;
    S2A=TS/2-S1B;
    S1B=TS/2-S2C;
    S2B= TS/2-S1C;
    S1C=TS/2-S2A;
    S2C=TS/2-S1A;

end
if(y==3)
    S1A=S1C;
    S2A=S2C;
    S1B=S2A;
    S2B=S1A;
    S1C=S2B;
    S2C=S1B;

end
if(y==4)
    S1A=TS/2-S2A;
    S2A=TS/2-S1A;
    S1B=TS/2-S2B;
    S2B= TS/2-S1B;
    S1C=TS/2-S2C;
    S2C=TS/2-S1C;

end
if(y==5)
    S1A=S1B;
```

```
    S2A=S2B;
    S1B=S2C;
    S2B=S1C;
    S1C=S2A;
    S2C=S1A;

end
if(y==6)
    S1A=TS/2-S2C;
    S2A=TS/2-S1C;
    S1B=TS/2-S2A;
    S2B= TS/2-S1A;
    S1C=TS/2-S2B;
    S2C=TS/2-S1B;
end
```

Appendix C: MATLAB Simulink Modeling

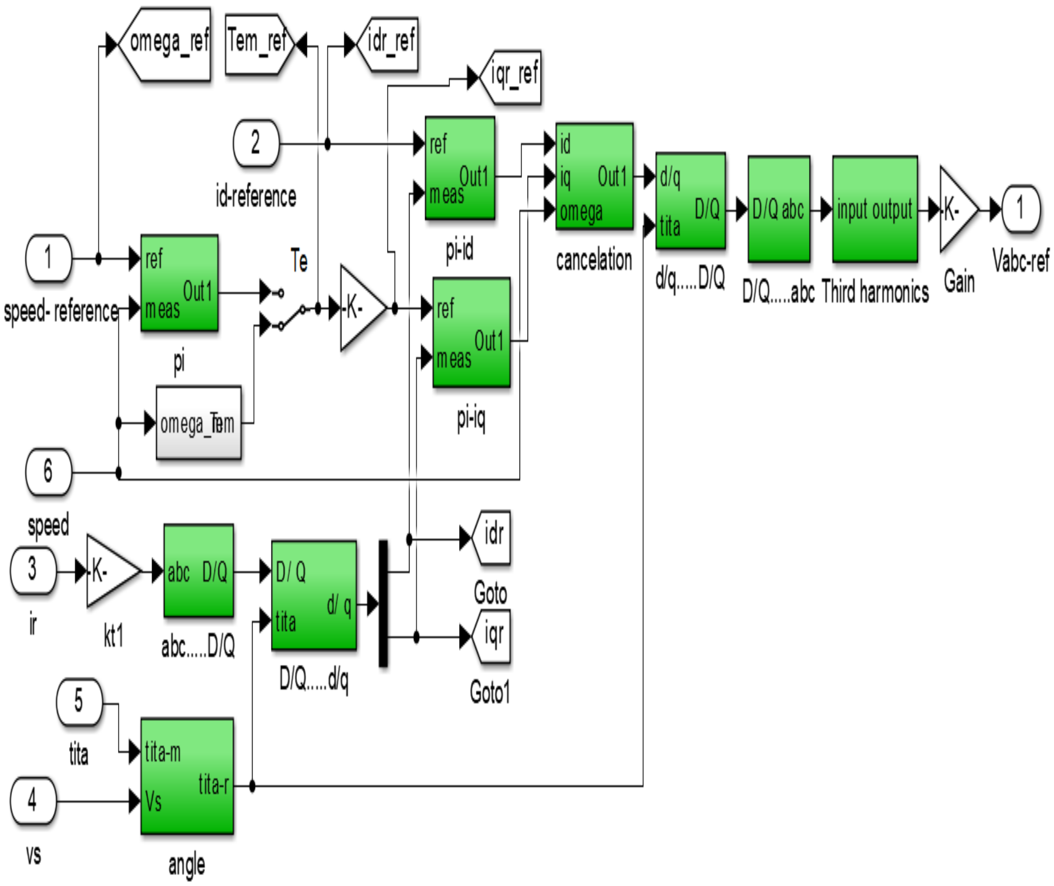

Figure A1: MATLAB Simulink subsystem model for RSC control system

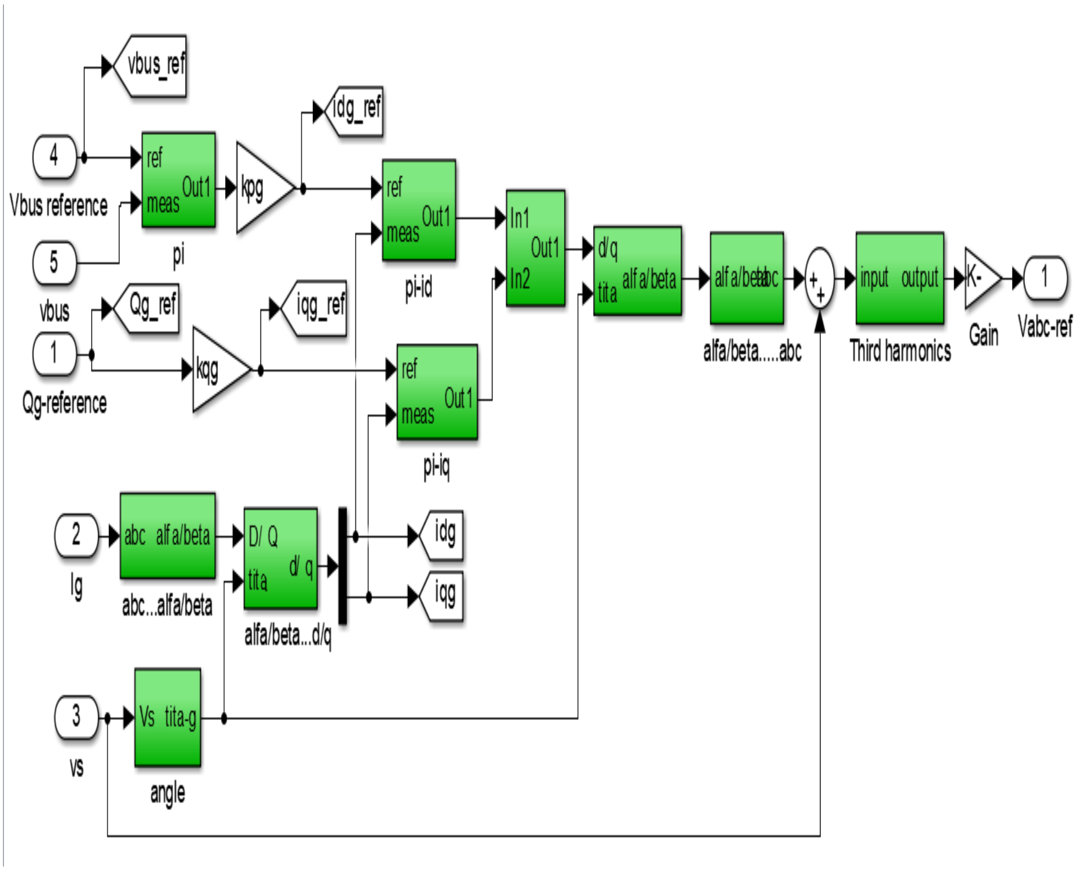

Figure A2: MATLAB Simulink subsystem model for GSC control system

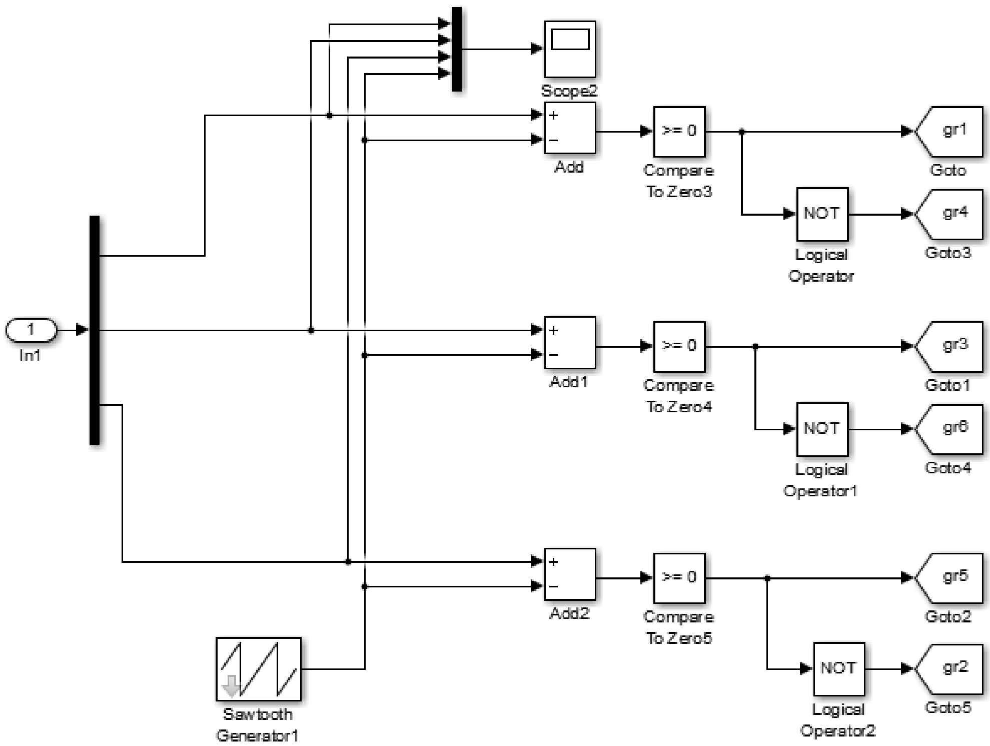

Figure A3: MATLAB Simulink subsystem model of SPWM for two level converters

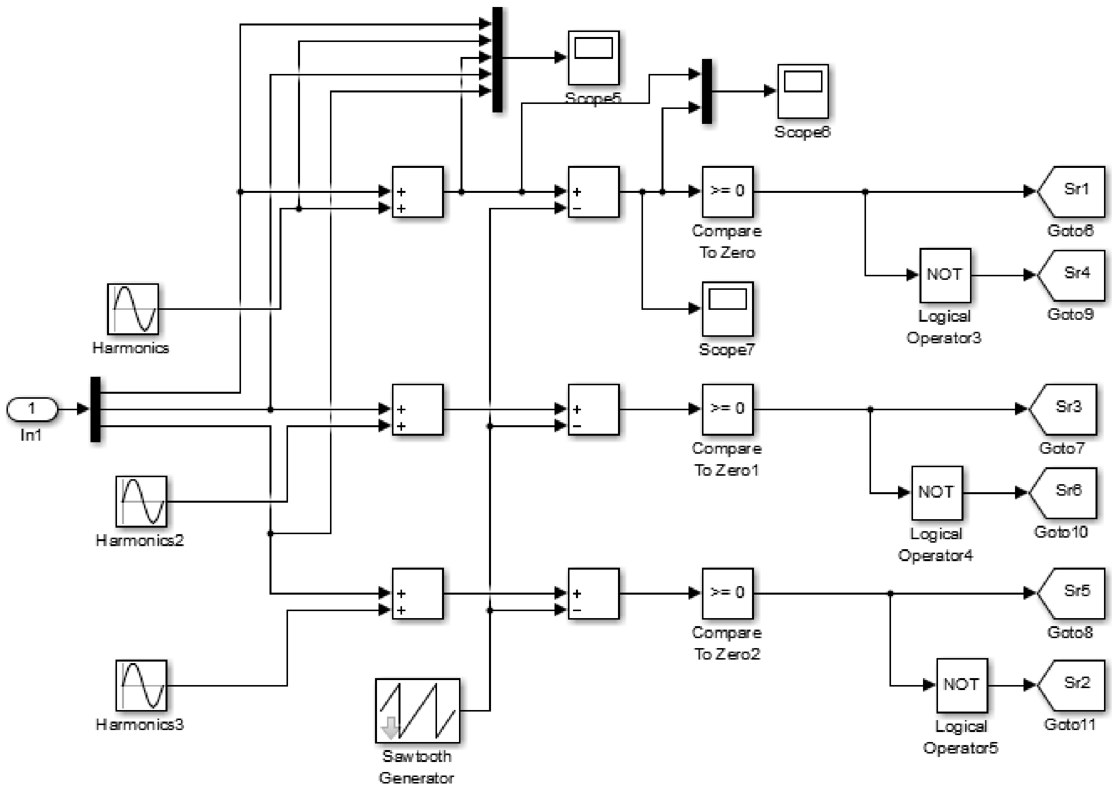

Figure A4: MATLAB Simulink subsystem model of THIPWM for two level converters

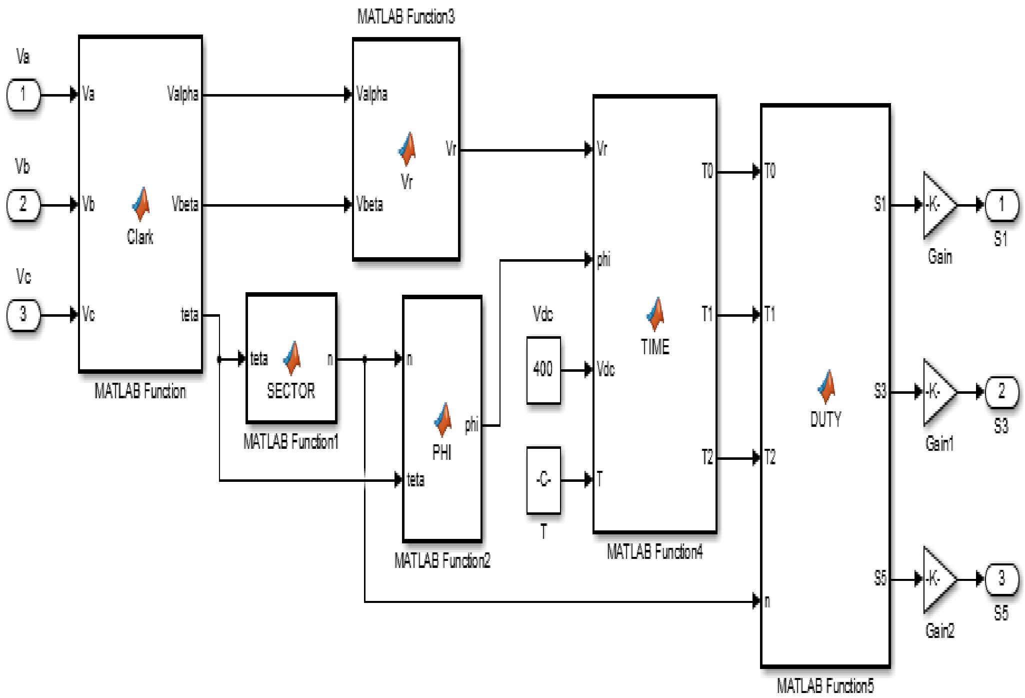

Figure A5: MATLAB Simulink subsystem model of SVPWM for two level converters

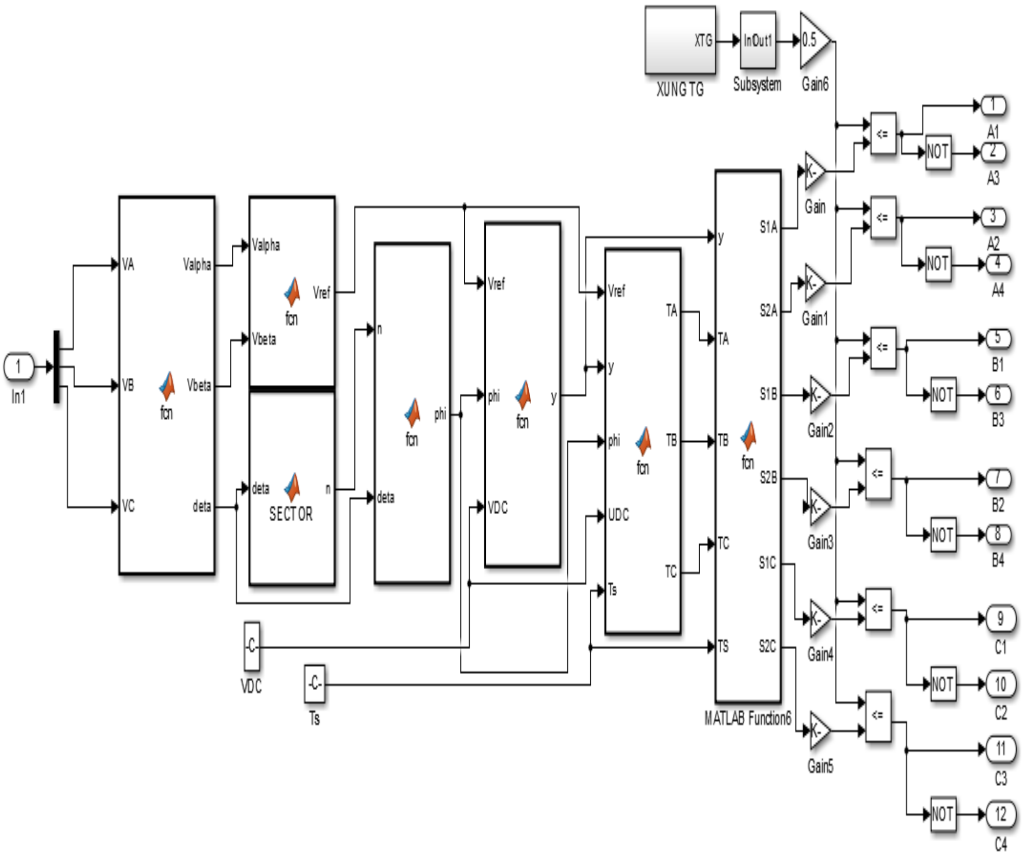

Figure A6: MATLAB Simulink subsystem model of SVPWM for three level NPC converters

Appendix D: Adama II wind turbine generator system data

Parameter	Value	Unite
Number of pole pairs	4	
Rated power	1.5	Mw
Rated voltage	690	V
Stator resistance	0.006243	Ω
Rotor resistance	0.011074	Ω
Stator inductance	0.1337	H
Magnetizing inductance	5.4749	mH

Appendix E: Controller parameters

Parameters	Gain value	
	K_p	K_i
DC bus voltage controller	8	400
Inner current controller in d axis	0.3016	56.8489
Inner current controller in q axis	0.3016	56.8489
PI-PLL controller	180	3200